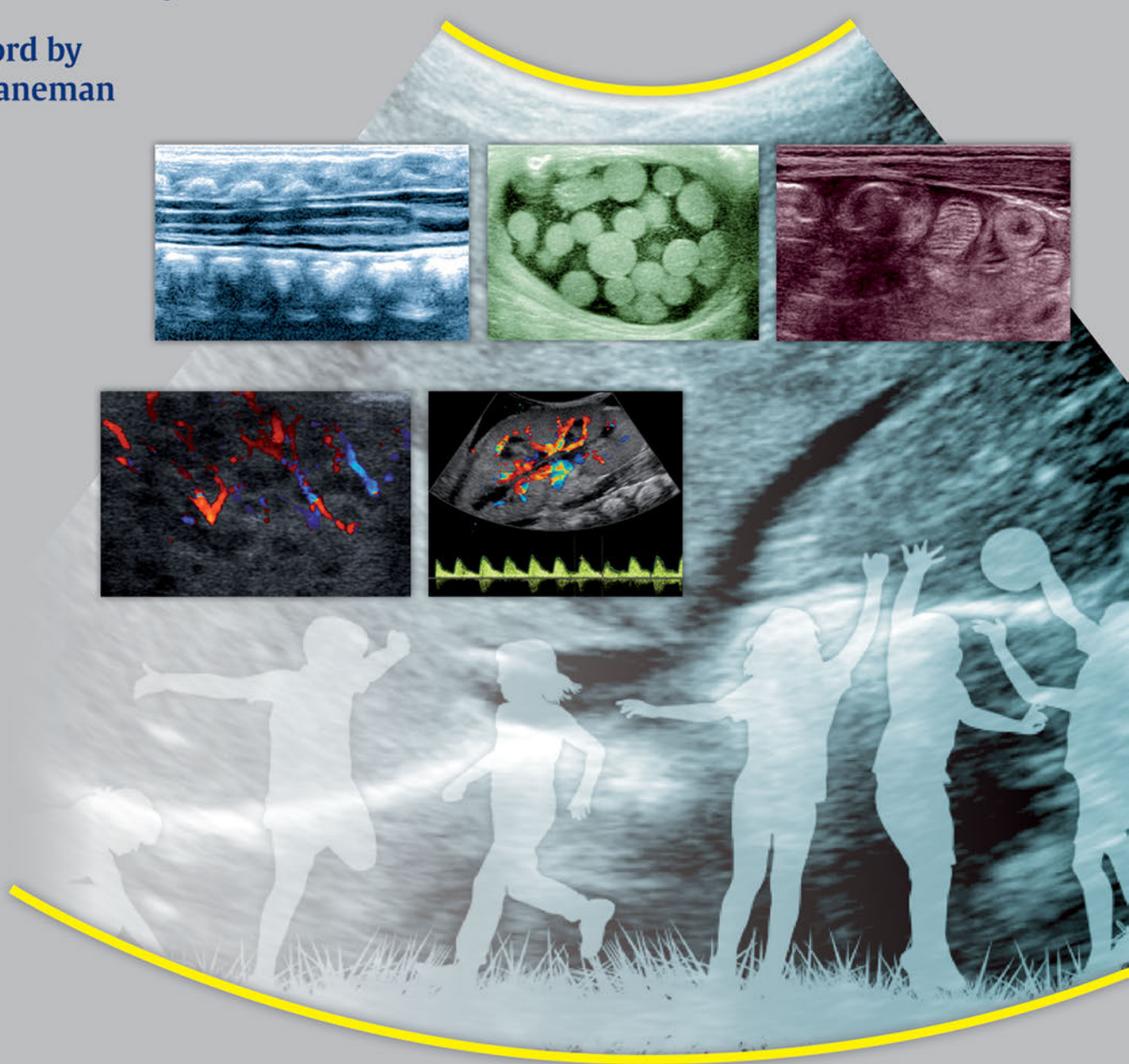
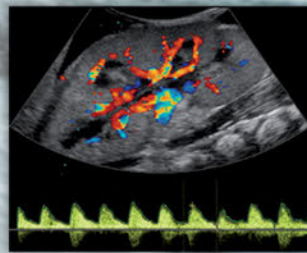
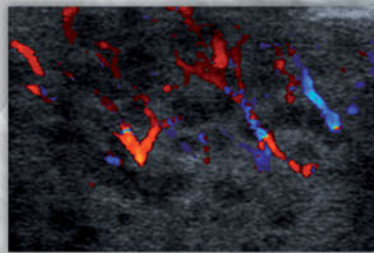
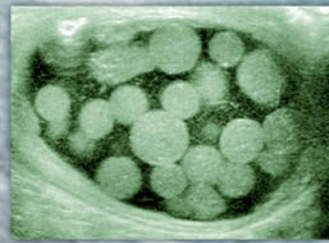
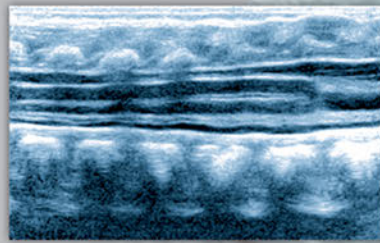


Diagnostic Pediatric Ultrasound

Erik Beek
Rick R. van Rijn

Foreword by
Alan Daneman



To access additional material or resources available with this e-book, please visit <http://www.thieme.com/bonuscontent>. After completing a short form to verify your e-book purchase, you will be provided with the instructions and access codes necessary to retrieve any bonus content.

Diagnostic Pediatric Ultrasound

Dr. Erik Beek, MD, PhD
Consulting Radiologist
Department of Radiology
Wilhelmina Children's Hospital
University Medical Center Utrecht
Utrecht, The Netherlands

Prof. Rick R. van Rijn, MD, PhD
Professor
Department of Radiology
Emma Children's Hospital
Academic Medical Center
Amsterdam, The Netherlands

Foreword by
Alan Daneman, BSc, MBBCh, FRANZCR, FRCPC

2,025 illustrations

Thieme
Stuttgart • New York • Delhi • Rio de Janeiro

Library of Congress Cataloging-in-Publication Data

Diagnostic pediatric ultrasound / [edited by] Erik Beek, Rick R. van Rijn.

p. ; cm.

Includes bibliographical references and index.

ISBN 978-3-13-169731-8 (hardback) –

ISBN 978-3-13-169741-7 (eISBN)

I. Beek, Erik, editor. II. Rijn, Rick R. van, editor.

[DNLM: 1. Ultrasonography–methods. 2. Child. 3. Infant. WN 208]

RJ51.U45

618.92'007543–dc23

2015006968

© 2016 by Georg Thieme Verlag KG

Thieme Publishers Stuttgart
Rüdigerstrasse 14, 70469 Stuttgart, Germany
+49 [0]711 8931 421, customerservice@thieme.de

Thieme Publishers New York
333 Seventh Avenue, New York, NY 10001 USA
+1 800 782 3488, customerservice@thieme.com

Thieme Publishers Delhi
A-12, Second Floor, Sector-2, Noida-201301
Uttar Pradesh, India
+91 120 45 566 00, customerservice@thieme.in

Thieme Publishers Rio, Thieme Publicações Ltda.
Edifício Rodolpho de Paoli, 25º andar
Av. Nilo Peçanha, 50 – Sala 2508
Rio de Janeiro 20020-906, Brasil
+55 21 3172 2297 / +55 21 3172 1896

Cover design: Thieme Publishing Group
Typesetting by Thomson Digital, India

Printed in China by Everbest Printing Ltd

ISBN 978-3-13169-731-8

Also available as an e-book:
eISBN 978-3-13169-741-7

Important note: Medicine is an ever-changing science undergoing continual development. Research and clinical experience are continually expanding our knowledge, in particular our knowledge of proper treatment and drug therapy. Insofar as this book mentions any dosage or application, readers may rest assured that the authors, editors, and publishers have made every effort to ensure that such references are in accordance with **the state of knowledge at the time of production of the book.**

Nevertheless, this does not involve, imply, or express any guarantee or responsibility on the part of the publishers in respect to any dosage instructions and forms of applications stated in the book. **Every user is requested to examine carefully** the manufacturers' leaflets accompanying each drug and to check, if necessary in consultation with a physician or specialist, whether the dosage schedules mentioned therein or the contraindications stated by the manufacturers differ from the statements made in the present book. Such examination is particularly important with drugs that are either rarely used or have been newly released on the market. Every dosage schedule or every form of application used is entirely at the user's own risk and responsibility. The authors and publishers request every user to report to the publishers any discrepancies or inaccuracies noticed. If errors in this work are found after publication, errata will be posted at www.thieme.com on the product description page.

Some of the product names, patents, and registered designs referred to in this book are in fact registered trademarks or proprietary names even though specific reference to this fact is not always made in the text. Therefore, the appearance of a name without designation as proprietary is not to be construed as a representation by the publisher that it is in the public domain.



This book, including all parts thereof, is legally protected by copyright. Any use, exploitation, or commercialization outside the narrow limits set by copyright legislation without the publisher's consent is illegal and liable to prosecution. This applies in particular to photostat reproduction, copying, mimeographing or duplication of any kind, translating, preparation of microfilms, and electronic data processing and storage.

Contents

3.5.1	Germinal Matrix–Intraventricular Hemorrhage	39	3.6.1	Pathology	70
3.5.2	Post-hemorrhagic Ventricular Dilatation	52	3.6.2	Congenital Abnormalities	78
3.5.3	White Matter Injury	60		Recommended Readings	94
3.5.4	Focal Infarction	64			
3.6	Term Infants	70			
4	Spine	98			
	<i>Samuel Stafrace and Erik Beek</i>				
4.1	Embryology	98	4.4	Pathology	103
4.1.1	Ascensus Medullaris	99	4.4.1	Non–Skin-Covered Back Masses: Open Lesions	103
4.2	Technique of Spinal Ultrasound	99	4.4.2	Skin-Covered Back Masses: Closed Lesions	104
4.3	Normal Sonographic Anatomy	100	4.4.3	Occult/Closed Lesions without a Mass	107
4.3.1	Normal Variants	102	4.4.4	Sacral Dimple	113
				Recommended Readings	113
5	Neck	116			
	<i>Erik Beek</i>				
5.1	Normal Anatomy and Variants	116	5.2.4	Pilomatrixoma	127
5.2	Pathology	119	5.2.5	Solid Tumors	127
5.2.1	Vessels of the Neck	119	5.2.6	Thyroid Gland	137
5.2.2	Cystic Lesions	120	5.2.7	Salivary Glands	138
5.2.3	Hemangiomas and Vascular Malformations	124	5.2.8	Thymus	143
			5.2.9	Miscellaneous Lesions	145
				Recommended Readings	151
6	Mediastinum	154			
	<i>Ingmar Gassner and Gisela Schweigmann</i>				
6.1	Normal Anatomy and Variants	154	6.2.2	Trachea	159
6.1.1	Thymus	154	6.2.3	Esophagus	159
6.1.2	Trachea	157	6.2.4	Congenital Vascular Anomalies	163
6.1.3	Esophagus	157	6.2.5	Mediastinal Masses	170
6.1.4	Heart and Great Vessels	157	6.3	Mediastinal Ultrasound in Intensive Care: Complications Associated with Central Venous Access	177
6.2	Pathology	157		Recommended Readings	179
6.2.1	Thymus	157			
7	Pleura and Thorax	182			
	<i>Joost van Schuppen and Rick R. van Rijn</i>				
7.1	Indications for Ultrasonography	183	7.3	Pathology	186
7.2	Anatomy and Normal Variants	183	7.3.1	Chest Wall	186
7.2.1	Thoracic Wall	183	7.3.2	Pleural Space	200
7.2.2	Pleura	184	7.3.3	Lungs	202
7.2.3	Lungs	184	7.3.4	Breast	202
7.2.4	Breast	184	7.3.5	Diaphragm	208
7.2.5	Diaphragm	186		Recommended Readings	211

8	Peritoneal Cavity and Retroperitoneal Space	214		
	<i>Rick R. van Rijn</i>			
8.1	Normal Anatomy	214	8.2.4	Peritonitis
8.2	Pathology	215	8.2.5	Pneumoperitoneum
8.2.1	Abdominal Vessels	215	8.2.6	Peritoneal Tumors.....
8.2.2	Lymphadenopathy	219	8.2.7	Retroperitoneal Tumors.....
8.2.3	Intraperitoneal Fluid Collections	221	8.2.8	Cystic Congenital Anomalies.....
				Recommended Readings
9	Liver and Biliary System	246		
	<i>Rick R. van Rijn and RAJ Nievelstein</i>			
9.1	Normal Anatomy and Variants	246	9.3.1	Congenital Anomalies
9.2	Normal Measurements	249	9.3.2	Infection.....
9.2.1	Portal Venous Flow	249	9.3.3	Acquired Biliary Pathology
9.2.2	Hepatic Arterial Flow	249	9.3.4	Trauma.....
9.2.3	Hepatic Venous Flow	249	9.3.5	Tumors.....
9.3	Pathology	249	9.3.6	Pneumobilia
			9.3.7	Miscellaneous Conditions
				Recommended Readings
10	Spleen	324		
	<i>Samuel Stafrace</i>			
10.1	Normal Anatomy and Variants	324	10.2	Pathology
10.1.1	Embryology	324	10.2.1	Abnormalities of Location and Number
10.1.2	Anatomical Considerations	324	10.2.2	Abnormalities of Size
10.1.3	Technique and Normal Ultrasound Appearances	325	10.2.3	Traumatic Injury of the Spleen
10.1.4	Echogenicity and Changes in Echogenicity with Age	325	10.3	Acknowledgements
10.1.5	Vascularity	327		Recommended Readings
10.1.6	Normal Variants.....	327		
10.1.7	Normal Splenic Size	331		
11	Pediatric Intestinal Ultrasonography	360		
	<i>Simon Robben</i>			
11.1	Esophagus	360	11.6.1	Other Causes of Colitis.....
11.2	Gastroesophageal Junction	363	11.7	Rectum
11.3	Stomach	364	11.8	Anus
11.4	Small Bowel	367	11.9	Neonatal Bowel Obstruction
11.5	Appendix	387	11.10	Conclusion
11.6	Large Bowel	393		Recommended Readings
12	Pancreas	416		
	<i>Maria Raissaki and Marina Vakaki</i>			
12.1	Examination Technique	416	12.3	Pathology
12.2	Normal Anatomy, Variants, and Pseudo-lesions	417	12.3.1	Developmental Anomalies
			12.3.2	Pancreatitis

12.3.3	Inherited Disorders	436	12.3.5	Cystic Masses	444
12.3.4	Neoplasms	440		Recommended Readings	449
13	Kidneys				452
	<i>Maria Beatrice Damasio, Ann Nystedt, Lil-Sofie Ording Muller, and Giorgio Pioggio</i>				
13.1	Normal Anatomy and Variants	452	13.8	Renovascular Disease	481
13.1.1	Kidneys	452	13.8.1	Renal Artery Stenosis	481
13.1.2	Ureters	455	13.8.2	Renal Vein Thrombosis	482
13.1.3	Bladder	456	13.9	Parenchymal Nephropathy	485
13.2	Congenital Anomalies of the Kidney and the Urinary Tract	456	13.9.1	Glomerular Nephropathies	487
13.2.1	Renal Hypodysplasia	457	13.9.2	Tubular Nephropathies	487
13.2.2	Ureteropelvic Junction Stenosis	457	13.9.3	Interstitial Nephropathies	488
13.2.3	Ureterovesical Junction Stenosis	457	13.9.4	Vascular Nephropathies	489
13.2.4	Ureterovesical Reflux	457	13.10	Renal Trauma	490
13.2.5	Duplicate Collecting System	460	13.10.1	Renal Trauma Grading	491
13.2.6	Horseshoe Kidney	461	13.11	Pediatric Renal Transplantation	491
13.3	Urolithiasis and Nephrocalcinosis	464	13.11.1	Early Postoperative Assessment	491
13.4	Kidney Cysts and Cystic Nephropathies	467	13.11.2	Differential Diagnosis of Early Graft Dysfunction	491
13.5	Autosomal-Dominant Polycystic Kidney Disease	469	13.11.3	Differential Diagnosis of Long-Term Graft Dysfunction and Imaging Aspects	496
13.5.1	Autosomal-Recessive Polycystic Kidney Disease	470	13.12	Bladder and Urethra	500
13.5.2	Nephronophthisis	472	13.12.1	Congenital Bladder Anomalies	500
13.5.3	Glomerulocystic Disease	472	13.12.2	Urethral Anomalies	502
13.5.4	Medullary Sponge Kidney Disease	472	13.12.3	Utricle	503
13.5.5	Multicystic Kidney Disease	472	13.12.4	Urachal Anomalies	503
13.5.6	Simple Cysts	473	13.12.5	Calculi	504
13.5.7	Complicated Cysts	473	13.12.6	Infection	504
13.6	Renal Tumors	474	13.12.7	Neoplasm	504
13.6.1	Malignant Tumors	474	13.13	Contrast-Enhanced Cystosonography	506
13.6.2	Benign Tumors	478		Recommended Readings	509
13.7	Urinary Tract Infection	480			
14	Adrenal Glands				512
	<i>Claire Gowdy and Annie Paterson</i>				
14.1	Embryology of the Adrenal Glands	512	14.5.2	Adrenal Hemorrhage in the Older Child	514
14.2	Normal Anatomy	512	14.5.3	Adrenal Cysts	514
14.3	Normal Sonographic Appearance	512	14.5.4	Adrenal Abscesses	517
14.4	Normal Variants	513	14.5.5	Congenital Adrenal Hyperplasia	517
14.5	Pathology	514	14.5.6	Adrenal Hyperplasia in Older Patients	518
14.5.1	Neonatal Adrenal Hemorrhage	514	14.5.7	Adrenal Hypoplasia	518
			14.5.8	Medullary Tumors: Neurogenic Tumors	519
			14.5.9	Medullary Tumors: Pheochromocytoma	520
			14.5.10	Adrenal Cortical Tumors	520

14.5.11	Other Adrenal Tumors	528	14.5.13	Wolman Disease	531
14.5.12	Miscellaneous Adrenal Masses	531		Recommended Readings	534
15	Sonography of the Female Genital Tract				536
	<i>Willemijn Klein</i>				
15.1	Normal Anatomy and Variants	536	15.2.3	Ovarian Tumors	551
15.1.1	Normal Measurements	538	15.2.4	Ovarian Torsion	560
15.2	Pathology	538	15.2.5	Pelvic Inflammatory Disease	560
15.2.1	Congenital Anomalies	538	15.2.6	Amenorrhea	560
15.2.2	Cloacal Malformation	540	15.2.7	Pubertas Praecox	568
				Recommended Readings	568
16	Male Genital Tract				570
	<i>Matteo Baldisserotto</i>				
16.1	Technique of Scrotal Ultrasound and Normal Ultrasound Anatomy	570	16.5	Epididymitis and Epididymo-orchitis	584
16.2	Hydrocele and Indirect Inguinal Hernia	570	16.6	Idiopathic Scrotal Edema	585
16.2.1	Hydrocele	570	16.7	Testicular Trauma	585
16.2.2	Indirect Inguinal Hernia	573	16.8	Cystic Transformation of the Rete Testis (Tubular Ectasia)	587
16.3	Scrotal Tumors	576	16.9	Epididymal Cyst	587
16.3.1	Testicular Tumors	576	16.10	Varicocele	588
16.3.2	Secondary Tumors of the Testes	576	16.11	Bilobed Testicle and Polyorchidism	589
16.3.3	Extratesticular Tumors and Masses	578	16.12	Undescended Testicle and Retractable Testicle	590
16.4	Testicular Torsion	580		Recommended Readings	591
16.4.1	Intravaginal Testicular Torsion	580			
16.4.2	Extravaginal Testicular Torsion	582			
16.4.3	Torsion of the Appendix Testis	583			
17	Musculoskeletal Ultrasound				594
	<i>Jim Carmichael and Karen Rosendahl</i>				
17.1	Pediatric Hip	594	17.2	Ultrasound of the Musculoskeletal System in the Older Child	598
17.1.1	Normal Development of the Hip	594	17.2.1	Arthritis	598
17.1.2	Ultrasound Examination for Developmental Dysplasia of the Hip	594	17.2.2	Soft-Tissue Masses: Lumps and Bumps	604
				Recommended Readings	615
18	Ultrasound-Guided Interventional Procedures: Biopsy and Drainage				618
	<i>Alex Barnacle and Derek Roebuck</i>				
18.1	Biopsy	618	18.2	Drainage Techniques and Equipment	625
18.1.1	Techniques and Equipment	618		Recommended Readings	627
18.1.2	Tumor Biopsy	620			
18.1.3	Nontumor Biopsy	623			
	Index				629

Video Contents

Chapter 3

Video 3.94 Doppler ultrasound shows flow in the bridging veins.

Chapter 6

Video 6.1 (1–4)

Video 6.1.1a, b Normal thymus.

Video 6.1.2 Trans-sternal transverse scan.

Video 6.1.3 Normal anatomy level of aortic arch.

Video 6.1.4 Normal esophagus.

Video 6.2 Cervical extension of normal thymus.

Video 6.4 (1–2) Subglottic hemangioma.

Video 6.4.1 The hemangioma compresses the tracheal lumen to a small gap (*arrowheads*).

Video 6.4.2 Color Doppler shows the high vascularity and the involvement of the adjacent soft tissues (i.e., thyroid).

Video 6.6 (1–2) Esophageal atresia with low fistula.

Video 6.6.1 The suction tube (*arrows*) lies in the nondistended proximal pouch (*arrowheads*).

Video 6.6.2 The distal esophagus is shown behind the heart.

Video 6.7 H-type tracheoesophageal fistula.

Video 6.8 Achalasia.

Video 6.12 (1–3) Left aortic arch with aberrant right subclavian artery.

Video 6.12.1 Left aortic arch with aberrant right subclavian artery.

Video 6.12.2 Left aortic arch with aberrant right subclavian artery.

Video 6.12.3 Left aortic arch with aberrant right subclavian artery.

Video 6.13 (1–2) Right aortic arch with aberrant left subclavian artery.

Video 6.13.1a, b Right aortic arch with aberrant left subclavian artery.

Video 6.13.2a, b Right aortic arch with aberrant left subclavian artery.

Video 6.14 (1–6) Double aortic arch.

Video 6.14.1 Double aortic arch.

Video 6.14.2 Double aortic arch.

Video 6.14.3 Double aortic arch.

Video 6.14.4 Double aortic arch.

Video 6.14.5 Double aortic arch.

Video 6.14.6 Double aortic arch.

Video 6.15 (1–2) Pulmonary artery sling.

Video 6.15.1 Pulmonary artery sling.

Video 6.15.2 Pulmonary artery sling.

Video 6.23 (1–3)

Video 6.23.1a, b Thrombus around central venous catheter in the right atrium.

Video 6.23.2 Fibrin sheath of a catheter left behind in the superior vena cava after removal of a central venous line.

Video 6.23.3 Embolization of a broken catheter fragment into the pulmonary artery.

Chapter 7

Video 7.8 Normal air containing lung.

Video 7.15 Normal movement of the diaphragm, M mode.

Video 7.17a, b A forked rib.

Video 7.18 Prominent cartilaginous rib.

Video 7.33 Thoracic venous malformation.

Video 7.40 Pleural fluid with thick echogenic strands after liver biopsy.

Video 7.42a Pneumonia complicated by empyema.

Video 7.42b Follow up shows a subpleural collection with a thick wall and debris.

Video 7.42c A 2-year-old boy with bronchopneumonia complicated by effusion. The video clearly shows motion of pleural fluid and the collapsed lung tissue during respiration.

Video 7.47a A 2-week-old premature with on chest x-ray a persistent opacification in the left upper lung. US shows hyperechoic tissue containing vascular structures.

Video 7.47b No air is visible in the lobe. The lung tissue resembles liver tissue.

Chapter 8

Video 8.6	Video clip shows the IVC located on the left side of the aorta.	Video 8.28	Upon compression flow is seen within the purulent fluid surrounding the small bowel loops.
Video 8.10	Video clip shows the hypertrophied collateral vein leading to the retroperitoneal space.	Video 8.31	Free air within the peritoneal cavity between the liver and the abdominal wall.
Video 8.16	Doppler US shows an extremely slow flow in the portal vein.	Video 8.35a	Video shows independent motion of the tumour in respect to the liver during respiration. This proves that there is no relation between these two structures.
Video 8.18	Video shows flow within the metastatic mass and flow within the ascites during respiration.	Video 8.35b	Video shows the extent to the tumour on an axial T2 weighted MRI.
Video 8.20	On respiration flow is visible within the ascites.	Video 8.38	Video shows the extent to the tumour on an axial T2 weighted MRI.
Video 8.24	Perforation of the gallbladder.	Video 8.42	Video shows the extent to the tumour on an axial T2 weighted MRI.
Video 8.26	Video clip shows flow of pus within the abscess. Note the deep extend of the abscess.	Video 8.49	During respiration there clearly is no relation between the cystic mass and the ovary.
Video 8.27	Video clip shows the flow of pus within the abscess upon compression. Note the rigidity of the surrounding infiltrated fat tissue.		

Chapter 9

Video 9.4	Thrombus formation in the umbilical vein.	Video 9.90	Neuroblastoma with encasement of the abdominal vessels.
Video 9.16	Choledochal cyst.	Video 9.98	Tumour in the liver hilum.
Video 9.21	Thick mucoid pus within the liver abscess.	Video 9.99	US shows air in the portal system.
Video 9.74	Mesenchymal hamartoma.	Video 9.101	Motion of air bubbles in the portal vein branches.
Video 9.79	Hepatoblastoma.		
Video 9.85	Hepatoblastoma.		

Chapter 10

Video 10.6	Air artefact from the lung obscuring the spleen.	Video 10.32	Splenic lymphoma.
-------------------	--	--------------------	-------------------

Chapter 11

Video 11.2	Juvenile polyp in descending colon.	Video 11.13b	Normal pylorus.
Video 11.4	Patient with mesenteric Burkitt lymphoma with infiltrative invasion of the mesentery	Video 11.14	Normal anatomical position of the D3 segment of the duodenum.
Video 11.5	Esophageal atresia without a tracheoesophageal fistula.	Video 11.17	Infant with malrotation and midgut volvulus, whirlpool sign.
Video 11.9	Boy with acute abdominal distention and vomiting.	Video 11.21a, b	Crohn's disease of the terminal ileum.
Video 11.11	hypertrophic pyloric stenosis.	Video 11.24	Lobulated character of the polyp and the vessels in the stalk.
Video 11.12	Acute lymphatic leukemia with massive nonstratified wall thickening of the stomach.	Video 11.25	Food particles simulating polyps or duplication cysts.
Video 11.13a	Hypertrophic pyloric stenosis.	Video 11.26a, b	Henoch Schönlein purpura.

Video 11.28	Meckel's diverticulum.	Video 11.48	Hydropic gangrenous appendix with a torsion at its base.
Video 11.30	Necrotizing enterocolitis and intestinal pneumatosis.	Video 11.53	Neutropenic colitis.
Video 11.31	Portal vein gas in Hirschsprung's disease.	Video 11.54	Pseudomembranous colitis.
Video 11.32	Pneumoperitoneum in necrotising enterocolitis.	Video 11.55	Pseudomembranous colitis.
Video 11.33	Sloughing of the mucosa in a premature infant with transient ischemia.	Video 11.57	Hemolytic uremic syndrome.
Video 11.35	Duplication cyst of the ileum in a newborn child.	Video 11.58	Juvenile polyp in the descending colon.
Video 11.37	Postsurgical resolving hematoma or haemorrhagic seroma resembling a duplication cyst	Video 11.59	Encrusted pellets of stools in the colon.
Video 11.38	Benign small bowel intussusceptions.	Video 11.60	Normal appendage of the colon.
Video 11.39	Extremely large benign small bowel intussusception.	Video 11.64	A newborn with a bucket handle deformity of the anus.
Video 11.46	Appendicitis.	Video 11.65	Jejunal atresia.
Chapter 16		Video 11.68	Newborn with cystic fibrosis and meconium ileus.
Video 16.6	Communicating hydrocele.	Video 11.72	Meconium peri-orchitis.
Video 16.7	Non-communicating hydrocele.	Video 16.12c	Inguinal hernia with omentum.
Video 16.12a	Scrotal hernia containing bowel loops, the testicle in the peritoneal cavity and an encysted hydrocele.	Video 16.19	Benign monodermal teratoma.
Video 16.12b	Inguinal hernia with a bowel loop.	Video 16.29	Torsioned spermatic cord.
		Video 16.47	Varicocele.
		Video 16.54a, b	Non-palpable testicles.

Foreword

It is with great pleasure that I write the Foreword of this book which is dedicated to describe the role and uses of sonography in neonates, infants, and older children.

For decades, sonography has played a major role in imaging protocols used in pediatric patients. The significant technical advances in sonographic equipment and the aggressive and imaginative approaches taken by many pediatric radiologists have facilitated the continuous expansion of the uses of sonography in the pediatric population. The pivotal role that sonography plays in pediatric imaging remains secure despite the advances of other imaging modalities, and its advantages have been well documented. The most significant factors are, firstly, that it does not use ionizing radiation which is extremely important in the pediatric age group and, secondly, that it is a relatively cheap modality (including equipment and running costs) compared with computed tomography and magnetic resonance imaging. Furthermore, equipment can be easily moved to the bedside where state-of-the-art examinations can be performed without moving patients who are too sick to be moved. Sonography is also ideally suited for use in pediatrics, particularly neonates and small children, in whom exquisite images can be obtained because of the small size of the patients.

Performing sonographic examinations in children is a great clinical and intellectual challenge. It is more than just a simple extension of the clinical examination. It requires a broad knowledge of the disease entities encountered in the pediatric age group, an understanding of the sonographic appearances of these diseases, and an ability to perform the examination with meticulous attention to technique in order to produce the highest quality images of both normal and abnormal findings. Although one should be guided by established protocols for each type of examination, one should never be constrained by these protocols. It is essential to perform examinations with an approach that enables one to be both aggressive in the search for abnormalities and flexible in adjusting the techniques used to suit the needs of the individual patient. This requires a thorough understanding of the equipment one is using and what factors need to be altered in order to optimize the images in pursuit of the most informative examination.

There has been a relentless expansion of the uses of sonography in pediatrics over the past four decades. However, sonography has not merely expanded by becoming another layer for imaging children. It has expanded by replacing other modalities as the imaging modality of choice in many clinical situations. The modalities that have been replaced are primarily those using ionizing radiation, such as plain radiographs, fluoroscopy, computed tomography, and angiography. Furthermore, sonography has also played a major role in facilitating or guiding interventional techniques in children.

This book addresses the issues related to sonographic imaging in pediatric patients extremely well. The text is very comprehensive and the images illustrating the wide variety of disease processes are of high quality. The authors have clearly made a tremendous effort to compile such an informative book.

The information contained in this book is of great value not only to trainees but also to pediatric radiologists and technologists who are involved in the care of sick children, as well as pediatricians and pediatric surgeons who may require a better understanding of the role of sonography in children and who desire to become more familiar with the sonographic appearances of the diseases they are dealing with.

The authors must be congratulated for the comprehensive text and high-quality images used in the book. It is a great honor to have been asked to write the Foreword of this book which is dedicated to a modality that has become so pivotal in pediatric imaging and which will definitely remain so for the foreseeable future.

*Alan Daneman, BSc, MBBCh, FRANZCR, FRCPC
Professor of Medical Imaging
Department of Medical Imaging
University of Toronto
Toronto, Canada*

*Staff Pediatric Radiologist
Department of Diagnostic Imaging
Division of Body Imaging
Hospital for Sick Children
Toronto, Canada*

Preface

Ultrasound is a marvelous imaging modality in pediatric radiology. Children are often lean and small and this creates favorable conditions for ultrasound. Anesthesia is not necessary and the exams can be done at the bedside. During the ultrasound examination the radiologist can not only image the patient but also obtain a clinical history, and thus be informed about the clinical situation of the patient in much more detail than any radiology request form can reveal.

In 1990 a book on pediatric ultrasound by Reinhard Schulz and Ulrich Willi was published. Its chapters were composed of a short text and many images. The book inspired us to publish a new book on diagnostic pediatric ultrasound, with a limited amount of text, many images and as a tribute to modern technology: on-line video clips. Video clips capture one of the most important aspects of ultrasound imaging, the ability to see motion in real-time.

The video clips have the same number as the images in the book which illustrate a related disease.

The book is intended for all health workers who perform pediatric ultrasound like pediatric-radiologists, general radiologists, radiology residents, pediatricians, and sonographers. It is the result of the efforts of many authors who describe the sonographic findings of a spectrum of diseases in their favorite organ system. This cooperation also gave the possibility to exchange images among the authors.

We and the authors have enjoyed working on this book and we hope that *Diagnostic Pediatric Ultrasound* will increase the knowledge of the readers, who would also enjoy the illustrations and video clips.

We like to thank all the authors for their contributions and Thieme for their support.

Erik Beek, MD, PhD
Rick R. van Rijn, MD, PhD

Contributors

Matteo Baldisserotto, MD, PhD

Consultant Paediatric Radiologist
Department of Radiology
School of Medicine
Pontificia Universidade Católica do Rio Grande do Sul
Brazil

Alex Barnacle, BM MRCP FRCR

Consultant Paediatric Interventional Radiologist
Department of Radiology
Great Ormond Street Hospital for Sick Children
London, United Kingdom

Erik Beek, MD

Consulting Radiologist
Department of Radiology
University Medical Center Utrecht
Utrecht, The Netherlands

Jim Carmichael

Consultant Paediatric Radiologist
Evelina London Children's Hospital
London, United Kingdom

Maria Beatrice Damasio, MD

Consultant Paediatric Radiologist
Department of Radiology
Giannina Gaslini Institute
Genova, Italy

Ingmar Gassner, MD

Consultant Paediatric Radiologist
Department of Radiology
Section of Pediatric Radiology
Innsbruck Medical University
Innsbruck, Austria

Claire Gowdy MRCP, CH, FRCR

Consultant Paediatric Radiologist
Paediatric Radiology
Royal Victoria Infirmary
Newcastle upon Tyne, United Kingdom

Handan Güleriyüz, MD

Consultant Paediatric Radiologist
Department of Pediatric Radiology
Dokuz Eylül University Medical School
Izmir, Turkey

Willemijn Klein, MD, PhD

Consultant Paediatric Radiologist
Department of Radiology and Nuclear Medicine
Radboud University Medical Center
Nijmegen, The Netherlands

Gerda Meijler, MD PhD

Consultant Neonatologist
Department of Neonatology
Isala Hospital
Zwolle, The Netherlands

Rutger Jan Nivelstein, MD

Consultant Paediatric Radiologist
Department of Radiology
University Medical Center Utrecht
Utrecht, The Netherlands

Ann Nystedt, MD

Consultant Paediatric Radiologist
Department of Radiology
Sørlandet Hospital Arendal
Arendal, Norway

Lil-Sofie Ording Muller, MD PhD

Consultant Paediatric Radiologist
Unit for Paediatric Radiology
Department of Radiology and Intervention
Oslo University Hospital
Oslo, Norway

Anne Paterson MBBS, MRCP, FRCR, FFR RCSI

Consultant Paediatric Radiologist
Radiology Department
Royal Belfast Hospital for Sick Children
Belfast, United Kingdom

Rob Peters, MSEE

Medical Physicist
Department of Physics & Medical Engineering
VU Medical Center
Amsterdam, The Netherlands.

Giorgio Piaggio, MD

Consultant Paediatric Nephrologist
Nephrology Unit
Giannina Gaslini Institute
Genoa, Italy

Maria Raissaki, MD, PhD

Assistant Professor in Paediatric Radiology
University Hospital of Heraklion
Crete, Greece

Prof. Rick R. van Rijn, MD, PhD

Professor
Department of Radiology
Emma Children's Hospital
Academic Medical Center
Amsterdam, The Netherlands

Prof. Simon Robben, MD, PhD

Consultant Paediatric Radiologist
Department of Radiology
Maastricht University Medical Center
Maastricht, The Netherlands

Derek Roebuck, MBBS, DMRD, FRCR, FRANZCR, MRCPCH

Consultant Paediatric Interventional Radiologist
Department of Radiology
Great Ormond Street Hospital for Sick Children
London, United Kingdom

Anne Smets, MD

Consultant Paediatric Radiologist
Pediatric Radiology Unit
Department of radiology
Emma Children's hospital
Academic Medical Center
Amsterdam, The Netherlands

Joost van Schuppen, MD

Consultant Paediatric Radiologist
Department of Radiology
Emma Children's Hospital
Academic Medical Center
Amsterdam, The Netherlands

Gisela Schweigmann, MD

Consultant Paediatric Radiologist
Department of Radiology
Section of Pediatric Radiology
Innsbruck Medical University
Innsbruck, Austria

Samuel Stafrace, MD, MRCP (UK), FRCR, FRCP (Edin)

Attending Physician – Radiology
Sidra Medical and Research Center
Doha, Qatar
Previously: Consultant Radiologist
Royal Aberdeen Children's Hospital
Aberdeen, Scotland, United Kingdom

Marina Vakaki, MD, PhD

Director of Radiology Department and Head of
Ultrasonography Unit
"P & A. Kyriakou" Children's Hospital
Athens, Greece

Linda de Vries, MD, PhD

Professor in Neonatology
Department of Neonatology
University Medical Center
Utrecht, The Netherlands

Abbreviations

¹²³ I-MIBG	iodine I 123 metaiodobenzylguanidine
¹⁸ F-FDG-PET	fluorodeoxyglucose F 18 positron emission tomography
^{99m} Tc-MDP	technetium Tc 99m methylene diphosphonate
AAST	American Association for the Surgery of Trauma
ACTH	adrenocorticotrophic hormone
ADPKD	autosomal-dominant polycystic kidney disease
AHW	anterior horn width
ALARA	as low as reasonably achievable
A-mode	amplitude mode
AP	anteroposterior.
APLS	Advanced Pediatric Life Support)
BESS	benign enlargement of the subarachnoid space
B-mode	brightness mode
CBH	cerebellar hemorrhage
CC	corpus callosum
CF	cystic fibrosis
CNS	central nervous system
CSF	cerebrospinal fluid
CSG	contrast-enhanced cystosonography
CT	computed tomography
cUS	cranial ultrasound
DDH	developmental dysplasia of the hip
DMSA	dimercaptosuccinic acid
ECMO	extracorporeal membrane oxygenation
ERCP	endoscopic retrograde cholangiopancreatography
ESPR	European Society of Paediatric Radiology
FAST	focused abdominal sonography for trauma
GCTTS	giant cell tumor of the tendon sheath
GERD	gastroesophageal reflux disease
GMH-IVH	germinal matrix–intraventricular hemorrhage
HIE	hypoxic–ischemic encephalopathy
IBD	inflammatory bowel disease
INRG	International Neuroblastoma Risk Group
INSS	International Neuroblastoma Staging System
IVC	inferior vena cava
JIA	juvenile idiopathic arthritis
LSV	lenticulostriate vasculopathy
MCE	multicystic encephalomalacia
MI	mechanical index

Abbreviations

M-mode	motion mode
MR	magnetic resonance
MRCP	magnetic resonance cholangiopancreatography
MRKH	Mayer-Rokitansky-Küster-Hauser (syndrome)
NAFLD	nonalcoholic fatty liver disease
NICH	noninvoluting congenital hemangiomas
NPV	negative predictive value
PAIS	perinatal arterial ischemic stroke
PET	positron emission tomography
PHVD	post-hemorrhagic ventricular dilatation
PLIC	posterior limb of internal capsule
PMA	postmenstrual age
PNET	primitive neuroectodermal tumor
PPV	positive predictive value
PRF	pulse repetition frequency
PRP	pulse repetition period
PSC	Primary sclerosing cholangitis
PTLD	post-transplant lymphoproliferative disorder
PVE	periventricular echodensities
PVHI	periventricular hemorrhagic infarction
PVL	periventricular leukomalacia
PVNS	pigmented villonodular synovitis
RI	resistive index
RICH	rapidly involuting congenital hemangiomas
SD	standard deviation
SELSTOC	self-limiting sternal tumor of childhood (SELSTOC)
SMA	superior mesenteric artery
SMV	superior mesenteric vein
SPEN	solid and papillary epithelial neoplasm
SPT	solid papillary tumor
TCD	transverse cerebellar diameter
TEA	term equivalent age
TGC	time gain compensation
TI	thermal index
TOD	thalamo-occipital distance
US	ultrasound
UTI	urinary tract infection
VACTERL	(vertebral abnormalities, anal atresia, cardiac abnormalities, tracheoesophageal fistula and/or esophageal atresia, renal agenesis and dysplasia, limb defects)
VCUG	voiding cystourethrography
VI	ventricular index
VUR	vesicoureteral reflux

Chapter 1

Examining the Child and Creating a Child-Friendly Environment

1.1	Child-Friendly Staff	2
1.2	Appointment	2
1.3	Appointment Letter	2
1.4	Waiting Area	2
1.5	Examination Room	3
1.6	Examination	4
1.7	How to Scan: Tips and Tricks	5
1.8	Private Room	6
1.9	Communicating the Results	6

1 Examining the Child and Creating a Child-Friendly Environment

Anne Smets

A pediatric radiology department welcomes children between 0 and 18 years of age who are sick or wounded, accompanied by worried or anxious parents or caregivers. Their stay in the radiology department is usually of short duration, and the ultimate challenge is to collect the necessary diagnostic information while limiting the amount of pain and distress. Getting the child to cooperate will increase our chances of performing this task with success and doing it in a child-friendly way will improve the experience of the child and his/her parents or caregivers. Performing an ultrasound examination on a calm child in the presence of trusting parents or caregivers will also make life easier for the hospital staff. Moreover, it will increase our chances of building a trusting relationship and hence laying the foundations for good collaboration with the child during future examinations. Providing good preparatory information and creating a child-friendly environment in the broadest sense of the words is the basis for a successful examination.

1.1 Child-Friendly Staff

Creating a child-friendly environment starts with the attitude of the staff, including the receptionist, radiology assistants, technicians, and doctors. All staff should be aware of the particular needs of pediatric patients, showing consideration and providing explanation and reassurance. They should be patient, enjoy working with children, and be comfortable with and around them. Uncertainty can be transmitted to the child and the parents, and this may very well result in inadequate examinations. The staff must be aware of the importance of building a rapport with the child and the anxious parents in order to pave the way for a good-quality examination and possible future examinations. Not everybody is capable of doing, or willing to do this; therefore, it is important to select dedicated pediatric personnel, even in a general radiology department setting. Without a committed pediatric team, child-friendly decoration and logistics are an investment of little value.

1.2 Appointment

When an appointment for an ultrasound examination is scheduled, several factors should be taken into account to find the most favorable time slot. If a child is to have several tests or examinations on the same day, it is best to schedule an ultrasound scan before any invasive examination that might be upsetting because a distressed child will be much less likely to cooperate. Also, crying will increase the amount of air in the stomach and bowel, rendering an abdominal ultrasound examination more difficult, if not inconclusive. If a child needs to be fasting for an examination of the upper abdomen, the session should be planned for as early as possible in the morning. Fasting infants should be scheduled right before the next feed.

1.3 Appointment Letter

It is often underestimated how a “benign” procedure such as an ultrasound can be perceived as a stressful event by children and their parents. It may be the child’s first visit to the radiology department, and the environment and the procedure may be unknown, which can be very intimidating. In addition, the parents and/or the child may be anxious about the findings of the examination. At best, the referring clinician will have explained what the ultrasound scan is about, including both the procedure and the possible outcome. However, supplementing this explanation with a clear information leaflet, provided with the appointment letter, which reiterates the ins and outs of the ultrasound scan, is a good practice. In our institution, we have added a section with tips from the child therapist team on how parents or caregivers can explain the procedure to a child in accordance with the age of the child. Including a contact telephone number in case there are still questions or concerns about the procedure is certainly useful.

The appointment letter should state the date and time of the appointment and the scan, where the patient is due, the type of scan, and which preparation is necessary (e.g., should the child have an empty stomach or a full bladder?).

1.4 Waiting Area

Examinations on children can be unpredictable and can take up more time than planned. However, keeping the waiting time for all children as short as possible should be a priority. Bored or fractious children are more difficult to examine. Annoyed parents can escalate their children’s anxiety and may direct their frustration at you, again rendering the ultrasound examination more challenging. This should be taken into account when the time slots for ultrasound scans are created. If a delay arises unexpectedly, take time to inform the parents and give them a reasonable and understandable explanation.

The waiting area should be a safe, friendly, and distracting area where children of any age and their parents can wait a short while before the examination is due (► Fig. 1.1). In our institution, we have intentionally opted for a closed area so that parents can focus on the administrative dealings while the child can play in a safe environment where he or she is unable to run off out of sight.

The administration desk has a lower part allowing children to see the person behind it, helping them to feel in control and included (► Fig. 1.2).

There is a television showing short cartoons (► Fig. 1.3), as well as books and magazines, a table with paper and crayons (► Fig. 1.4), and lots of washable toys. Other types of distracting items can be offered. At the Royal Belfast Hospital for Sick Children, a collage has been made with medical supplies (► Fig. 1.5). This has proved to be very popular with the children, who try to spot things the nurses and doctors have been using.



Fig. 1.1 Example of a waiting area that appeals to children. It is a closed area so that children cannot run off.



Fig. 1.2 A low administration desk allows children to participate and feel included.



Fig. 1.3 A television set showing short cartoons.



Fig. 1.4 Area where children can read, draw, or play.



Fig. 1.5 Collage made up of medical supplies. Courtesy of A. Paterson, Royal Belfast Hospital for Sick Children, Belfast, Northern Ireland.

It is also worth having a quiet corner for very ill or injured children and bedridden patients who are not interested in this kind of distraction.

1.5 Examination Room

To facilitate patient flow, it can be convenient to have two changing rooms per examination room. Having a baby changing area in the changing room will allow parents to dress and undress their infant, thus improving the patient flow (► Fig. 1.6). A toilet within the changing room allows for quick post-micturition scans.

The examination room should also be a friendly environment. The room should be large enough to accommodate a child along with the parents, siblings, and strollers, and there should be enough room to exchange the couch for an inpatient in his or her own bed. The room temperature should be warm enough for partially undressed patients; an infrared lamp can add extra warmth for newborns, who lose heat easily when undressed. The decoration should appeal to children of all ages (► Fig. 1.7, ► Fig. 1.8, ► Fig. 1.9, ► Fig. 1.10).



Fig. 1.6 Encouraging parents to dress and undress their infants in the changing room will improve patient flow.



Fig. 1.7 The lights on the wall representing the positions of the moon are appreciated by all children, regardless of their age.



Fig. 1.8 Drawing on the wall in the digital radiography room at the Wilhelmina Children's Hospital, Utrecht, The Netherlands. Courtesy of E. Beek.



Fig. 1.9 Drawing on the wall of the fluoroscopy room at the Wilhelmina Children's Hospital, Utrecht, The Netherlands. Courtesy of E. Beek.

1.6 Examination

For almost all children, the presence of parents will be beneficial. Adolescents should be given the choice of having their parents present during the scan or not.

It is important for the radiologist to build a good rapport with the child and parents before starting the examination. If all people involved feel at ease, the chances of a successful diagnostic examination will be good.

It is usually the technician or radiology assistant who will invite the patient and parents into the room. This person will introduce himself or herself and once again explain the procedure at a level appropriate to the child's understanding. When you walk into the scanning room and introduce yourself properly to both the child and the parents, make sure the child is feeling safe. This can be a sitting position on a parent's lap or, if the child feels confident enough, on the couch. It is not necessary to undress the child completely; pulling up tops and loosening trousers or skirts is usually sufficient.

Taking a few minutes to have a chat with the child and the parents will help to put everyone at ease. You should enter the room with a full knowledge of the patient's history, the results of any previous examinations, and the clinical information delivered for this examination. It is also important in this short introduction to take a short history and ask questions about what is worrying the child and/or the parents and what has been previously discussed with the referring physician. Acknowledging their feelings about the examination and the results is important. Use this time also to tell them that you will need to concentrate during the examination but that you will inform them of the results when the scan is finished, if they wish. Some parents will prefer hearing the results and some explanation from you, whereas others may want to wait for the appointment with the referring physician if there are no urgent matters to be dealt with.

Tell the child again what you will do, as a repeated explanation will help to diminish anxiety. Be honest about what will happen; an ultrasound scan is a painless test unless the region of interest is painful!



Fig. 1.10 Detail of a wall drawing at the Wilhelmina Children's Hospital, Utrecht, The Netherlands. Courtesy of E. Beek.



Fig. 1.11 Allowing children to hold the transducer together with you will enhance their feeling of being in control and increase their cooperation.



Fig. 1.12 The coupling gel ought to be warm in a pediatric radiology department.



Fig. 1.13 Climbing the couch alone will make children feel in control.

1.7 How to Scan: Tips and Tricks

Sedation is almost never needed for ultrasonography, although if the child is young and too restless for the examination of a small lesion and will be sedated for another procedure, it may be convenient to use that moment to examine the child under these conditions.

For abdominal examinations, an empty stomach is necessary in most cases. Babies can become very restless when hungry, making this examination difficult. If sucking on a pacifier or a parent's finger does not help, a drop of sucrose on the pacifier or finger may do the trick. Some children will feel more secure and in control if they can hold the transducer together with the doctor (► Fig. 1.11).

Warming the gel will prevent a shock effect when the cold gel touches the child's skin. This can be done in a gel warmer or small oven (► Fig. 1.12). Make sure to check the temperature of the gel with your fingers before starting your examination.

An adjustable position in height will allow children to climb on the couch or bed by themselves, which will give them a feeling of being in control (► Fig. 1.13).

A large couch allows flexibility in positioning, and mothers can lie down next to their infants to breast-feed them and comfort them during the examination. A parent can lie on the couch together with the child or sit next to you with the child on his or her lap (► Fig. 1.14 a–c).

Distraction is an excellent way to help a child cope with an unfamiliar situation such as an ultrasound scan, and it will reduce stress and anxiety. It also helps the child from getting bored lying on his or her back for more than 10 minutes. It is good to have an arsenal of distracting toys at hand for the youngest, such as musical toys and books, materials for bubble blowing, and so forth. During scans on inpatients, parents may not be present; make sure you have someone (a radiology assistant or play therapist) to help you hold and entertain the child while you focus on the examination. Older children can be distracted



Fig. 1.14a–c Different scanning positions can be attempted when children are too afraid to lie down on the couch by themselves. Parents can help with immobilizing their children while comforting them.

by a conversation, joke telling, singing, and other similar activities. However, distraction should not be forced upon a child who is very upset or in pain.

1.8 Private Room

If there is enough space in your department, you may want to have a private room as an extension to the ultrasound scanning room. In this room, mothers can continue breast-feeding their babies after the scan in order to free the examination room for another patient. It can be used to discuss more complex or serious results in private when this discussion cannot wait, and a pediatric specialist can be called in to see the patient there immediately.

1.9 Communicating the Results

The results must be reported to the referring physician as soon as possible. Parents might prefer to hear the results from you instead of waiting for the appointment with the referring physician. When the results of the test are normal, it will be easy to reassure the parents and prevent days of worrying before the appointment with the referring physician. If you need to compare the results with those of previous or other examinations,

tell the parents so. If your findings are worrisome and you need to make sure there is no delay in action (surgery, more tests, or referral to a specialist), tell the parents there are things you need to discuss with the referring physician while they wait in the waiting area or in a private room. Together with the referring physician, you can decide what should be said and done, when and by whom.

Adolescents may not ask questions for fear of appearing stupid. Make sure they have understood what you need them to know.

Tips from the Pro

- Schedule ultrasound examinations for children wisely.
- Provide clear information about the ultrasound scan beforehand.
- Make sure your department welcomes children of all ages.
- Time in the waiting room should be pleasant but kept as short as possible.
- Enter the examination room well informed and prepared.
- Take time to build rapport.
- Have distraction tools at hand and/or have someone to help you.
- Be prepared for how you will communicate the results.

Recommended Readings

- Alexander M. Managing patient stress in pediatric radiology. *Radiol Technol* 2012; 83: 549–560
- Goske MJ, Reid JR, Yaloo-Poltorak D, Hewson M. RADPED: an approach to teaching communication skills to radiology residents. *Pediatr Radiol* 2005; 35: 381–386
- Harrison D, Beggs S, Stevens B. Sucrose for procedural pain management in infants. *Pediatrics* 2012; 130: 918–925
- Johnson AJ, Steele J, Russell GB, Moran R, Fredericks KP, Jennings SG. Decreasing pediatric patient anxiety about radiology imaging tests: prospective evaluation of an educational intervention. *J Child Health Care* 2009; 13: 370–382
- Piira T, Sugiura T, Champion GD, Donnelly N, Cole AS. The role of parental presence in the context of children's medical procedures: a systematic review. *Child Care Health Dev* 2005; 31: 233–243
- Safdar N, Shet N, Bulas D, Knight N. Handoffs between radiologists and patients: threat or opportunity? *J Am Coll Radiol* 2011; 8: 853–857

Chapter 2

Physics and Artifacts

2.1	Basic Principles of Ultrasound	10
2.2	Echoscopic Image Construction	13
2.3	Transducers	15
2.4	Resolution	16
2.5	Artifacts in Sonography	17
2.6	Advances in Echoscopic Image Construction	19
2.7	Biological Effects and Safety	20

2 Physics and Artifacts

Rob Peters

Ultrasound imaging is a popular imaging technique in clinical practice. It has been used for over 6 decades. Medical ultrasound is relatively inexpensive, noninvasive, and portable; it has good spatial and temporal resolution; and it is safe. Ultrasound imaging is based on the use of the echo of a sound wave to produce an image of the insonated area. It is derived from techniques like SONAR (sound navigation ranging) and non-destructive material testing.

The first clinical ultrasound image was produced by Karl and Friedrich Dussik in Vienna in 1946. They used a transmission technique, similar to the technique used in X-ray imaging. In 1949, the first pulse echo was described. After that, 2D gray-scale images were produced. In 1956, Ziro Kaneko introduced the Doppler technique. In 1965, Siemens introduced the VIDOSON, the first real-time 2D gray-scale system.

In 1971, the first commercially available array transducer-based systems were introduced simultaneously by Professor Klaas Bom of Erasmus University in Rotterdam, The Netherlands (the Multiscan system) and by Toshiba (the SSD-12). In 1979, Professor Bom in conjunction with Professor Wladimiroff, an obstetrician, introduced the Minivisor, the first portable ultrasound imager.

After these advances, ultrasound scanners were made available by many companies. The techniques evolved into applications like life 3D and elastography, and the developments are still going fast.

2.1 Basic Principles of Ultrasound

2.1.1 Ultrasonic Waves

Ultrasound is defined as sound having a frequency higher than 20 kHz. This is beyond the upper limit of the human audible spectrum. Frequencies used in medical ultrasound typically range from 1 to more than 20 MHz.

Ultrasonic waves are longitudinal compression waves. Longitudinal means that the movement of the particles of the medium is parallel to the direction of the wave movement. This is a contrast to transverse waves, like waves on water. Here, the movement of the particles is perpendicular to the direction of the wave. In longitudinal pressure waves, the movement of the particles leads to regions of compression and expansion corresponding to high- and low-pressure areas, respectively.

2.1.2 Wave Propagation in Homogeneous Media

The degree of compression is related to properties of the propagation medium. These properties are characterized by the acoustic impedance, Z

$$Z = \rho c \quad (\text{kg} \cdot \text{m}^{-2} \cdot \text{s}^{-1}) \quad (2.1)$$

with ρ being the density of the medium [$\text{kg} \cdot \text{m}^{-3}$] and c being the speed of sound in the medium [ms^{-1}]. ▶ **Table 2.1** lists various properties of materials and tissues.

The frequency (f) of the ultrasonic wave is unaffected by the propagation medium. The wavelength (λ), however, is related to the medium by the following equation:

$$\lambda = \frac{c}{f} \quad [\text{m}] \quad (2.2)$$

2.1.3 Wave Propagation in Inhomogeneous Media

Just like visual light, sound breaks and reflects on discontinuities in media (▶ **Fig. 2.1**), according to Snell's law:

$$\frac{\sin \alpha_i}{c_1} = \frac{\sin \alpha_r}{c_1} = \frac{\sin \alpha_t}{c_2} \quad (2.3)$$

Reflection

The reflection coefficient R_p describes the fraction of sound pressure that is reflected on an interface and is given by the following equation:

$$R_p = \frac{P_i}{P_r} = \frac{Z_2 \cdot \cos \alpha_i - Z_1 \cdot \cos \alpha_t}{Z_2 \cdot \cos \alpha_i + Z_1 \cdot \cos \alpha_t} \quad (2.4)$$

with P_i and P_r representing the incident pressure amplitude (height) and the reflected pressure amplitude, respectively.

For a perpendicular incidence ($\alpha = 0^\circ$, $\cos \alpha = 1$), this formula simplifies as follows:

$$R_p = \frac{P_i}{P_r} = \frac{Z_2 - Z_1}{Z_2 + Z_1} \quad (2.5)$$

Intensity is the amount of power (energy per unit of time) per unit area. It is proportional to the square of the pressure amplitude:

$$I \propto P^2 \quad (2.6)$$

In case of a perpendicular incidence, the intensity reflection coefficient thus becomes:

$$R_i = \frac{I_i}{I_r} = \left(\frac{Z_2 - Z_1}{Z_2 + Z_1} \right)^2 \quad (2.7)$$

Table 2.1 Acoustic properties of various materials and tissues

Material/Tissue	ρ [$\text{kg} \cdot \text{m}^{-3}$]	c [ms^{-1}]	Z [$\text{kg} \cdot \text{m}^{-2} \cdot \text{s}^{-1}$] ($\times 10^6$)	
Air		1.2	330	0.0004
Lung		300	600	0.18
Fat		924	1,450	1.34
Water		1,000	1,480	1.45
Kidney		1,041	1,565	1.63
Blood		1,058	1,560	1.65
Liver		1,061	1,555	1.65
Muscle		1,068	1,600	1.71
Skull bone		7,500	4,080	30.6

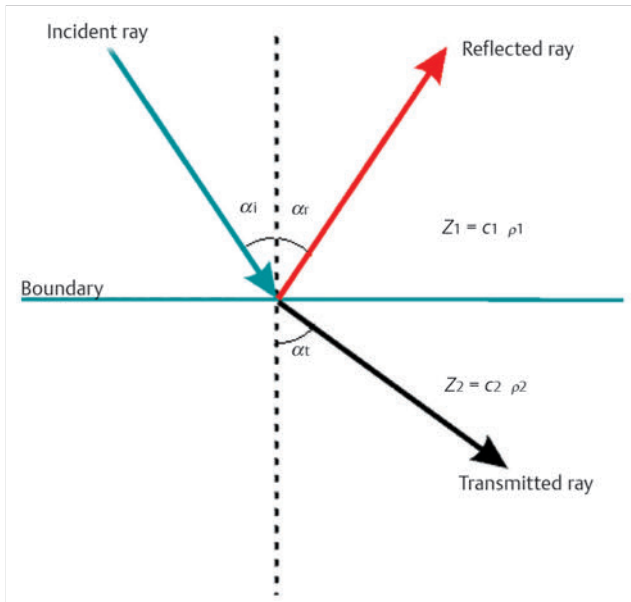


Fig. 2.1 Reflection and refraction on discontinuities in media.

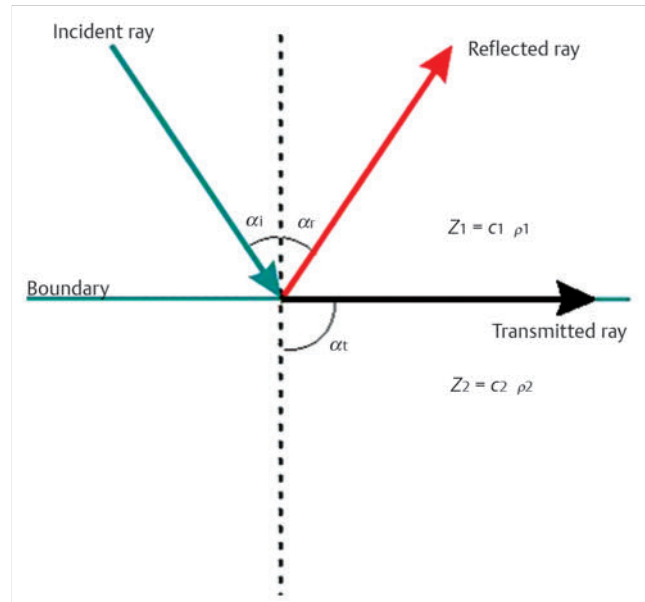


Fig. 2.2 Reflection at critical angle.

with I_i and I_r representing the incident intensity and the reflected intensity, respectively.

R_i ranges between 0 and 1. At 0, no energy is reflected; no echo occurs. This is when $Z_1 = Z_2$. There is no discontinuity in the medium and no boundary to reflect on. At $R_i = 1$, all energy in the incident wave is reflected. No energy is transmitted through the boundary. This occurs when there is a great difference between Z_1 and Z_2 ($Z_1 \ll Z_2$ or $Z_1 \gg Z_2$).

As can be seen in ► **Table 2.1**, the acoustic impedance values of biomaterial are in the order of 1.3 to $1.7 \times 10^6 \text{ kg}\cdot\text{m}^{-2}\cdot\text{s}^{-1}$. This leads to reflection coefficients in the order of 0.02. This means that 2% of the intensity of an incidence wave reflects on the boundary and 98% is transmitted and can produce echoes of adjacent structures. Note that without these small differences in the acoustic impedance of biomaterials, ultrasound imaging would not be possible.

Refraction

As seen in ► **Fig. 2.1**, the transmitted wave is refracted. An interesting phenomenon called total reflection occurs when, given $c_2 > c_1$, the angle of incidence α_i gets beyond a critical value called α_c . This angle is called the critical angle (► **Fig. 2.2**). The refracted wave does not penetrate the second medium. It travels along the interface. Hence $\alpha_t = 90^\circ$.

We get the critical angle α_c by substitution of $\sin \alpha_t = 1$ into Eq. 2.3:

$$\sin \alpha_c = \frac{c_1}{c_2} \quad (2.8)$$

At an interface from fat to muscle, we get $\sin \alpha_c = 1,450/1,600$. This gives a critical angle of 65° .

Scattering

A smooth boundary between two media, with the dimensions of the boundary much larger than the wavelength of the

ultrasonic wave, causes reflection, as has been explained previously. This type of reflection is called specular or smooth reflection. The roughness of an interface leads to so-called non-specular reflection. The reflection of the incident wave is spread over a range of reflection angles. The same occurs on small objects in a tissue, about the size of the wavelength or smaller. Non-specular reflection is also called diffuse reflection or scattering.

In case of scattering, the incident wave is spread over a range of reflection angles. This means that the intensity of backscatter, the part of the scattered signal that can be detected by the ultrasound system, is quite small.

Attenuation

Scattering and energy absorption in the tissue cause an attenuation of the ultrasound beam. This attenuation occurs exponentially with the distance that the ultrasound wave travels through the medium. In ► **Fig. 2.3**, the attenuation of ultrasound in liver tissue is shown for different frequencies in relation to the penetration depth. It must be taken into account that the total distance traveled by the ultrasound pulse and the echo is twice the penetration depth.

The relative loss of acoustic intensity is expressed in the attenuation coefficient μ [dB/(MHz·cm)].

A decibel is not a unit, but it indicates a ratio—in this case, the ratio between the intensity of the incident wave and the transmitted wave. The relative intensity in decibels is defined as follows:

$$\text{Relative intensity} = 10 \log_{10} \left(\frac{I_2}{I_1} \right) \quad (2.9)$$

An intensity ratio of 10^6 equals 60 dB. A ratio of 2 equals 3 dB, whereas a ratio of 0.5 equals -3 dB. The logarithmic relation compresses the values of the intensity ratio into a more manageable number range.

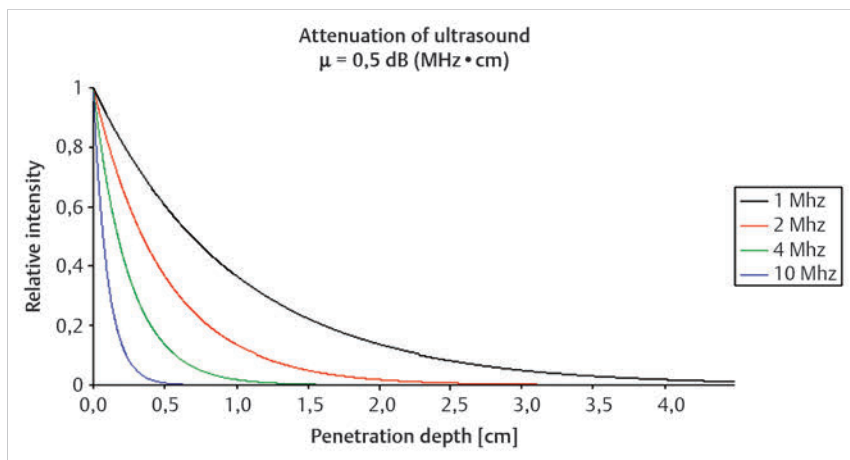


Fig. 2.3 Attenuation of ultrasound in liver tissue.

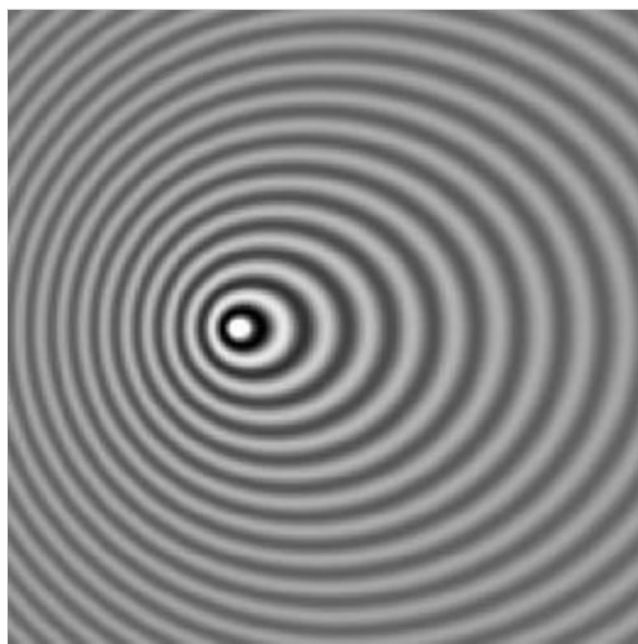


Fig. 2.4 Doppler effect.

2.1.4 Doppler Echo Doppler Effect

The Doppler effect is a change in the frequency of a sound due to the relative motion of the source and the receiver. This change in frequency is called the Doppler shift. In daily practice, we hear the Doppler effect when the siren of an ambulance passes by. When the vehicle is approaching, the pitch is high. As the ambulance passes by, the pitch gets lower.

In ultrasound imaging, we encounter moving objects such as blood cells. The ultrasonic wave reflects on these cells. The cells thus become transmitters of sound (the echo). In ► Fig. 2.4, the sound source moves to the left. The wavelength on the left is smaller than the wavelength on the right. The opposite happens to the frequency. Perpendicular to the direction of movement (up and down), no change in wavelength occurs. Therefore, there is no change in frequency in these directions.

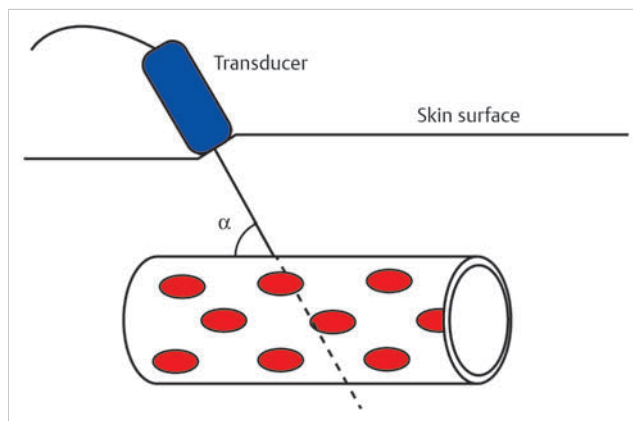


Fig. 2.5 Angle of insonation.

The change in frequency due to the Doppler effect, also called the Doppler shift, is given by the following equation:

$$\Delta f = \cos(\alpha) \cdot \frac{2 \cdot f_{\text{send}} \cdot v}{c} \tag{2.10}$$

with f_{send} the ultrasound frequency of the incident wave, v the speed of the reflector (cell), c the speed of sound, and α the angle of insonation, as visualized in ► Fig. 2.5. To calculate v , Eq. 2.10 can be rewritten as follows:

$$v = \frac{\Delta f \cdot c}{2 \cdot f_{\text{send}} \cdot \cos(\alpha)} \tag{2.11}$$

The Doppler shift and thus the velocity profile can be presented in a Doppler spectrogram (► Fig. 2.6).

From typical values of $f_{\text{send}} = 4 \text{ MHz}$, $c = 1,480 \text{ ms}^{-1}$, $v = 0,5 \text{ ms}^{-1}$, and $\alpha = 30^\circ$, we obtain a Doppler shift of 2,350 Hz (Eq. 2.10). This lies in the audible range. Presenting this Doppler shift through a loudspeaker can be of help for the positioning of the probe and can even help in diagnostics. During pregnancy, the blood flow in the umbilical arteries can be monitored by acoustic presentation of the Doppler shift. Pathologies give characteristic changes in Doppler shift patterns, and these can easily be revealed audibly. This simple but very effective ultrasonic device is standard equipment for a midwife.

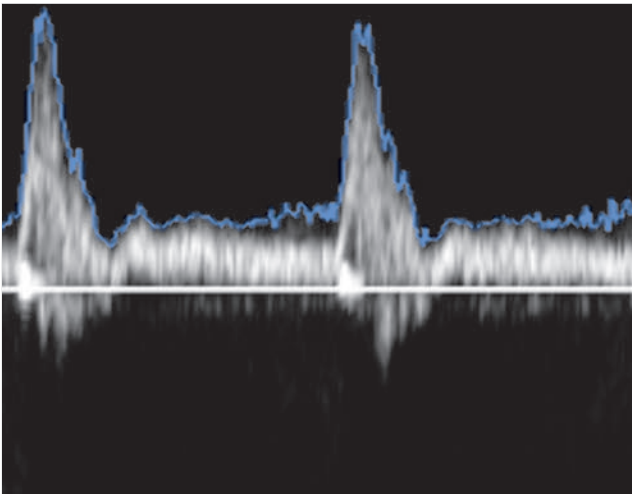


Fig. 2.6 Doppler spectrogram with maximum-velocity envelope (blue).

For a typical ultrasound Doppler measurement, f_{send} is known and c is assumed. The angle of insonation is set on the console of the ultrasound machine. If the angle of insonation is kept small, slight changes in positioning of the ultrasound transducer, introducing small changes in α , have little effect on the determination of v . However, if we increase the angle, a little error in α leads to an increasing error in v . Assuming $\alpha = 30^\circ$ and $v = 0.5 \text{ ms}^{-1}$, a deviation of 3° in the real α (compared with the assumed α) gives rise to an error of up to 3% in the determination of v . The same measurement at $\alpha = 60^\circ$ causes an error of up to 10% in the determination of v . Thus, for Doppler measurements, the angle of insonation should be kept as small as possible.

Continuous Wave Doppler

Continuous wave Doppler transmits and receives ultrasound continuously. The velocity can easily be determined by extraction of the Doppler shift through demodulation of the ultrasound echo. Thus, there is no principal upper limit to the velocities that can be measured.

However, there is no information about the period of time that the sound needed to travel back and forth, and therefore no spatial information is available.

Pulsed Wave Doppler

In pulsed wave Doppler, one sample is taken from every received pulse. This results in a set of samples describing a signal that happens to have the same frequency as the Doppler shift. It is a kind of demodulation through undersampling.

If no ultrasound pulse is emitted before the echo of the prior pulse has been received, spatial information is contained in the time it took for the echo to arrive. However, because of the sampling, the maximum velocity that can be measured is limited. It is related to the pulse repetition frequency according to the sampling theorem of Nyquist–Shannon.

The Nyquist–Shannon theorem states that given a continuous signal with no components higher than half the sample

frequency, the original signal can be perfectly reconstructed from the samples.

2.2 Echoscopic Image Construction

Image construction is basically performed by sequentially emitting a beam of small bursts of ultrasound, called pulses, followed by a period of listening to their echoes. The longer it takes for an echo to arrive, the farther away the boundary that caused this echo. With knowledge of the direction of the incident pulse, information about the spatial position of the boundary is obtained.

The time between repetitive pulses determines the maximal distance from which echoes can be processed. When echoes up to a depth of 15 cm are detected, and assuming a speed of sound of $1,480 \text{ ms}^{-1}$, a minimal pulse repetition period (PRP) of $(2 \times 0.15)/1,480 = 203 \text{ } \mu\text{s}$ is needed. Thus, the maximal pulse repetition frequency (PRF) in this example is 4.9 kHz.

The intensity of the echo tells something about the change in acoustic impedance at the boundary. This then provides information about the anatomical structures that form the boundary.

Echoes originating from similar boundaries can differ in intensity because of attenuation of the signal. The deeper the structure, the more attenuation. This attenuation can be compensated for by using time gain compensation (TGC), usually a set of sliders on the console of the ultrasound machine. TGC enhances echoes from deeper structures.

The origin of received echoes varies from specular reflection to scattering. This leads to a wide dynamic range of intensities of these echoes. In order to be able to present this information in gray notes on the screen, dynamic range compression has to be performed. This is done by so-called logarithmic compression. The logarithmic relation compresses the values of the intensity ratio into a more manageable number range. In image construction, this means that a huge range of echo intensities can be represented within the limited amount of gray notes at our disposal.

2.2.1 Amplitude Mode

In amplitude mode (A-mode), one line of ultrasound pulses is used. Along this scan line, the A-line, echoes are generated by tissue boundaries. The amplitudes of these echoes are plotted against the distance from the probe. The A-mode (► Fig. 2.7) is currently used in ophthalmology applications for precise distance measurements of the eye.

2.2.2 Brightness Mode

In brightness mode (B-mode; ► Fig. 2.8), a 2D image is built out of multiple scan lines. The intensity of the echo is represented in gray levels. The B-mode image is the image type commonly used in ultrasound imaging. It presents a real-time 2D slice through the insonated object and is used for examination of anatomy and function.

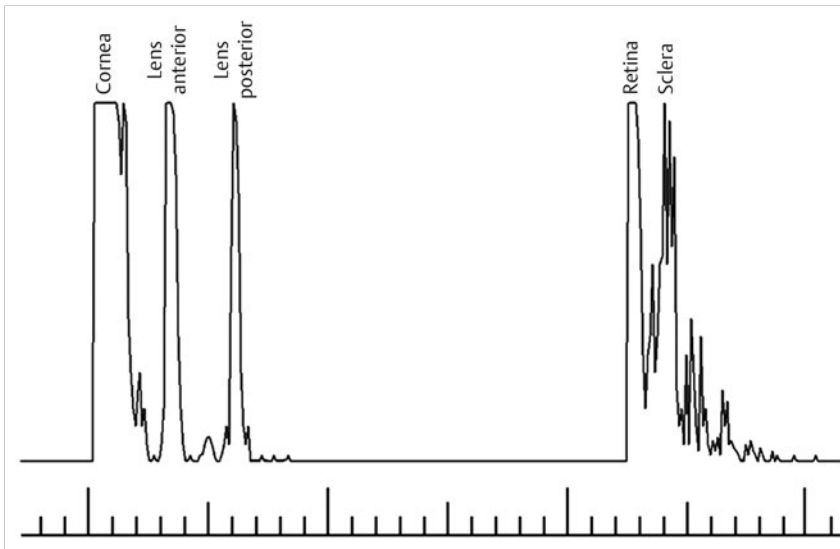


Fig. 2.7 Amplitude mode.

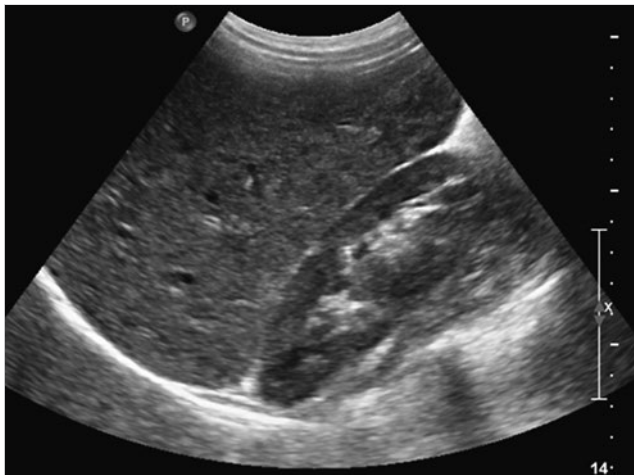


Fig. 2.8 Brightness mode.

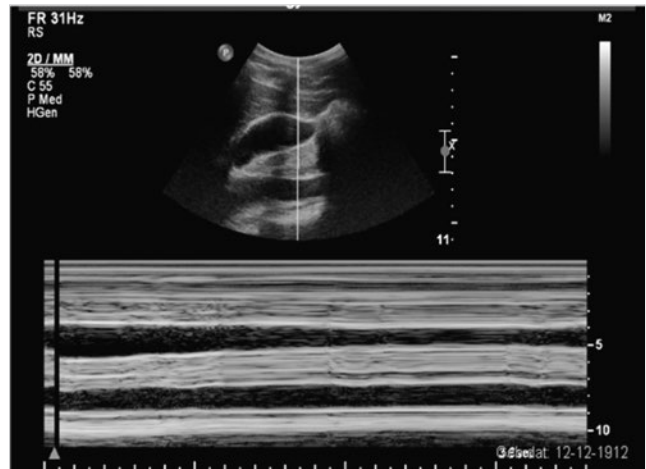


Fig. 2.9 Motion mode of the inferior vena cava.

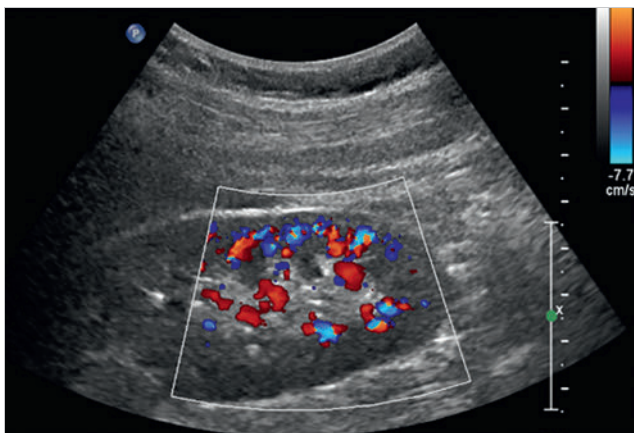


Fig. 2.10 Color Doppler.

2.2.3 Motion Mode

In motion mode (M-mode) ultrasound, one scan line in the B-mode image is selected. This scan line passes through a moving anatomical structure (► Fig. 2.9). The changes in intensity of this one scan line are plotted in relation to time.

M-mode can provide excellent temporal resolution of motion patterns. In cardiology, it is used in the evaluation of heart valves and other heart anatomy.

2.2.4 Color Doppler

In color Doppler, velocity information is merged with the B-mode image. The velocity is represented in color scale. Color Doppler images are widely used (► Fig. 2.10). In vascular examinations, it adds information about blood flow. Also, it can visualize perfusion and detect a stenosis.

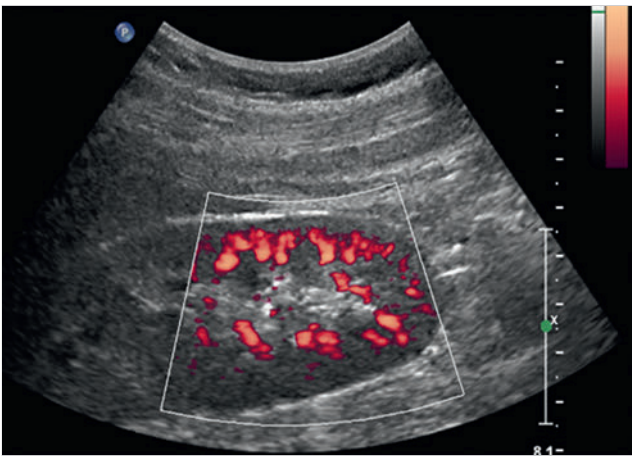


Fig. 2.11 Power Doppler.

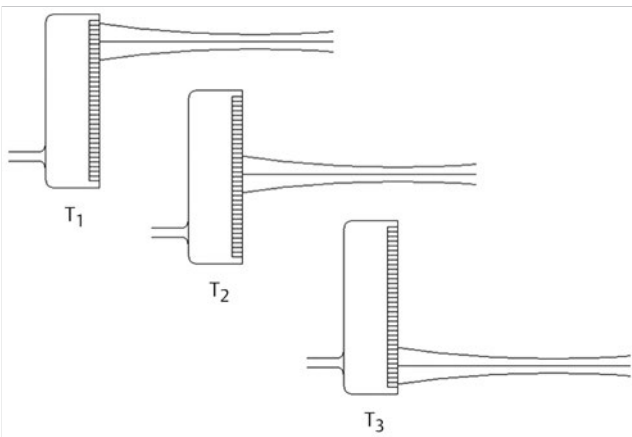


Fig. 2.13 Linear array transducer.

2.2.5 Power Doppler

In duplex mode, velocities can be derived by pulsed wave Doppler. The colors overlying the B-mode image represent velocity values at that particular spot. The underlying calculations are time-consuming. In power Doppler, just the total strength of the Doppler signal (power) is used for color representation. Directional information is ignored. This dramatically improves sensitivity. The shorter computing time can be translated into a higher temporal resolution and/or a higher spatial resolution.

Power Doppler procedures are little affected by the angle of insonation (► Fig. 2.11). It is superior in its visualization of small vasculature and is used to visualize perfusion.

2.3 Transducers

The ultrasonic pulse is generated by exciting the crystal with an electric pulse (► Fig. 2.12). A piezoelectric crystal generates an

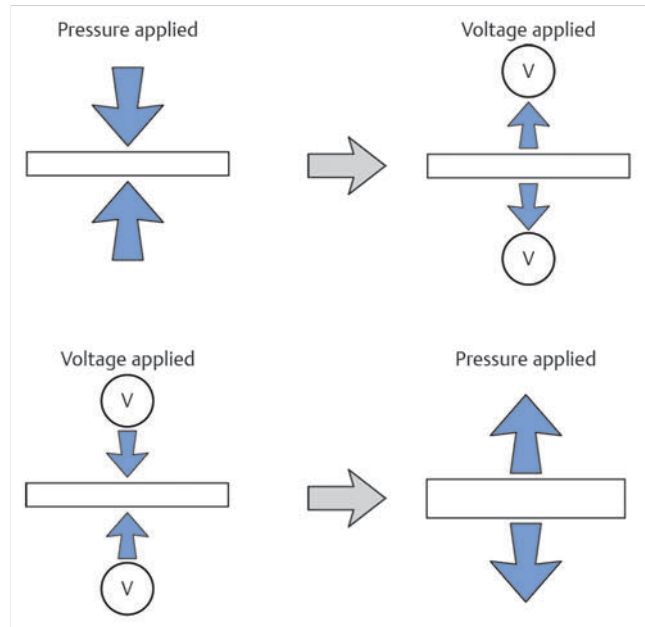


Fig. 2.12 Piezoelectric effect.

electric signal when it is deformed. On the other hand, when an electric signal is applied, the crystal deforms. Thus, the crystal can be used for both generating and receiving signals.

The ultrasonic pulse is generated when echoes exit the crystal. Then, the crystal is switched to receiving mode for incoming echoes. After a certain time, the pulse repetition time, when no echoes are expected to be received anymore, the next pulse is generated, and so on.

2.3.1 Types of Transducers

There are two basic forms of ultrasound transducers or probes: linear/curvilinear array and phased array transducers. They are identified by the way in which the ultrasound beam is produced, and by the field-of-view coverage.

Linear Array

The linear array transducer consists of an array of crystals. Sequentially, a group of adjacent crystals are fired, resulting in an active transducer area. Thus, a single scan line is created. Then, the group of crystals are shifted one or more elements and another scan is performed, generating the next line of echo information. Thus, the ultrasound beam sequentially sweeps across the region of interest. The number of scan lines is approximately equal to the number of crystals (► Fig. 2.13).

Mounting the array of crystals on a flat transducer surface produces a rectangular image. The width of the image and number of scan lines are the same at all tissue levels.

Mounting the array of crystals on a curved transducer surface produces a trapezoidal image. This type of transducer is known as a curved array transducer. The density of the scan lines

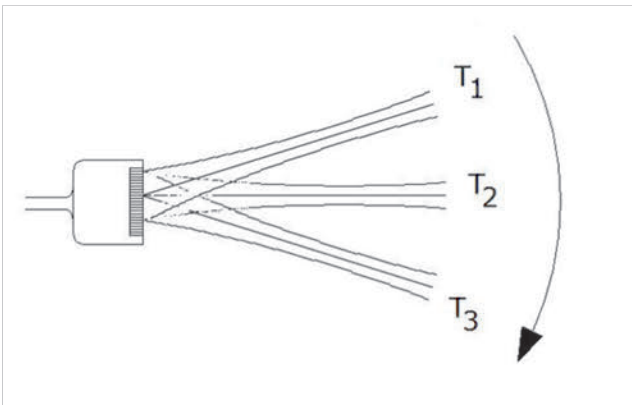


Fig. 2.14 Phased array transducer.

decreases with increasing distance from the transducer. The linear array transducer has the advantage of a wide field of view.

Phased Array

The crystals of a phased array transducer are typically tightly grouped together, forming a small footprint (► Fig. 2.14). In a phased array transducer, unlike in a linear array transducer, all crystals are simultaneously used to generate an ultrasound beam.

The angle of individual scan lines is manipulated by tuning the delay in firing of individual crystals. This is called electronic beam steering (► Fig. 2.15). The same technique is also used in electronic focusing (► Fig. 2.16).

Phased array transducers are used in cases with a small entrance window, such as in neonatal brain imaging, in which the width of the neonatal fontanel can be a limiting factor.

2.4 Resolution

In echoscopic imaging, the spatial resolution is not uniform throughout the image. It depends on the beam-forming process.

2.4.1 Axial Resolution

Axial resolution or longitudinal resolution is the minimum distance that can be discerned between two reflectors located in the direction of the ultrasound beam.

Axial resolution depends on the wavelength of the ultrasound pulse and is better with a short wavelength. So, the higher the frequency, the shorter the wavelength and thus the higher the axial resolution. Focusing has no influence on the axial resolution.

2.4.2 Lateral Resolution

Lateral resolution is the minimum distance that can be discerned between two reflectors located perpendicular to the beam direction. Lateral resolution is related to the width of the ultrasound beam. When the width of the ultrasound beam is narrow, the lateral resolution is high. With focusing, the lateral resolution is highest in the focal zone.

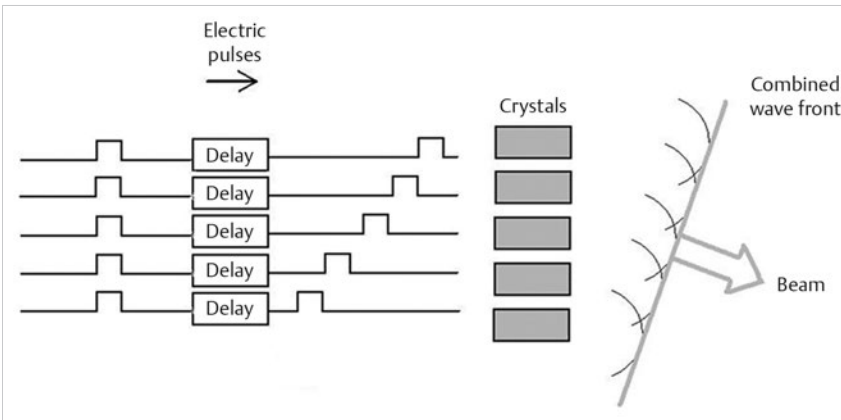


Fig. 2.15 Beam steering.

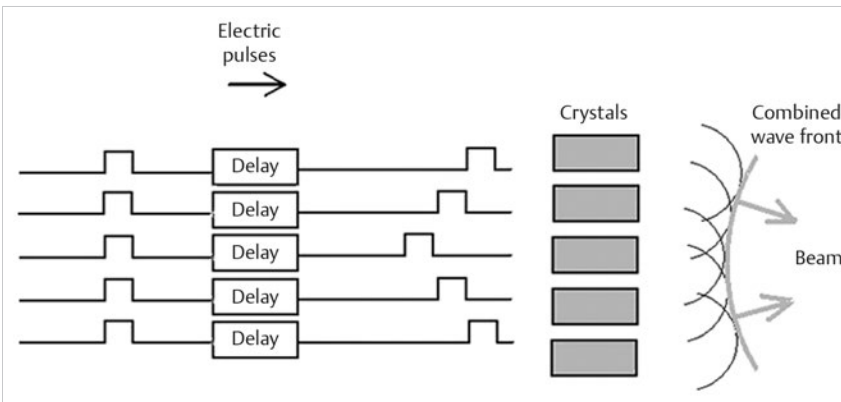


Fig. 2.16 Electronic focusing.

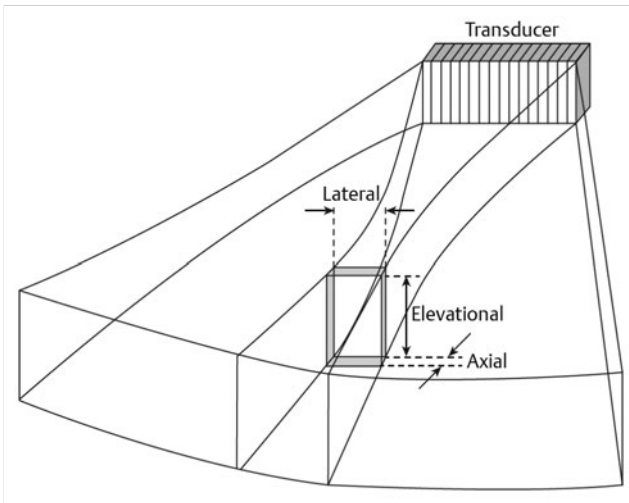


Fig. 2.17 Ultrasound imaging resolutions.

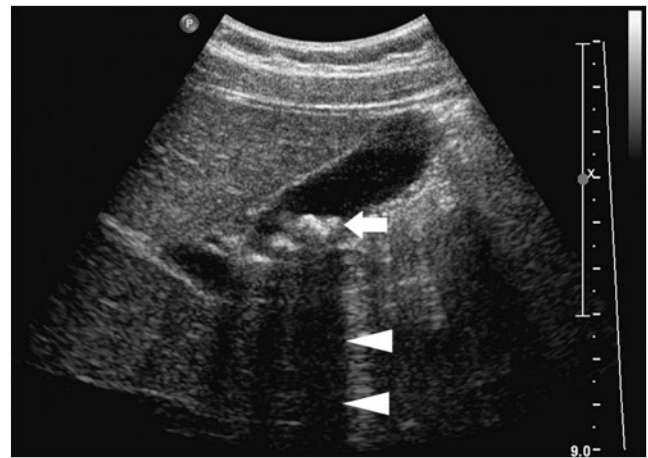


Fig. 2.18 Posterior shadowing (arrowheads) behind gallstones (arrow).

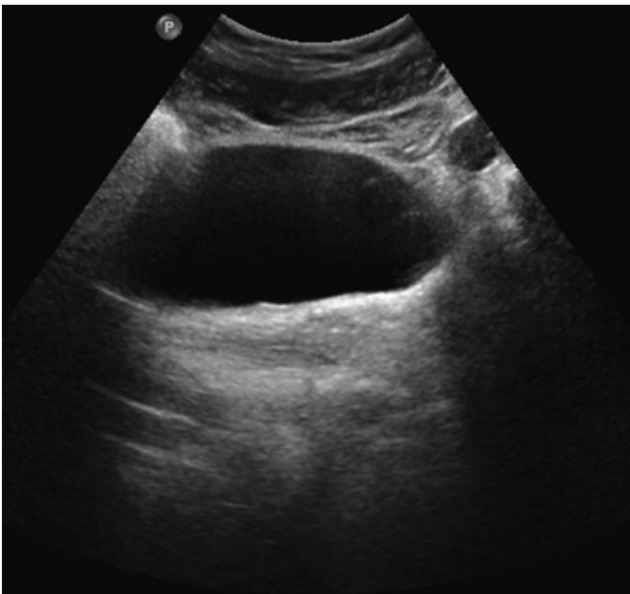


Fig. 2.19 Enhancement artifact behind the urinary bladder.

2.4.3 Elevational Resolution

Elevational resolution or slice thickness is the thickness of the ultrasound beam. It is perpendicular to the image plane. Slice thickness is related to the height of the crystals, in much the same way as lateral resolution is related to the width of the ultrasound beam (► Fig. 2.17). A fixed focal length lens is used to optimize slice thickness at a fixed focal distance.

2.5 Artifacts in Sonography

An artifact is defined as an incorrect display of anatomy. There are many distinguishable types of artifacts in ultrasound imaging. A set of commonly occurring artifacts is discussed here.

2.5.1 Artifacts in 2D Ultrasound

A main reason for these artifacts is the fact that in echoscopic image construction, a set of basic assumptions is made. Some important assumptions are the following:

- The width of the sound bundle is infinite.
- Sound travels in a straight line.
- Sound travels with a constant velocity.
- Pressure wave reflects only once.
- A received reflection is coming from the last emitted pulse.

Failure to comply with these assumptions leads to artifacts such as those discussed in the next sections.

Shadowing

Shadowing (► Fig. 2.18) occurs when no echo is received from a region distal to an object or an interface (tissue dropout) because of high attenuation, reflection, or refraction of the incident beam. It occurs with bone or stones. Shadowing can be distinguished by slightly tilting or rocking the transducer. The hypoechoic area will follow the movement of the transducer.

Enhancement

Enhancement is somewhat related to shadowing (► Fig. 2.19). It occurs distal to objects with low attenuation. Because of the low attenuation, the echoes of distal structures have a relatively high intensity. Enhancement occurs distal to fluid-filled cavities such as the gallbladder or cysts. It can also be seen deep to very homogeneous tissue. Again, slightly tilting or rocking the transducer reveals the artifact.

Reverberation

Reverberation artifact is also known as the comet tail artifact (► Fig. 2.20). It arises when an ultrasound pulse is trapped between two closely spaced, highly reflective boundaries. Part of the pulse is reflected between the boundaries, thus causing it to move back and forth.



Fig. 2.20 Reverberation artifact at the diaphragm (arrow).

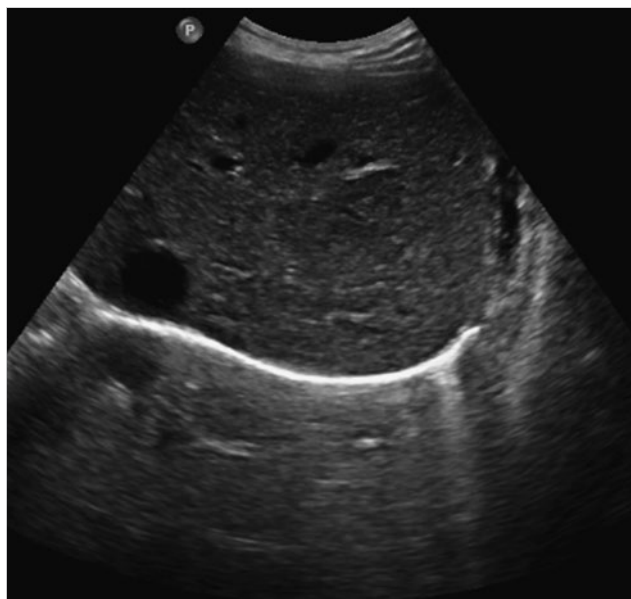


Fig. 2.21 Mirror artifact of the liver above the diaphragm.

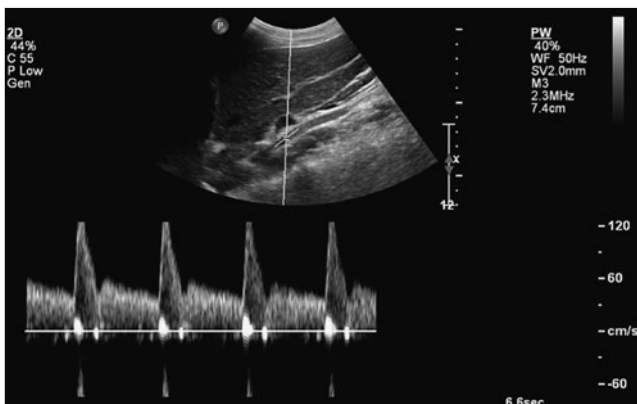


Fig. 2.22 Aliasing in the Doppler spectrogram. The peaks of the spectrum are shown below at -40 cm/s.

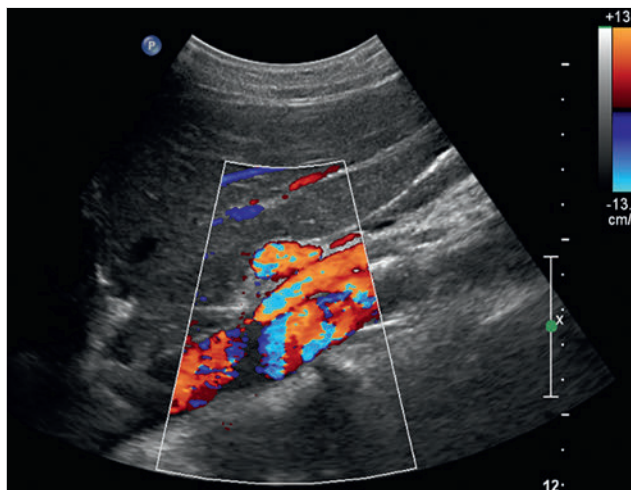


Fig. 2.23 Aliasing in color Doppler imaging of the aorta and superior mesenteric artery. The velocity scale, -13 to $+13$ cm/s, is too low.

On every reflection, a small part of the intensity is transmitted through the boundary and received by the transducer. The delay of these echoes is related to the number of times that the pulse was reflected in its trap. It takes these echoes longer to reach the transducer. Thus, they are displayed as a series of echoes at an increasingly greater depth. Again, slightly tilting or rocking the transducer reveals the artifact.

Mirror Artifacts

When a highly reflective surface is distal to an object, ghosts of the object are displayed distal to the highly reflective surface. The ghost is generated by multiple reflections caused by the same phenomenon as described with the reverberation artifact.

The mirror artifact typically arises at, for instance, the diaphragm, where an erroneous image of the liver is displayed in the thorax (► Fig. 2.21).

2.5.2 Artifacts in Doppler Ultrasound

Aliasing

Aliasing is a common artifact in pulsed wave Doppler. It is due to undersampling. The ultrasound echo is sampled at the PRF. According to the Nyquist–Shannon criterion, the PRF must be larger than twice the maximum Doppler shift. If the Nyquist–Shannon criterion is not followed, frequencies cannot uniquely be distinguished. Higher frequencies fold back into the spectrum (► Fig. 2.22). In the Doppler spectrogram, aliasing appears as in ► Fig. 2.22.

Aliasing in a color Doppler image is shown in ► Fig. 2.23. In color Doppler imaging, aliasing and turbulence look quite similar. However, in turbulence, the gradient from positive to negative velocities always passes a region of zero velocity. This means there is always a black line between red and blue colors. In a case of aliasing, no black line is present.

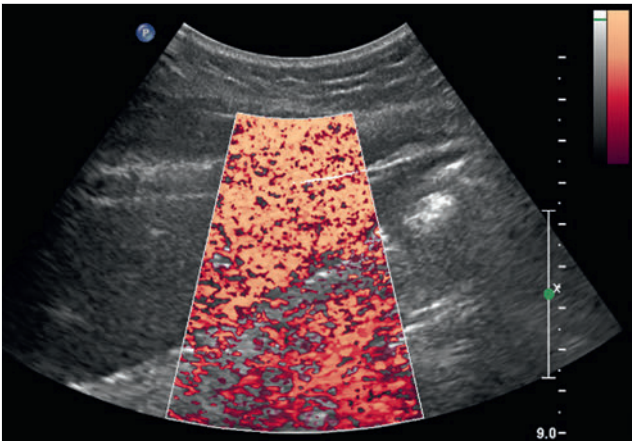


Fig. 2.24 Flash artifact.

Flash Artifact

All movements, including unintended movements, result in a Doppler shift. A characteristic flash artifact occurs in liver echoscopy (► Fig. 2.24). When the patient coughs, the organ moves, and this movement shows in a span of color in the color or power Doppler image.

In Chapter 17, examples and tips are provided in the section 17.2.2, regarding the application of technical factors in ultrasound.

2.6 Advances in Echosopic Image Construction

Progress in technology has made it possible to improve image quality and has opened up new sources of information within the ultrasound echo. As examples of this progress, compound imaging, harmonic imaging, and elastography are discussed.

2.6.1 Compound Imaging

In compound imaging, beam steering is used to produce a set of echoscopic images with a different (lateral) angle for each image. The images are summed into one combined image. The combined image has a better quality because image noise is reduced. Furthermore, curved and irregular structures are better visualized.

2.6.2 Harmonic Imaging

The speed of sound is slightly pressure-dependent. The higher the pressure, the higher the speed of sound. Thus, as it propagates through tissue, the ultrasound wave, consisting of areas of higher and lower acoustic pressure, deforms. In parts at higher acoustical pressure, the ultrasound wave moves faster than in parts at lower acoustic pressure.

In signal theory, this deformation means that higher harmonics are introduced. The higher harmonics, called tissue harmonics, can be used for ultrasound image construction, which results in images with higher resolution. Because the harmonics are generated inside the tissue and not emitted by the transducer, their propagation path through the tissue is relatively

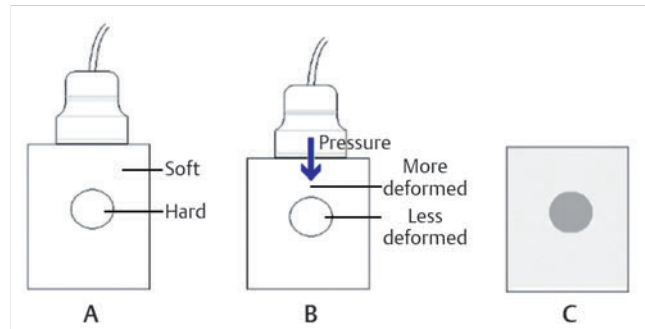


Fig. 2.25 Ultrasound elastography: applying external pressure.

short. Echosopic images produced with higher harmonics have better resolution at greater depths than do images made only with the fundamental frequency.

Harmonic imaging has its roots in contrast ultrasound. In contrast ultrasound, an (air) bubble within the ultrasound bundle is deformed because of the variable acoustic pressure of the pressure pulse. At low pressure variations, deformation is linear. At high pressure variations, deformation becomes a linear. Alinearity introduces harmonics in the echo of the bubble. The intensity of these harmonics is high in contrast to that of tissue harmonics. Imaging only the high-intensity harmonics in contrast ultrasound enables the visualization of perfusion.

2.6.3 Elastography

Ultrasound elastography reveals functional information by monitoring tissue deformation. It is kind of palpation using ultrasound. Information about the stiffness of tissue is obtained.

Axial Deformation

By manipulating the transducer (compression), the underlying tissue can be deformed. Areas of low stiffness are deformed more than areas of high stiffness. The degree of deformation reveals information about the stiffness of the tissue.

In ► Fig. 2.25, an echo transducer is placed on an object containing a soft and a hard area. Repeatedly pushing the transducer causes the object to deform, with relatively more deformation in the soft area. The variations in the echo image during deformation then are represented in an elastographic image of the object. This is a color Doppler-like image that can be color-coded (soft, medium, hard) and merged into a B-mode image. Thus, the relative stiffness of tissues can be determined.

Lateral Deformation

Quantitative measurement of tissue stiffness is possible with so-called shear wave elastography. The ultrasound pulses invoke a shear wave that travels perpendicular to the ultrasound wave, parallel to the surface. The frequency of the shear wave is orders less than the frequency of the ultrasound wave (► Fig. 2.26).

Through imaging with an extremely high frame rate (100–200 times faster than in conventional systems), the shear wave is monitored as it travels through the tissue. Thus, the speed of sound in the tissue can be measured. The stiffness of tissue is

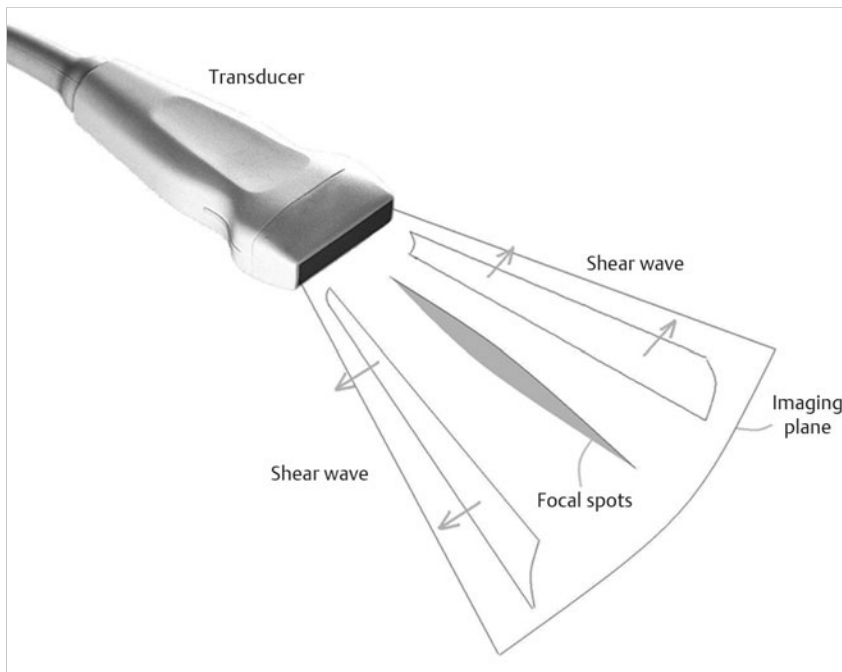


Fig. 2.26 Ultrasound elastography: shear waves.

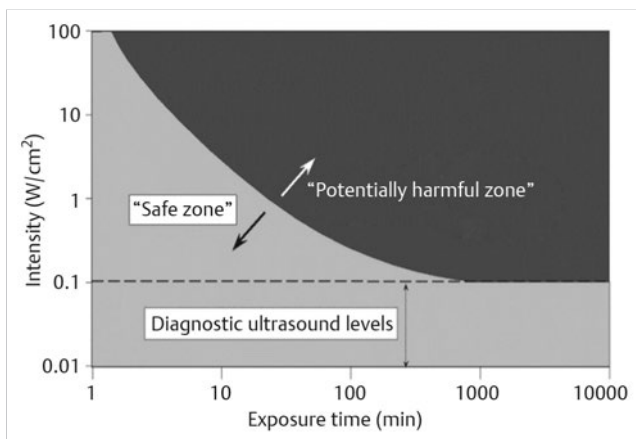


Fig. 2.27 Safe use of ultrasound.

directly related to the speed of sound. Shear wave elastography depicts tissue stiffness in real time. It is a user-independent method.

Shear wave elastography is used in assessing liver fibrosis. Other fields of application are in the evaluation of breast and prostate cancers and in the evaluation of nodules.

2.7 Biological Effects and Safety

Diagnostic ultrasound has an outstanding safety record. Significant harmful bioeffects on either patients or operators of diagnostic ultrasound imaging equipment have never been reported. However, high-intensity ultrasound can cause

biological effects by thermal and mechanical mechanisms. These effects are used in high-intensity, focused ultrasound for the treatment of tumors.

The acoustic energy is absorbed in the tissue and converted into heat and motion. The ability of the tissue to drain thermal energy is characterized by the thermal index (TI). Absorption increases with ultrasound frequency and varies with tissue types. Related to high attenuation, acoustic energy is absorbed much more in bone than in soft tissue. This can cause significant heat deposition at the bone–tissue interface.

Mechanically, ultrasound can evoke particle movement. When high energy is applied over a short period, implosion and cavitation can occur. However, the intensities used in echoscopic imaging are limited by the manufacturers and are far below the threshold at which deleterious cavitation effects, such as implosions, might occur. The mechanical index (MI) is an estimation for the induction of cavitation.

Taking into account intensity and exposure time, ► Fig. 2.27 gives an indication of the safe use of ultrasound. No biological effects have been shown at intensity levels under $100 mW/cm^2$, shown by the dashed line in ► Fig. 2.27. For intensities above $100 mW/cm^2$, exposure to acoustic energy should be applied prudently, with the principle of as low as reasonably achievable (ALARA) in mind.

Food and Drug Administration regulations require TI and MI to be displayed. The TI implemented is that of cranial bone. The display of TI and MI gives the operator feedback about the power dissipation within the patient. Guidelines, such as those composed by the safety group of the British Medical Ultrasound Society, give the operator recommended scan times related to TI and MI settings. If there is a clinical need to exceed these guidelines, the ALARA principle should be followed.

Chapter 3

Neonatal Cranial Ultrasonography

3.1	Ultrasound Anatomy of the Neonatal Brain	22
3.2	Maturation Changes and Distinction between Physiologic and Pathologic Echogenic Areas in the Neonatal Brain	26
3.3	Timing of Examinations	31
3.4	Measurements	36
3.5	Preterm Infants: Pathology	39
3.6	Term Infants	70

3 Neonatal Cranial Ultrasonography

Gerda Meijler,¹ Linda de Vries,¹ and Handan Gülerüz²

The neonatal skull is easily accessible by ultrasound because of its small size and multiple acoustic windows. In sick or preterm neonates, serial brain imaging is indicated to follow brain development and injuries. As minimal handling is recommended, ultrasonography, which can be performed at the bedside, is the preferred tool to visualize the brain of both preterm and high-risk full-term neonates. For a successful neonatal cranial ultrasound (cUS) examination, the experience of the sonographer and the use of a modern, portable ultrasound machine with appropriate transducers and presets are required. In addition, the examiner should take the necessary precautions to prevent hypothermia, infection, and disturbance of the infant.

Besides bedside imaging, there are other major advantages of cUS compared with other imaging modalities, including that it is safe, does not involve ionizing radiation, and is relatively cheap. cUS can reliably diagnose most congenital anomalies, hemorrhagic lesions, calcifications, and many forms of hypoxic-ischemic injury. It is, however, less reliable than magnetic resonance imaging (MRI) for subtle lesions and does not depict myelination.

In this chapter, we will discuss ultrasound anatomy of the neonatal brain, how to differentiate normal findings from (subtle) abnormalities, the optimal timing of ultrasound examinations, and the most frequently occurring brain lesions of the preterm infant.

3.1 Ultrasound Anatomy of the Neonatal Brain

For a routine ultrasound examination of the neonatal brain, the anterior fontanel is used as the acoustic window. Appropriate

presets and well-fitting, appropriate transducers are used. The scan frequency for a standard examination is set at 7.5 to 8 MHz.

The examination includes assessing anatomy, maturation, and the presence of abnormalities by:

- Systematically scanning the whole brain in the coronal (from frontal to occipital) and sagittal (from right to left) planes, recording images in at least six standard coronal and five standard sagittal planes.
- Additionally recording images of (suspected) abnormalities in two planes.

Examples of the standard coronal planes, showing the anatomical structures in both the very preterm and the full term infant's brain, are presented in ▶ Fig. 3.1, ▶ Fig. 3.2, ▶ Fig. 3.3, ▶ Fig. 3.4, ▶ Fig. 3.5, ▶ Fig. 3.6, ▶ Fig. 3.7, ▶ Fig. 3.8, ▶ Fig. 3.9. For details on the anatomical structures seen in these planes, we refer to recent literature.

Scanning through the anterior fontanel generally allows an accurate assessment of most supratentorial structures. The posterior parts of the brain, the infratentorial structures, and the brainstem are further away from the transducer, especially in larger preterm and full-term neonates. These structures can therefore only be reliably assessed if the supplemental acoustic windows (posterior fontanel, mastoid fontanels, and temporal windows) are additionally used. For detailed descriptions on how to use the supplemental windows for cUS and on the anatomical structures visualized while scanning through these windows, we refer to recent literature.

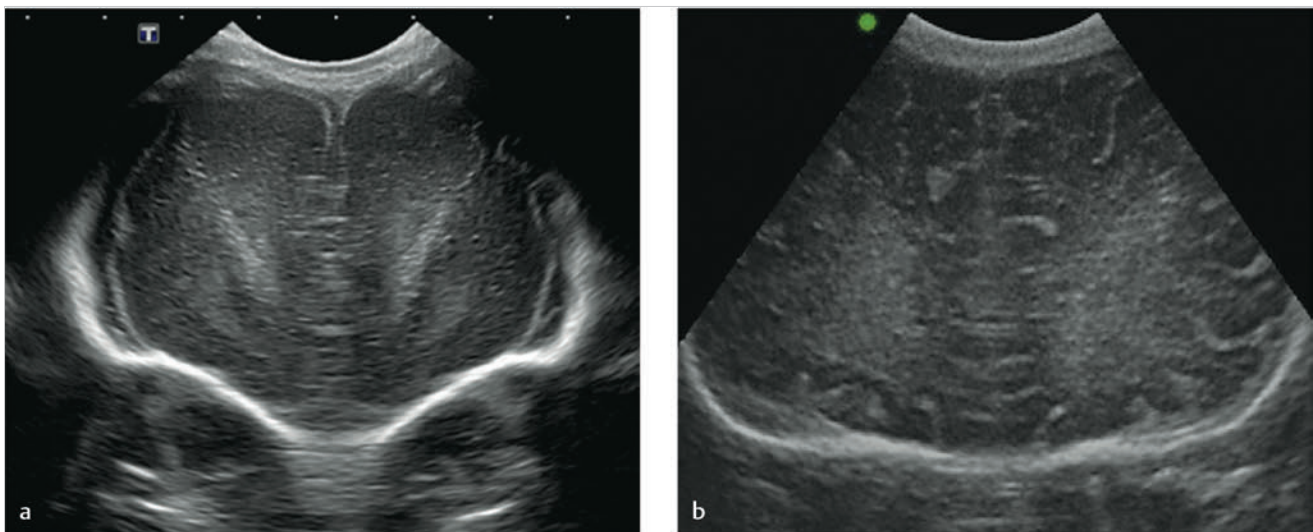


Fig. 3.1a,b First coronal plane through the frontal lobes. a Preterm neonate, GA 26 weeks. b Term neonate.

¹Sections 3.1 to 3.5 are contributed by Dr. Gerda Meijler and Dr. Linda de Vries.

²Section 3.6 is contributed by Dr. Handan Gülerüz.

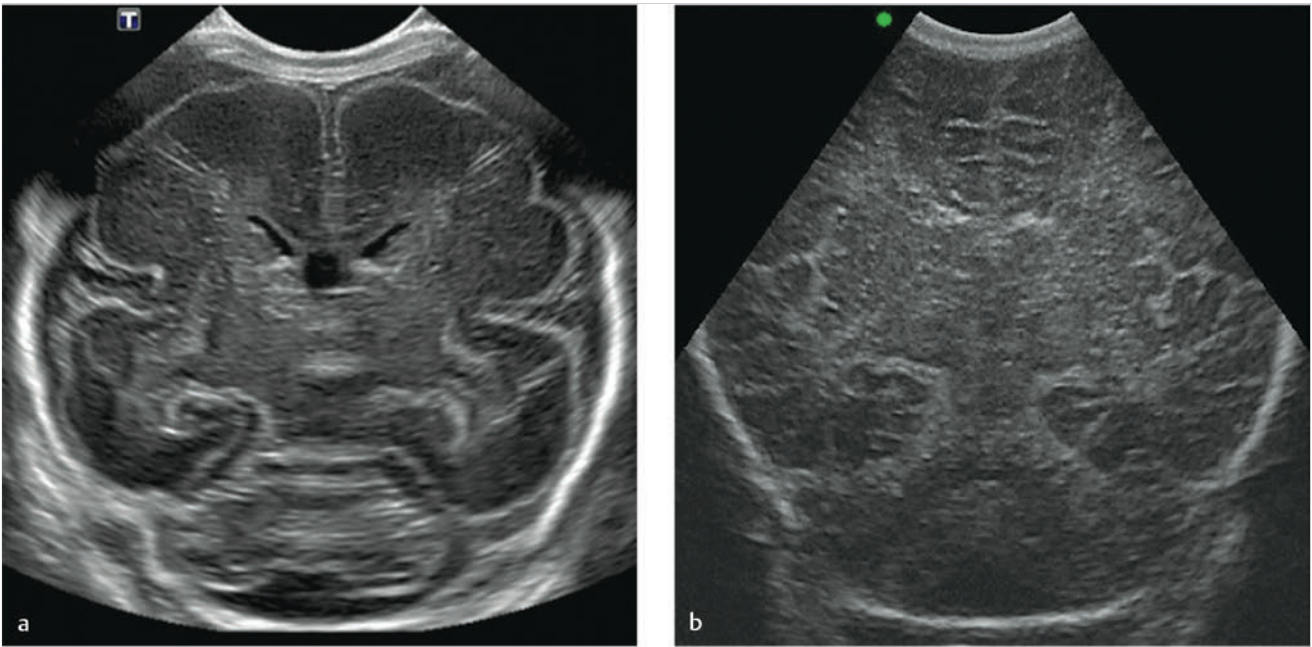


Fig. 3.2a,b Second coronal plane through the frontal horns of the lateral ventricles. a Preterm neonate, GA 26 weeks. b Term neonate.

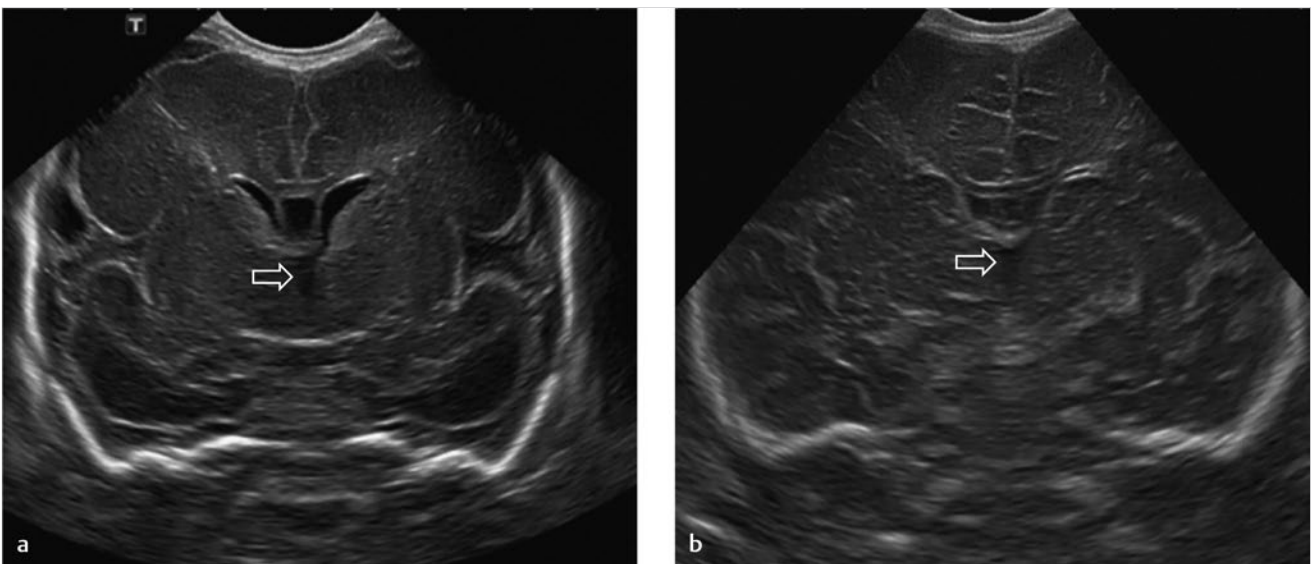


Fig. 3.3a,b Third coronal plane through the third ventricle (arrows). a Preterm neonate, GA 26 weeks. b Term neonate.

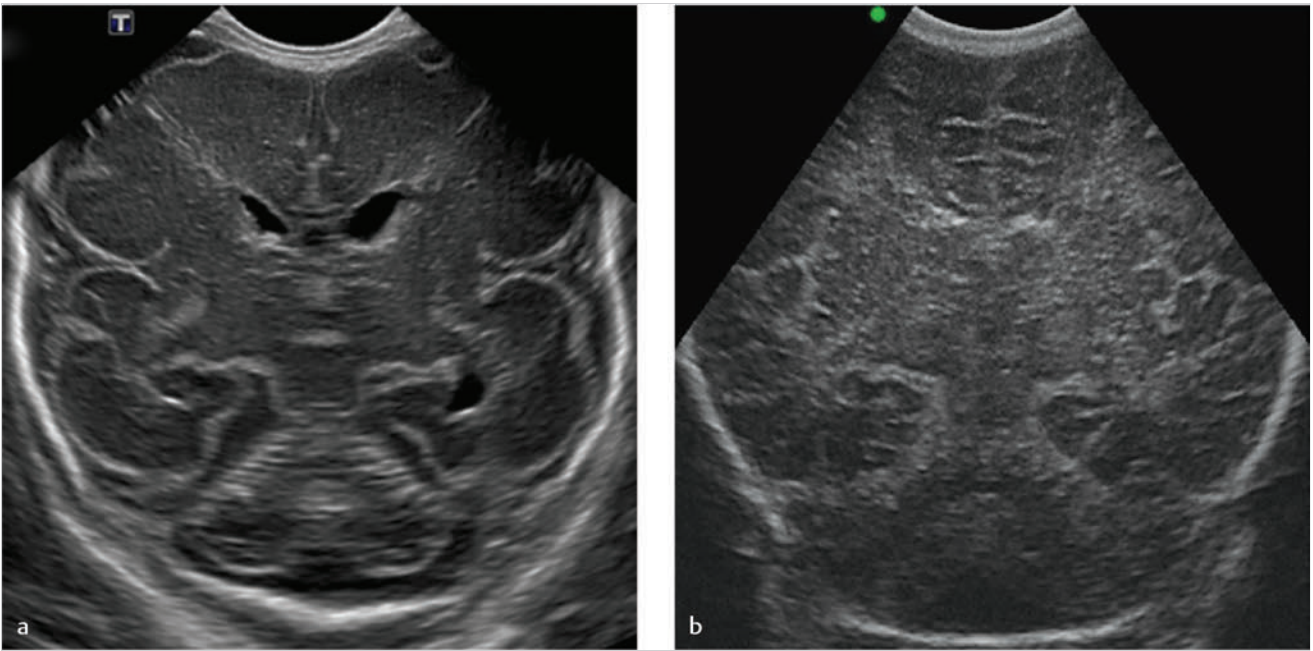


Fig. 3.4a,b Fourth coronal plane through the bodies of the lateral ventricles. a Preterm neonate, GA 26 weeks. b Term neonate.

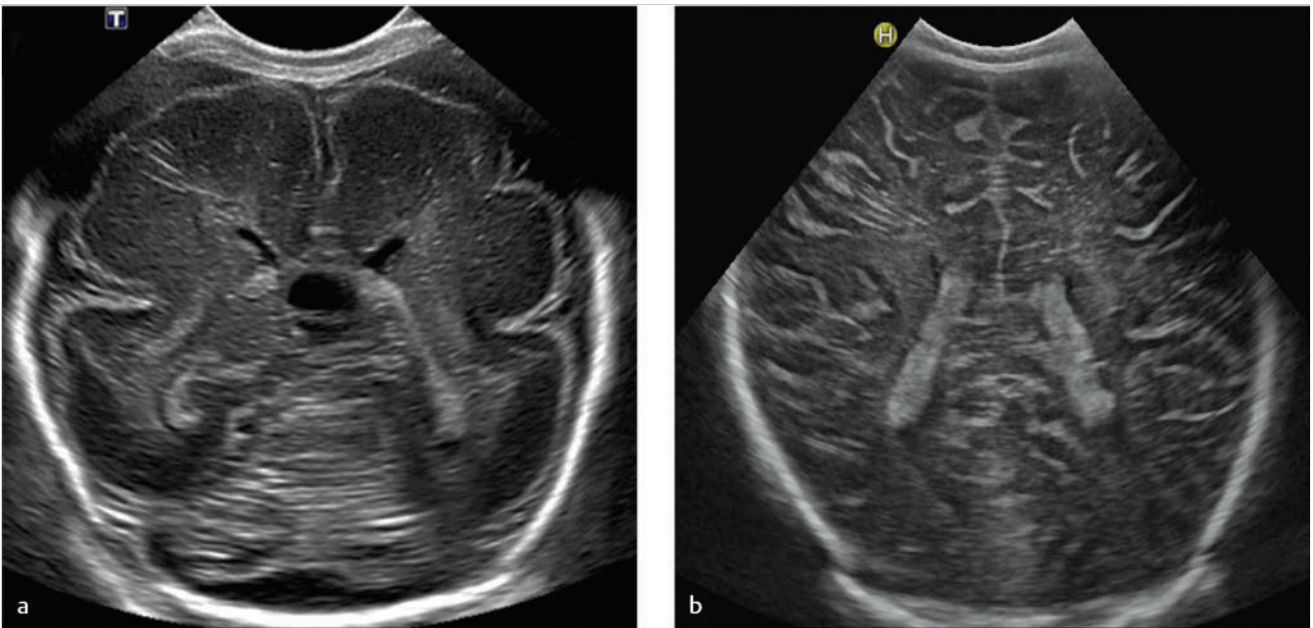


Fig. 3.5a,b Fifth coronal plane through the trigone of the lateral ventricles. a Preterm neonate, GA 26 weeks, scanned at postmenstrual age 29 weeks. b Term neonate.

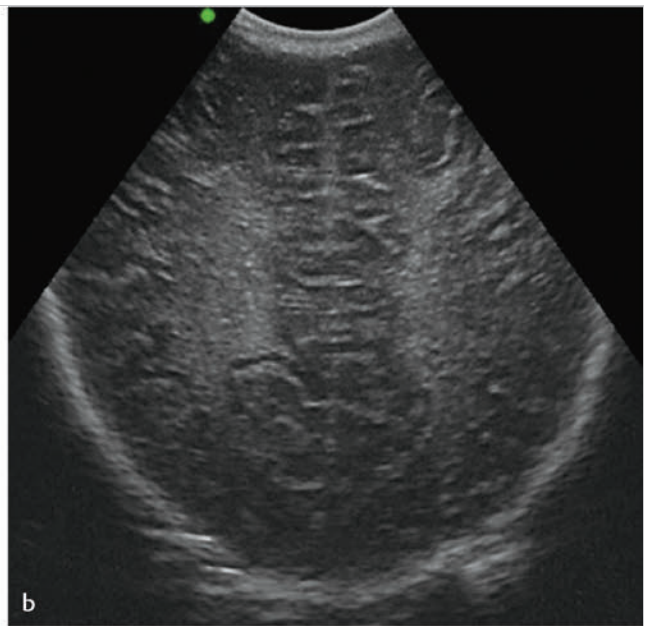
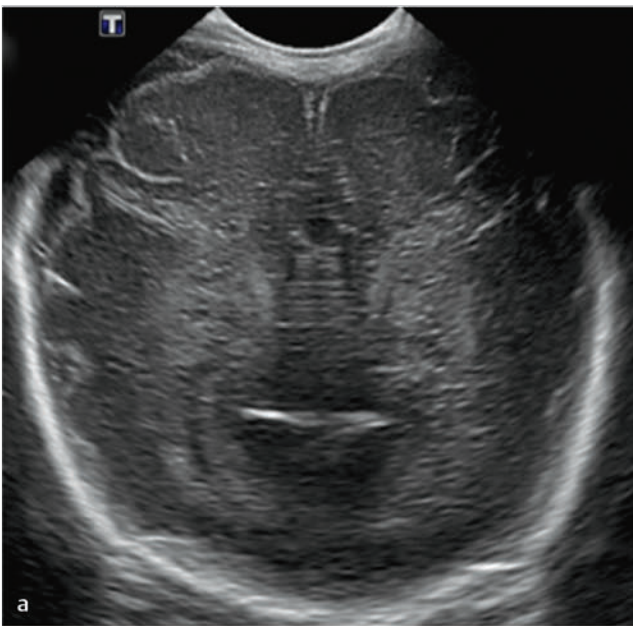


Fig. 3.6a,b Sixth coronal plane through the bodies of the lateral ventricles. a Preterm neonate, GA 26 weeks, scanned at postmenstrual age 29 weeks. b Term neonate.

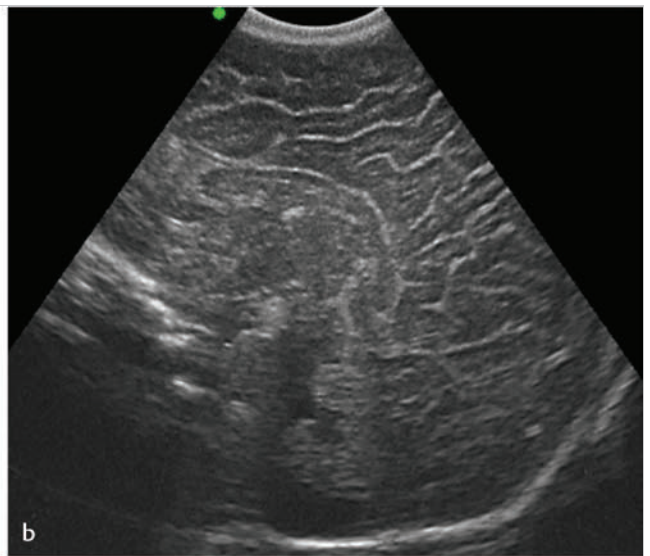


Fig. 3.7a,b Midsagittal plane through corpus callosum, third and fourth ventricles. a Preterm neonate, GA 26 weeks. b Term neonate.

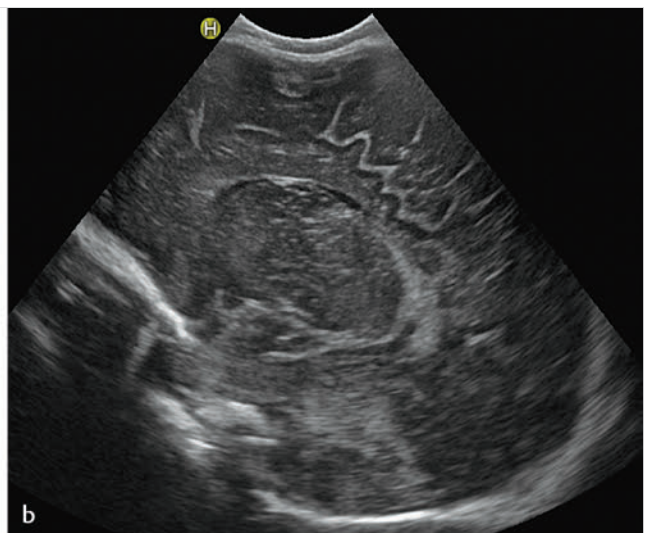
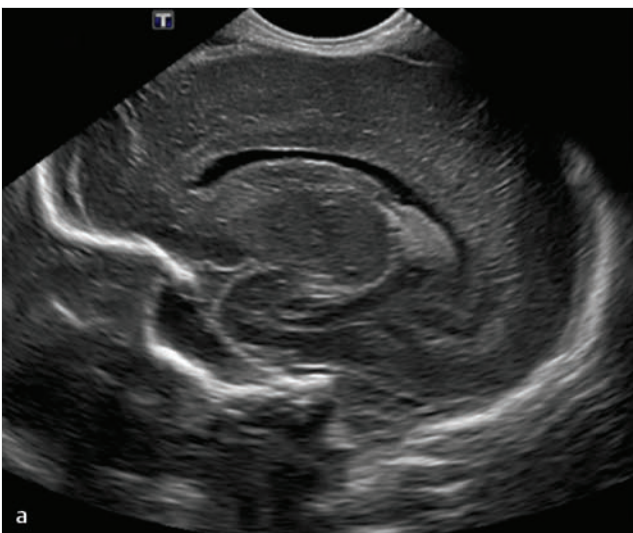


Fig. 3.8a,b Parasagittal plane through lateral ventricle. a Preterm neonate, GA 26 weeks. b Term neonate.

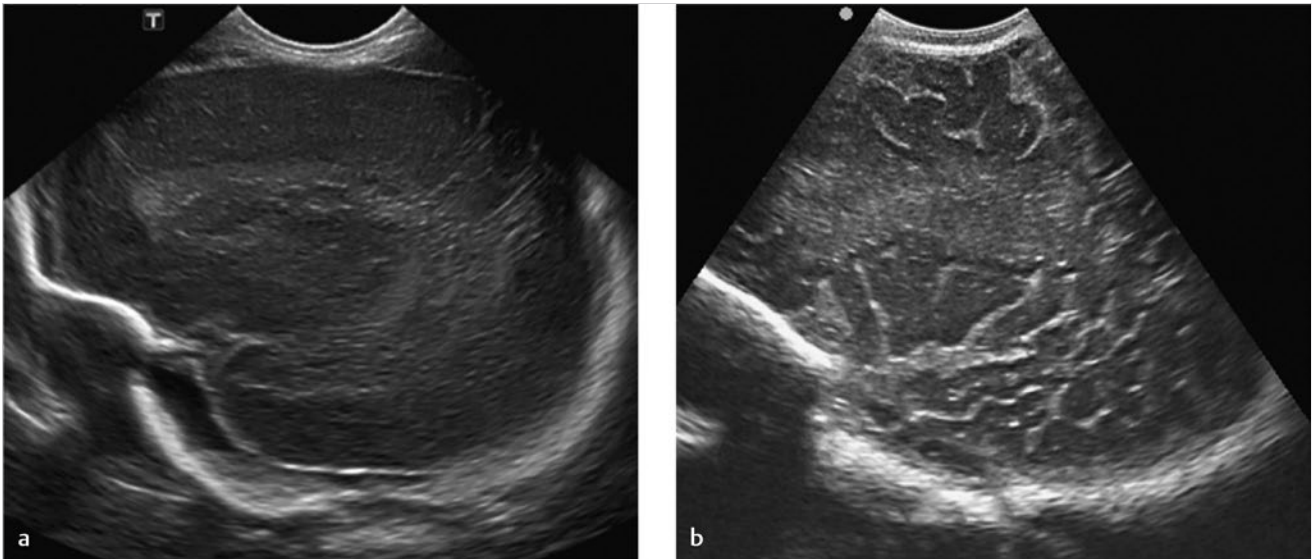


Fig. 3.9a,b Parasagittal plane through insula. a Preterm neonate, GA 30 weeks. b Term neonate.

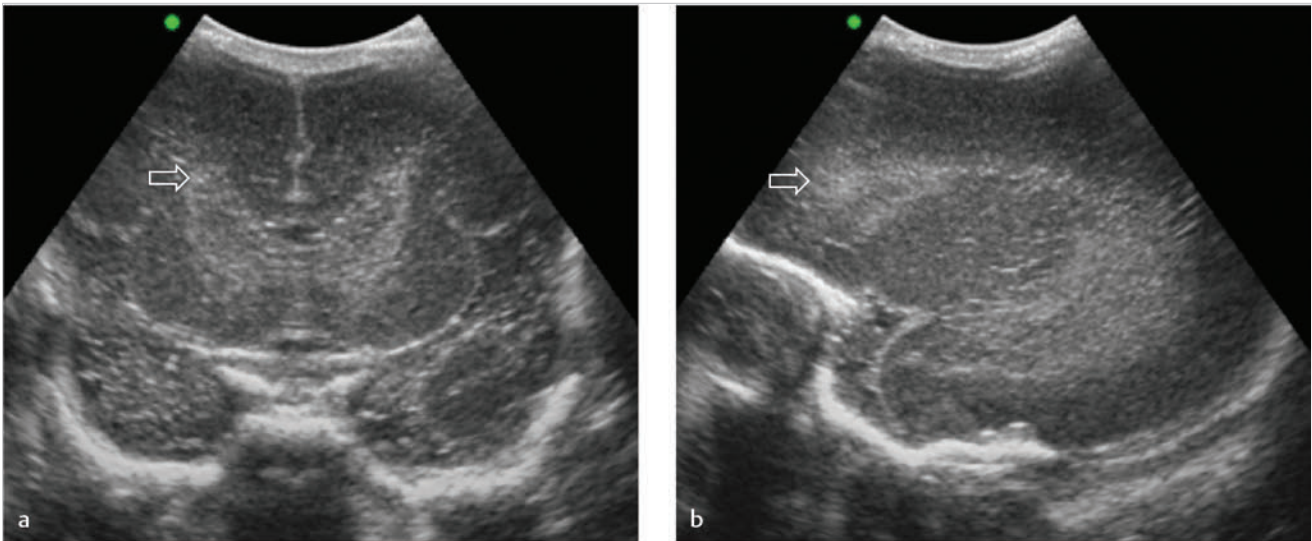


Fig. 3.10a,b Physiologic frontal echodensities (arrow) in preterm neonate, GA 26 weeks. a Coronal plane. b Parasagittal plane.

3.2 Maturation Changes and Distinction between Physiologic and Pathologic Echogenic Areas in the Neonatal Brain

Areas of echogenicity are often seen in the neonatal brain. Some of these are normal and related to maturational changes, whereas others may reflect (serious) injury. The distinction is not always easy.

3.2.1 White Matter

The immature white matter is characterized by its very high water content, almost complete absence of myelin, and, in cases of very preterm birth, additionally by migrating glial cells.

So-called frontal echodensities (subtle, homogeneous, symmetric echogenic zones in the frontal white matter and bilateral echogenic lines around/below the lateral ventricles on anterior coronal cUS scans) are related to this glial cell migration and seen in preterm neonates before term equivalent age (TEA; ▶ Fig. 3.10 and ▶ Fig. 3.11). Frontal echodensities should be



Fig. 3.11 Physiologic echogenic lines (*arrow*) around the frontal horns of the lateral ventricle in very preterm neonate, GA 26 weeks.

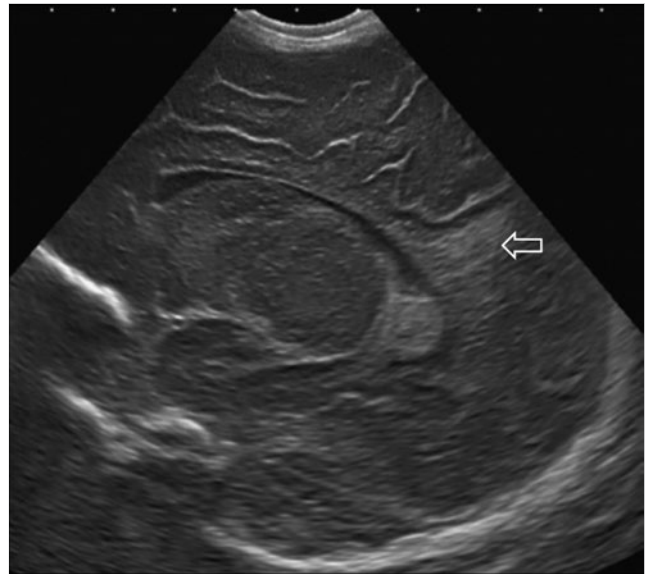


Fig. 3.13 Physiologic “flag-shaped” echogenicity in the parietal white matter (*arrow*). Full-term neonate, GA 38 weeks.

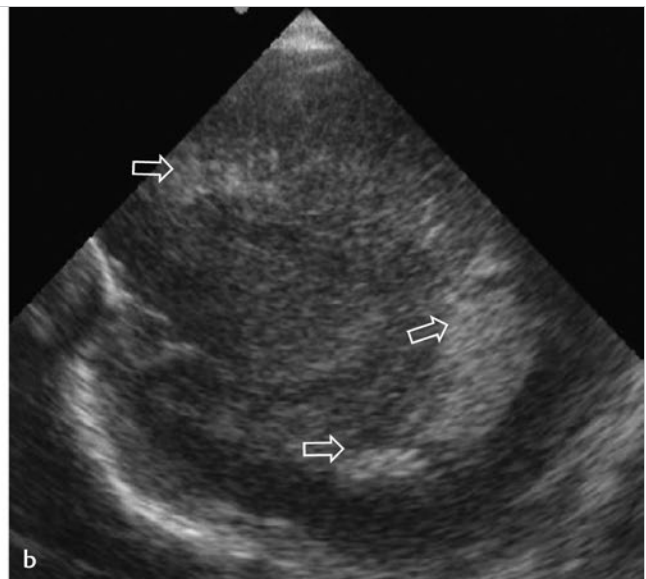
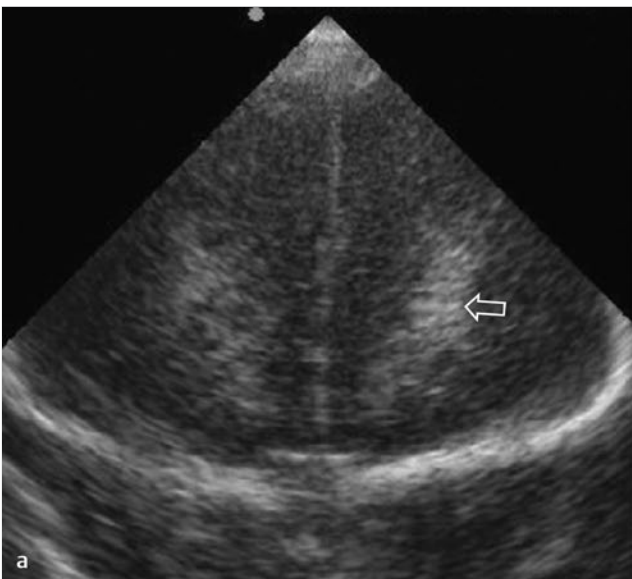


Fig. 3.12a,b Nonphysiologic PVE in a preterm neonate, GA 30 weeks. **a** Coronal plane showing the frontal, inhomogeneous, asymmetric PVE (*arrow*). **b** Right parasagittal plane showing patchy, inhomogeneous PVE in the frontal, parietal, and temporal white matter (*arrows*).

distinguished from nonphysiologic periventricular echodensities (PVE) that may indicate white matter injury. These are more echogenic, less homogeneous, and less symmetric (► **Fig. 3.12**). “Flag-shaped” echogenicities in the parietal white matter on parasagittal scans, subtle echogenic blushes superolaterally from the lateral ventricles, and linear echogenicities running parallel to the trigone of the lateral ventricles on coronal scans are all

considered physiologic phenomena in both preterm and full-term neonates (► **Fig. 3.13**, ► **Fig. 3.14**, ► **Fig. 3.15**). These echogenicities are symmetric and homogeneous, and they tend to fade with age. The latter are thought to represent the optic radiation. These normal echogenicities should be distinguished from pathologic PVE in the parietal white matter, which are likely to represent white matter injury (► **Fig. 3.16**).

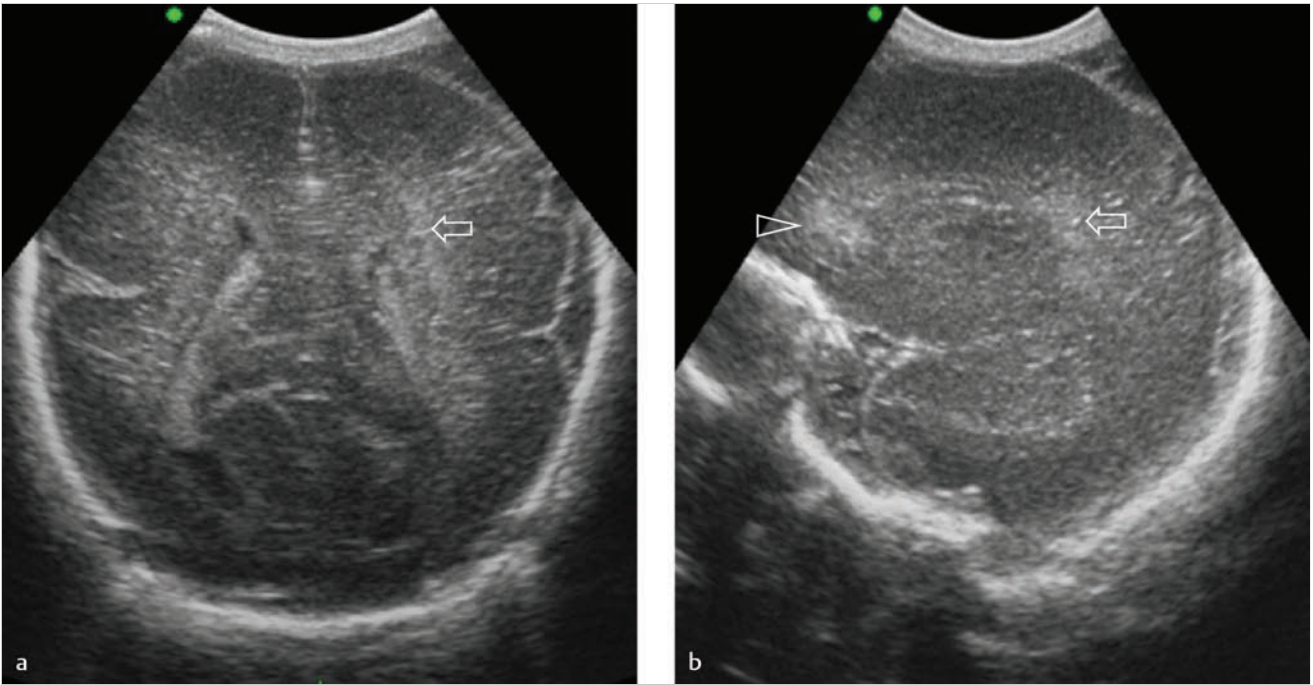


Fig. 3.14a,b Physiologic echogenic blush in the parietal white matter (arrows). Preterm neonate, GA 27 weeks. a Coronal plane. b Parasagittal plane. Also note frontal echodensity (arrowhead), a physiologic finding at this age.

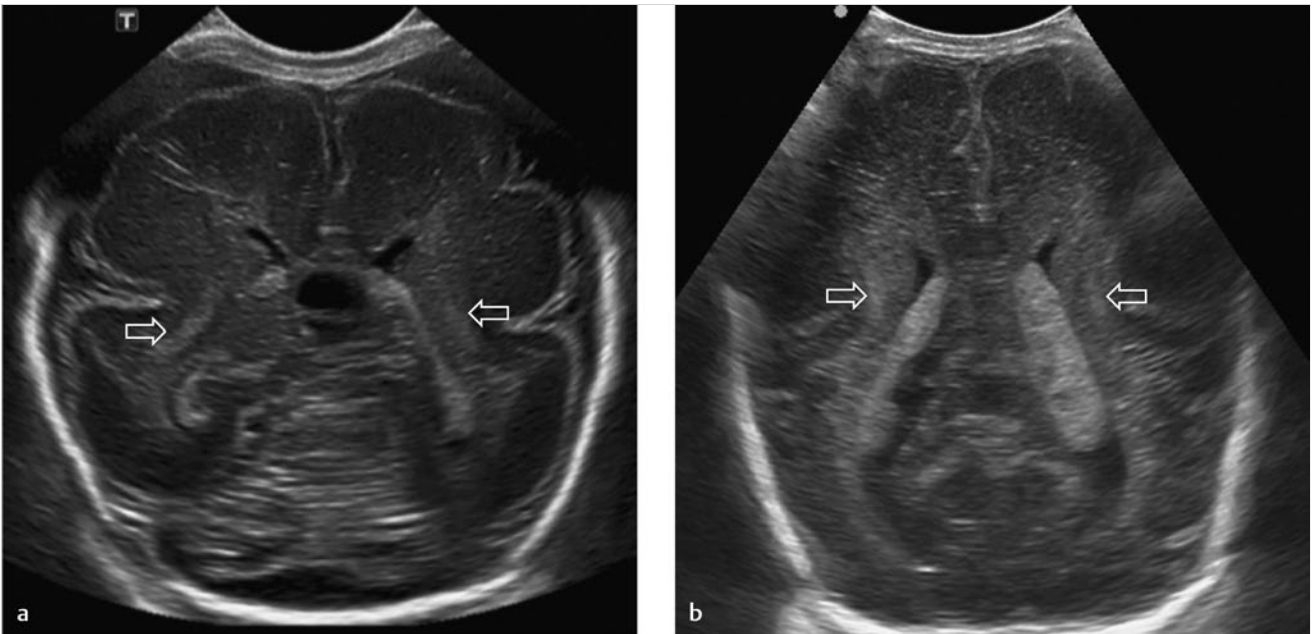


Fig. 3.15a,b Physiologic echodensities parallel to the trigone of the lateral ventricles (arrows) in the coronal plane. a Preterm neonate, GA 26 weeks. b Full-term neonate.

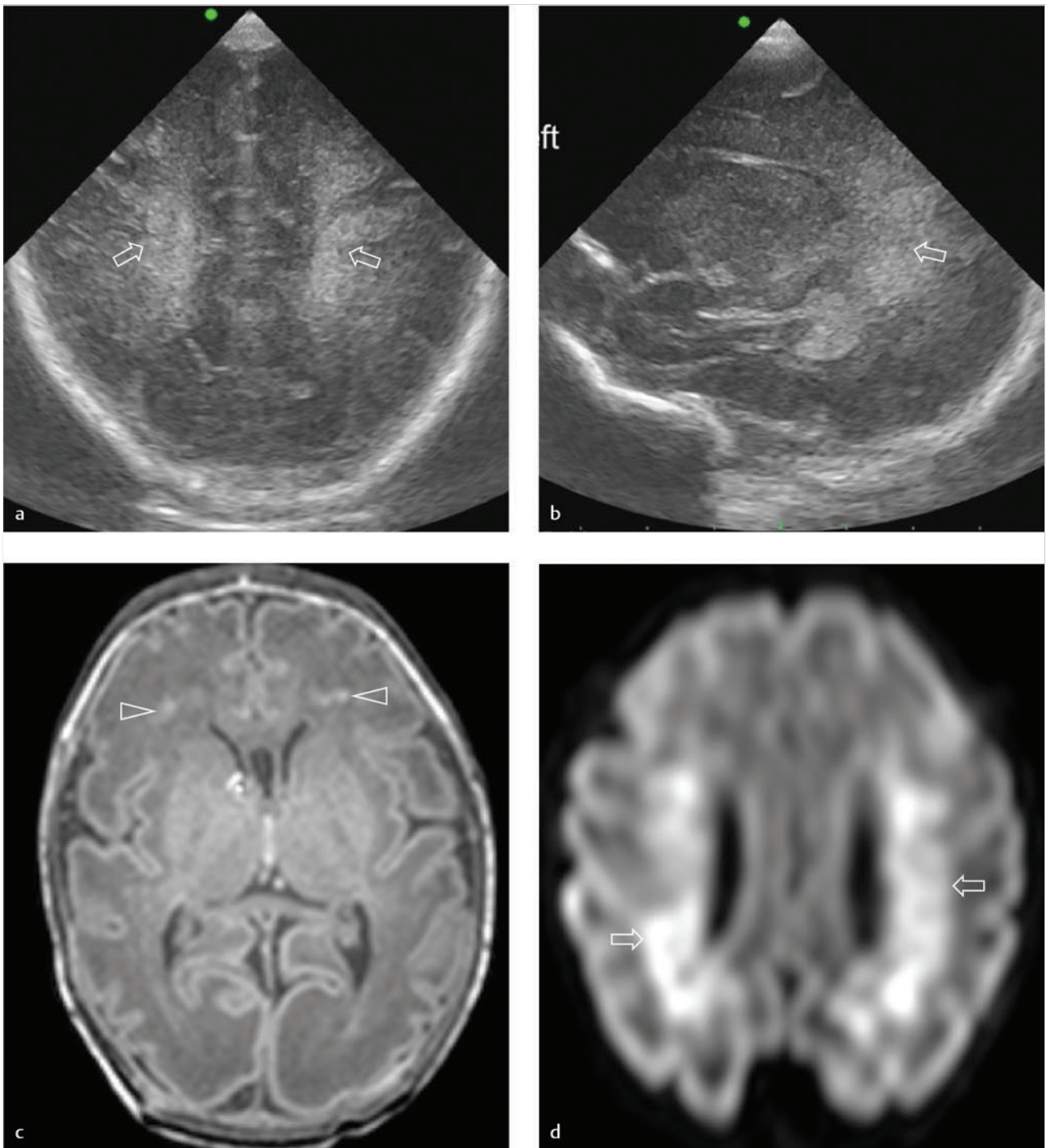


Fig. 3.16a-d Coronal (a) and parasagittal (b) cranial ultrasound images: nonphysiologic echodensities in the parietal white matter (arrows). c T1-weighted transverse MRI showing multiple punctate white matter lesions in the frontal white matter (arrowheads), also showing small right-sided GMH. d Diffusion-weighted MRI showing extensive diffusion restriction throughout the parietal and occipital white matter (arrows). Preterm neonate, GA 34 weeks. MRI performed 3 days after birth. (continued)

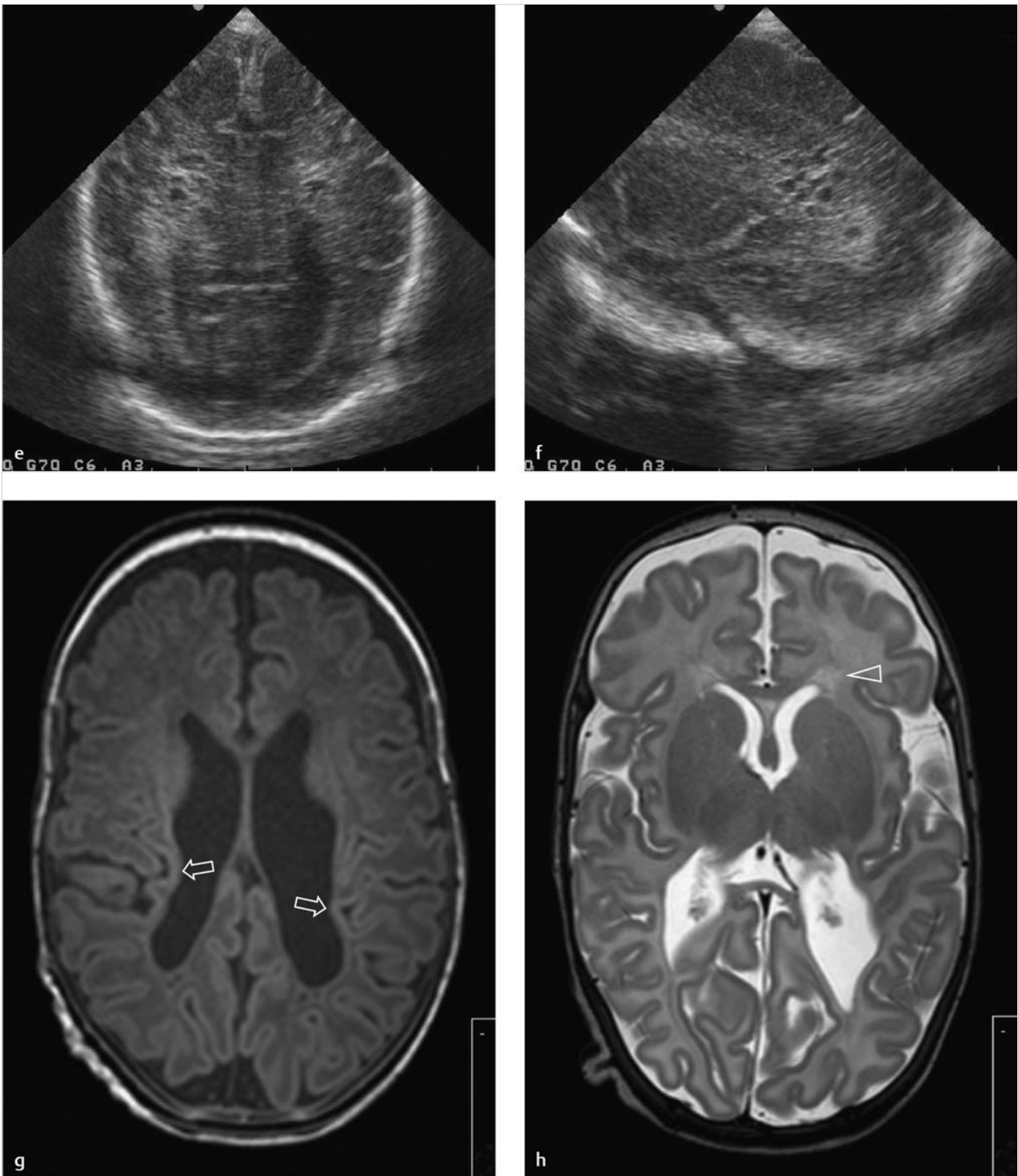


Fig. 3.16e-h (continued) e (coronal) and f (parasagittal) cUS images: 2 weeks later cystic lesions have developed in the parietal white matter, still surrounded by abnormal PVE. g T1-weighted transverse MR image at high ventricular level, showing irregular dilatation of the ventricular system and deep sulci due to severe white matter loss, nearly abutting the ventricular wall, indicating white matter loss (arrows). h T2-weighted transverse MR image at mid-ventricular level, showing the abnormally shaped lateral ventricles and abnormal signal intensity in the frontal white matter (arrow heads). Also note the small right-sided IVH. MRI performed around TEA.

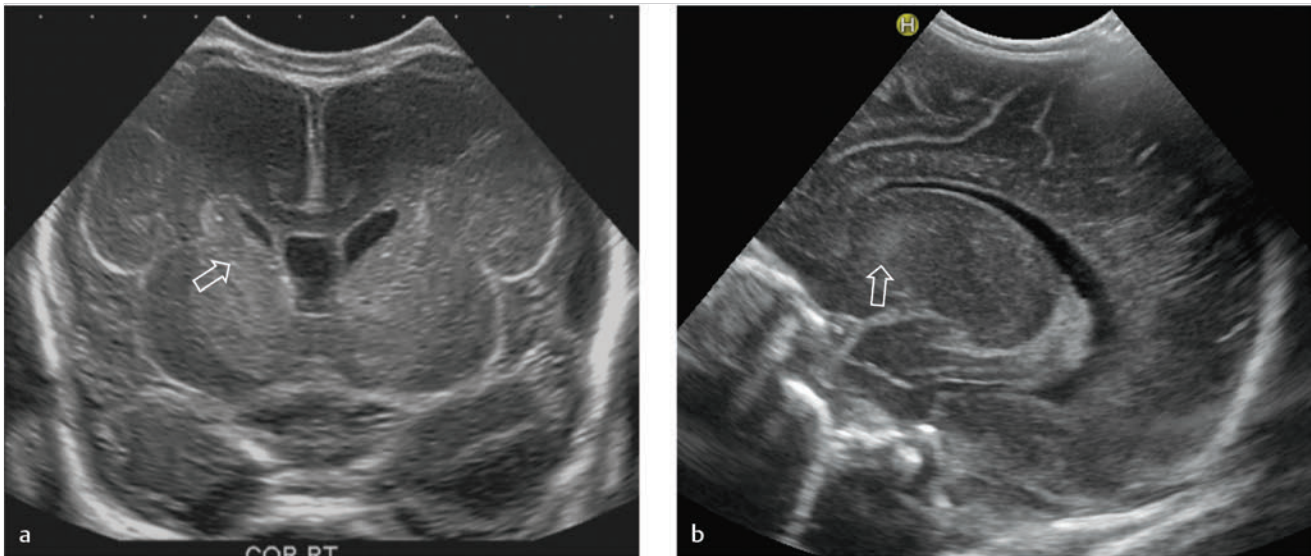


Fig. 3.17a,b Physiologic echogenicity of the basal ganglia (arrows) in preterm neonates. a Coronal plane, preterm neonate, GA 26 weeks. b Parasagittal plane, preterm neonate, GA 29 weeks.

3.2.2 Deep Gray Matter

The immature deep gray matter has a higher cell and tissue density than the immature white matter and therefore appears relatively echogenic compared with the surrounding white matter on ultrasound scans performed in preterm infants before TEA. Especially the caudate nucleus and globus pallidus may look strikingly echogenic. The echogenicity is symmetric and homogeneous and tends to fade with age (► Fig. 3.17).

Echogenicity in the deep gray matter should, however, never be considered a normal phenomenon in (near)-term neonates or in preterm neonates beyond TEA. In this age group, it most likely represents hypoxic-ischemic injury, which is associated with serious consequences for outcome. The echogenicity may also be subtle and symmetric and often includes the thalami. A zone of low echogenicity can sometimes be seen between the basal ganglia and thalami, representing the internal capsule. This may cause a so-called onion peel appearance, whereby the echogenic basal ganglia and thalami are seen as separate echogenic structures and are interspersed by the low echogenicity of the internal capsule (► Fig. 3.18).

Other echodensities in the deep gray matter, resulting from infarction or hemorrhage, are more echogenic, asymmetric, focal, and easily distinguishable from physiologic echodensities (► Fig. 3.19).

Lenticulostriate vasculopathy is characterized by linear or punctate hyperechoic areas in the basal ganglia and thalami. It is probably caused by a benign vasculitis of the lenticulostriate vessels and suggestive of mineralization of the arterial wall. It is seen in healthy preterm neonates, but also in association with various abnormal conditions such as central nervous system infections, metabolic disorders, and chromosomal abnormalities. It can easily be distinguished from the aforementioned physiologic deep gray matter echogenicity in preterm infants as it is linear or punctate and follows a typical vascular pattern (► Fig. 3.20).

Tips from the Pro

In summary, white matter echogenicities are likely to be physiologic if they have the following characteristics:

- The echogenicity does not exceed that of the choroid plexus;
- The echogenicity is homogeneous and symmetric;
- The echogenicity fades with age.

Echogenicity in the deep gray matter is likely physiologic if it is seen in the preterm period, fades with age, and does not persist beyond TEA. It is subtle, homogeneous, and symmetric. The internal capsule should not be visible as a separate entity.

3.3 Timing of Examinations

The optimal timing and frequency of examinations is of great importance. In the preterm infant, cUS performed on the first day of life will first of all diagnose an antenatally or perinatally acquired lesion (see ► Fig. 3.16; ► Fig. 3.21 and ► Fig. 3.22) or congenital anomaly (► Fig. 3.23). Secondly, it enables the detection of (new) lesions within hours or days after the onset. Most of these lesions are clinically silent. Once the diagnosis is made, the evolution of the lesion over time should be assessed. In infants with germinal matrix-intraventricular hemorrhage (GMH-IVH), this enables timely recognition of post-hemorrhagic ventricular dilatation (PHVD), a potentially serious condition that may need intervention. Another serious complication of GMH-IVH is periventricular hemorrhagic infarction (PVHI). This lesion and its evolution can be diagnosed and followed if serial cUS scans are performed on a regular basis. In preterm infants with nonphysiologic PVE, sequential imaging will show whether the echogenicity will resolve without cystic evolution or whether cystic changes occur. Small cystic lesions develop only 3 to 6 weeks after the abnormal echogenicity is

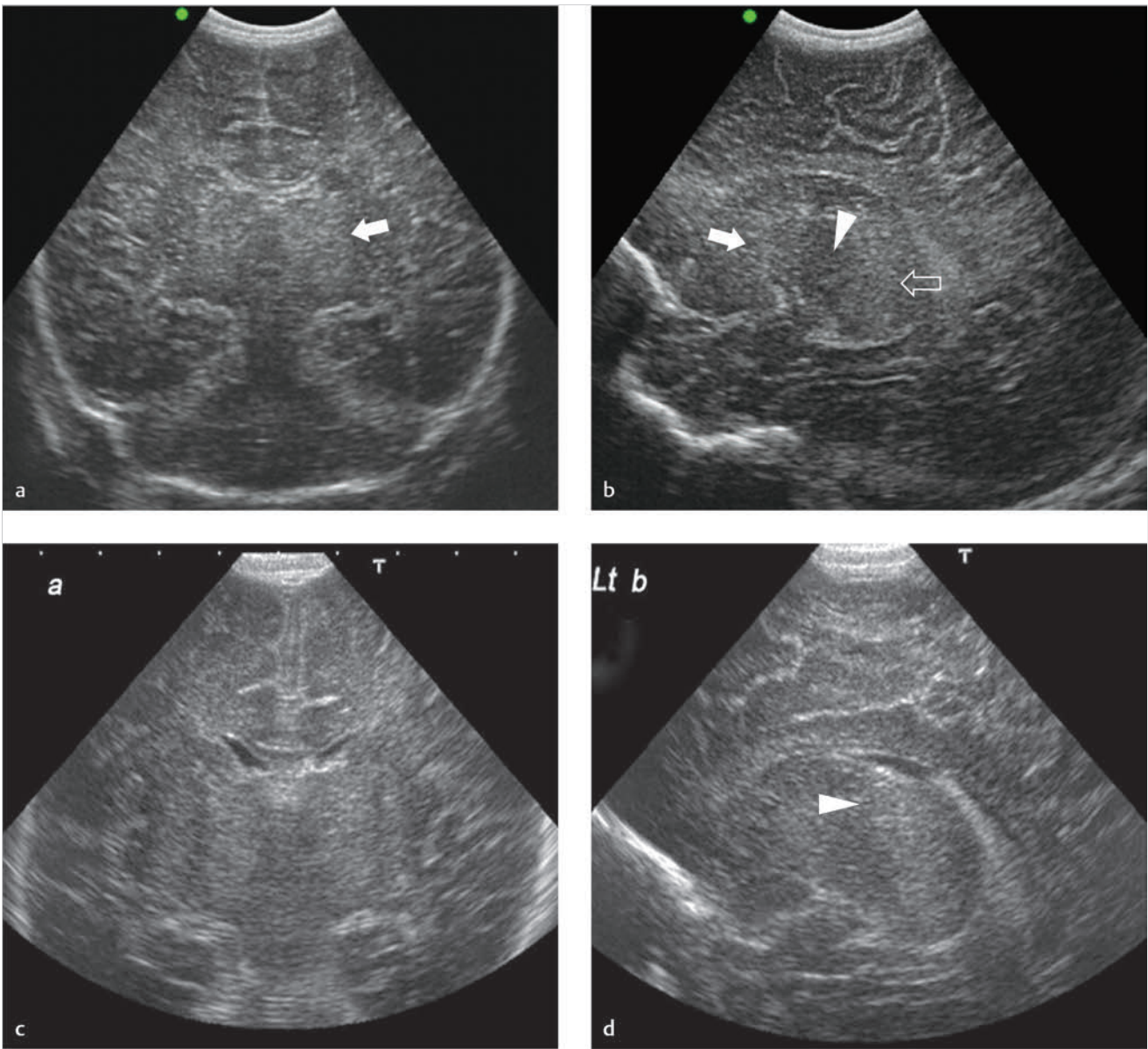


Fig. 3.18a–d Abnormal echogenicity in the basal ganglia (*arrow*) and thalami (*open arrow*) in two full-term neonates with hypoxic-ischemic deep gray matter injury following acute perinatal asphyxia. (a, c) Coronal planes. (b, d) Parasagittal planes, also showing a zone of low echogenicity representing the internal capsule (*arrowheads*).

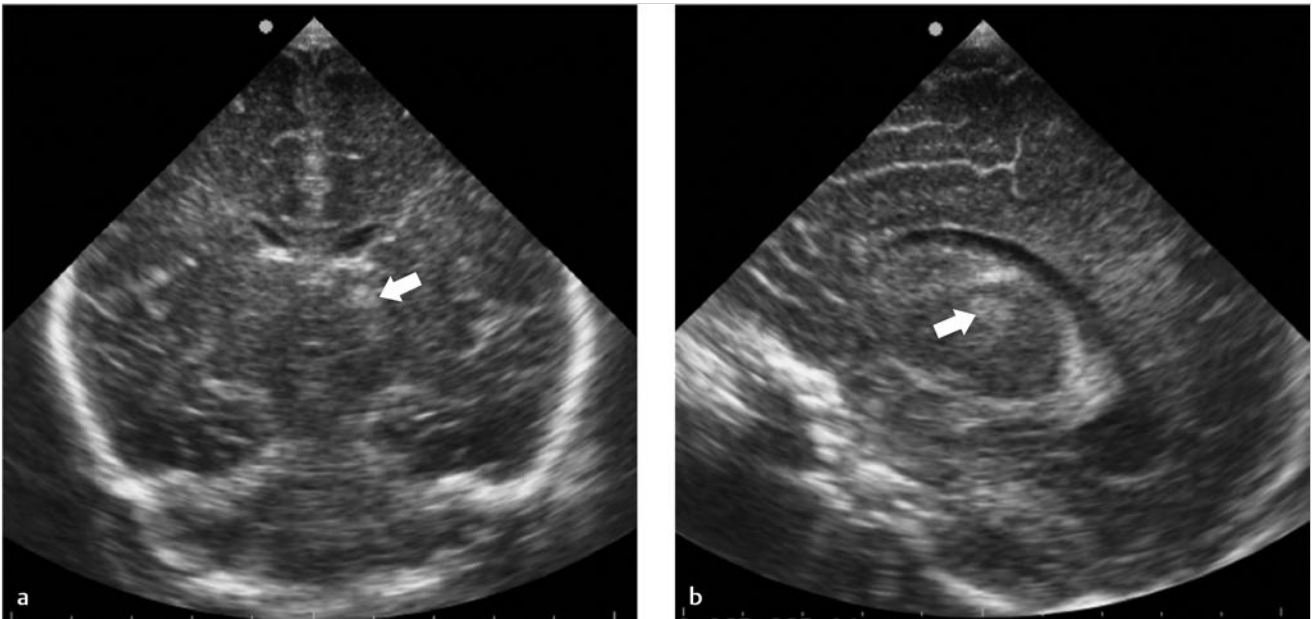


Fig. 3.19a,b Focal echogenic lesion in the left thalamic area (*arrows*) representing infarction. Near-term neonate, GA 36 weeks. a Coronal plane. b Parasagittal plane.

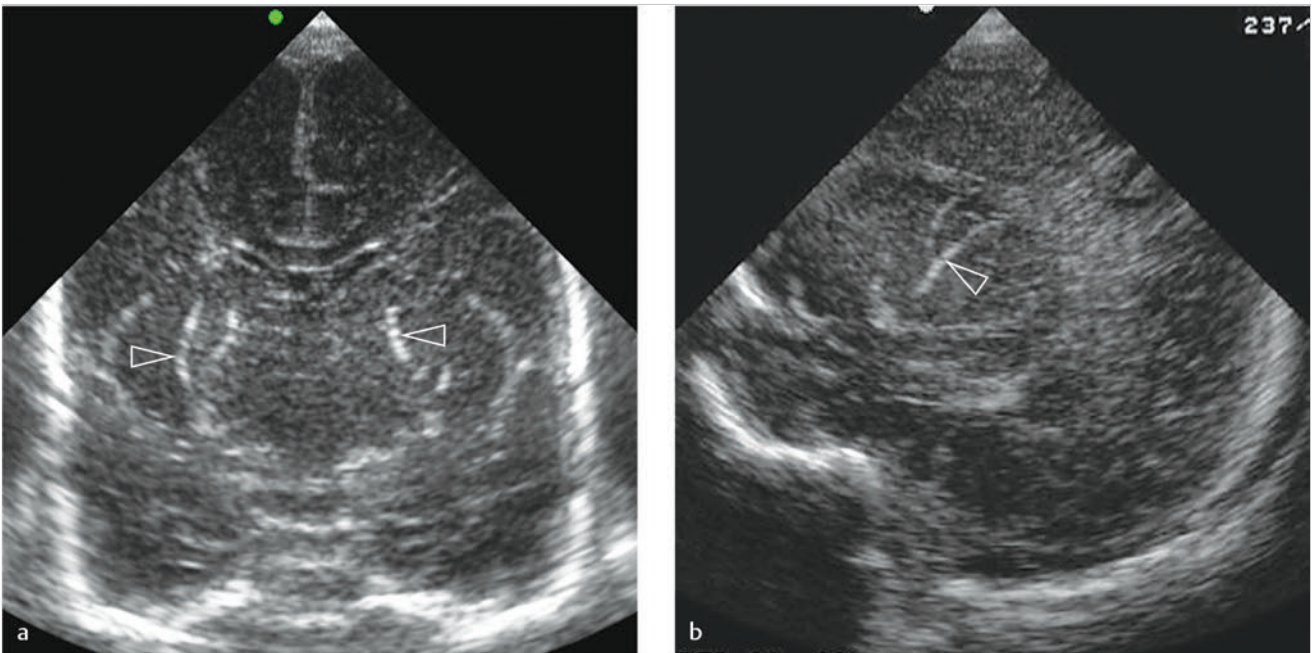


Fig. 3.20a,b Lenticulostriate vasculopathy (*arrowheads*) in a near-term neonate with viral meningoencephalitis. a Coronal plane. b Parasagittal plane.

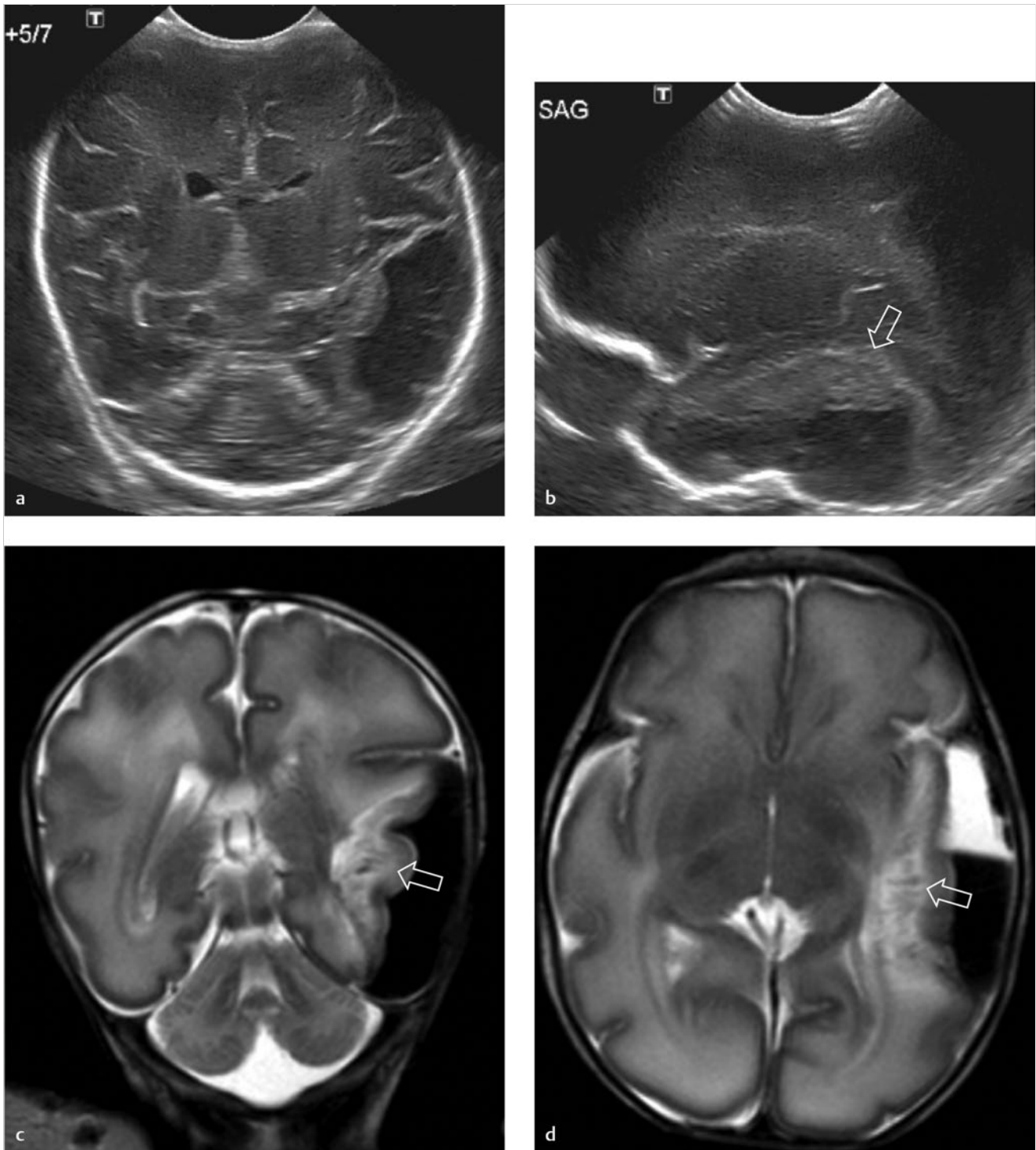


Fig. 3.21a–d Preterm neonate, GA 30 weeks, 5 days. Large left-sided subdural hemorrhage. **a, b** Coronal, resp. parasagittal cUS showing the large extra-axial hemorrhage in the temporal region. Also showing increased echogenicity in the temporal lobe (*arrows*) and compression of the left lateral ventricle. **c, d** Coronal, resp. transverse T2-weighted MRI showing, besides the extra-axial hemorrhage, abnormal signal intensity in the left temporal lobe adjacent to the extra-axial hemorrhage (*open arrows*) due to multiple small hemorrhages and tissue compression. The remainder of the brain parenchyma has a normal aspect for this age. MRI performed on day 6 after birth.

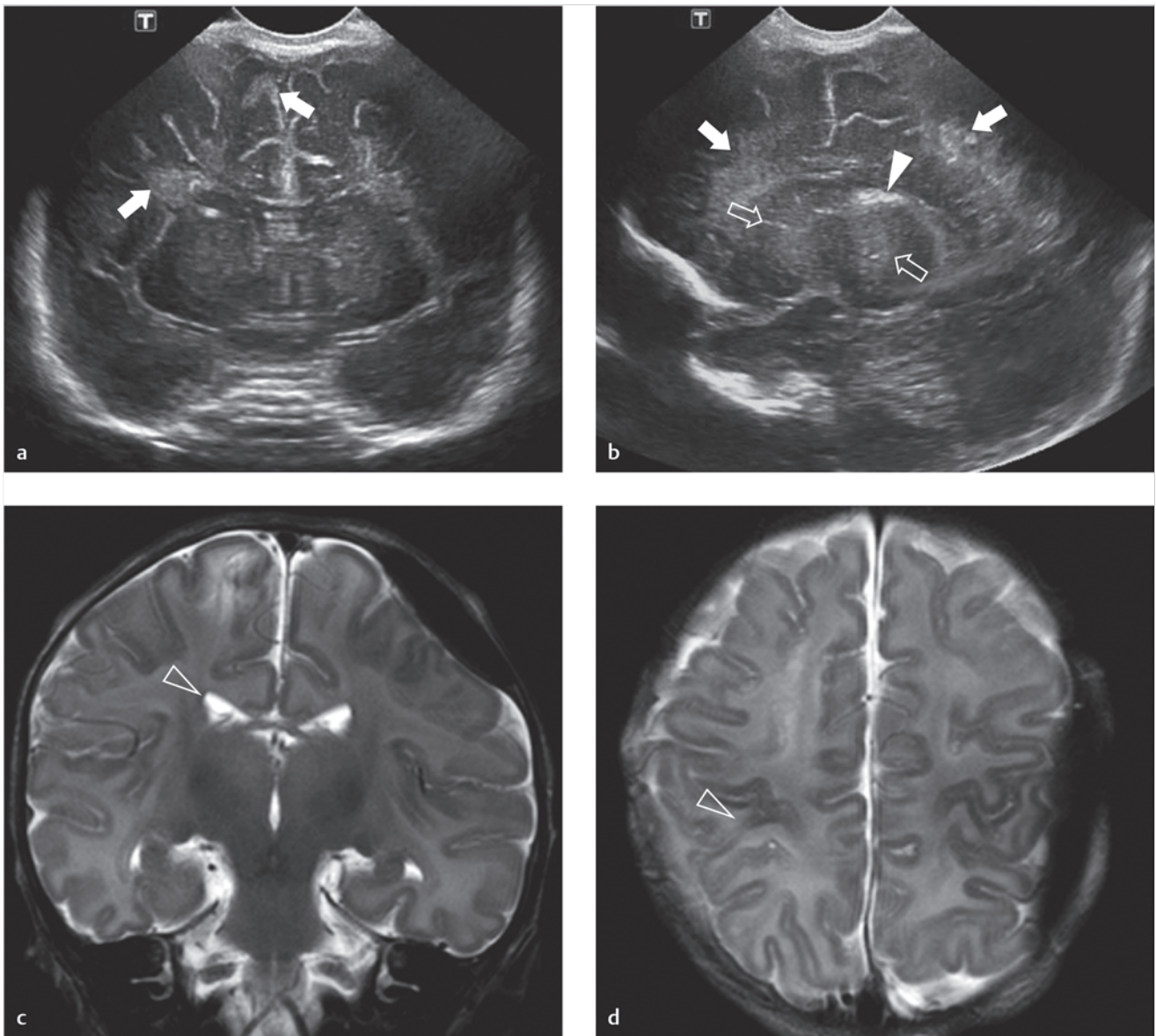


Fig. 3.22a–d Full-term neonate, traumatic delivery. **a, b** Coronal, resp. parasagittal cUS images showing increased echogenicity in the frontoparietal white matter (*arrows*) consistent with swelling or ischemia. Also showing increased echogenicity in the basal ganglia and thalami (*open arrows*), again related to edema or ischemia. Furthermore, there is a small hemorrhage in the thalamocaudate notch (*arrowhead*). **c, d** Coronal, resp. transverse (supraventricular level) T2-weighted MRI showing a left parietal epidural hematoma with some mass effect upon the adjacent frontal and parietal lobe. Areas of abnormal signal intensity in the white matter (*open arrowheads*). MR imaging performed 1 month after birth. The epidural hemorrhage was missed with cUS because of its high and peripheral location, being outside the scope of cUS.

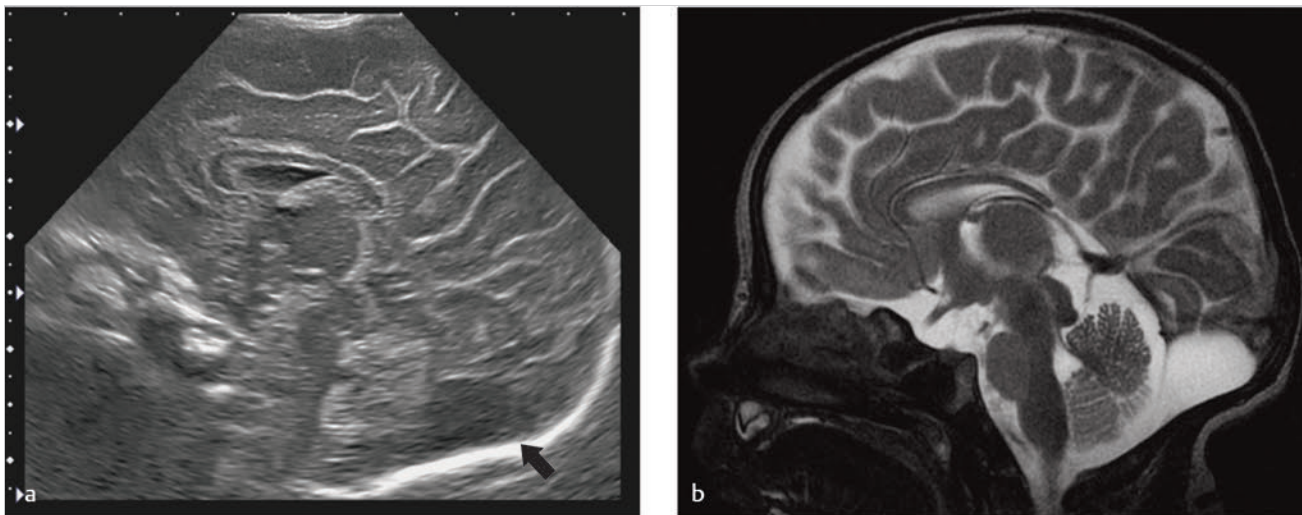


Fig. 3.23a,b Preterm neonate, GA 34 weeks. **a** Midsagittal cUS showing retrocerebellar fluid collection (*arrow*). The cerebellar vermis and other midline structures have a normal appearance. **b** Midsagittal T2-weighted MRI confirming a retrocerebellar cerebrospinal fluid collection without mass and with a normally developed cerebellar vermis, probably representing a small arachnoid cyst.

first seen and tend to resolve within several weeks. They may thus not be visible around TEA. In most infants, some degree of ventriculomegaly, resulting from white matter loss, will then be recognized. Not only cystic periventricular leukomalacia (PVL) but also nonphysiologic PVE of longer duration without cystic evolution (noncystic PVL) is associated with suboptimal neurodevelopmental outcome. Therefore, it is important to know the total duration of abnormal echogenicity.

Although GMH-IVH generally develops within the first few days after birth and is thus diagnosed on cUS scans performed during the first week of life, white matter injury may develop at any time during the neonatal period. Late-onset cystic PVL may occur following sepsis, viral infections, necrotizing enterocolitis, surgery, or recurrent apneic spells (► Fig. 3.24). It is therefore important to perform serial cUS scans from the day of birth until TEA and to increase the number and intensity of cUS examinations following any acute deterioration (► Table 3.1).

A cUS examination around TEA is recommended in every very preterm neonate (GA < 32 weeks). It enables the detection/evaluation of the following:

1. Late-onset cystic PVL;
2. Focal infarction;
3. The later stages of cystic PVL and PVHI;
4. Ventriculomegaly resulting from white matter loss in infants with diffuse, noncystic white matter injury;
5. Ventricular dilatation and white matter injury due to PHVD.
6. In the preterm neonate, serial cUS scans from birth until TEA are needed to detect and follow brain injury.

In the preterm neonate, serial cUS scans from birth until TEA are needed to detect and follow brain injury. ► Table 3.1 shows an example of a scan protocol used in our hospitals. The frequency of cUS examinations should be increased when injury is seen and following any clinical deterioration or recurrent apneic spells.

For other useful scan protocols, we refer to recent literature.

Table 3.1 Cranial ultrasound scan protocol for preterm infants

GA at birth (weeks)	23–26	27–32	33–37
Postnatal age	Days 1, 2, 3, ^a 7 ^a	Days 1, 3, ^a 7 ^a	Day 3 ^a
	2 weeks	2 weeks	
	Weekly to PMA 31 weeks	Weekly to PMA 31 weeks	Before discharge
	Alternating weeks to PMA 35 weeks	At PMA 32 weeks or before discharge	
	TEA	TEA	

Abbreviations: GA, gestational age; PMA, postmenstrual age; TEA, term equivalent age.
 Note: ^aInclude scanning through posterior fontanel and mastoid fontanel.

3.4 Measurements

3.4.1 Ventricular Measurements

In preterm neonates with progressive ventricular dilatation, mostly due to PHVD, it is recommended to perform serial measurements of the ventricular system. The decision to treat ventricular dilatation depends largely on these measurements. In order to prevent any further increase in ventricular size and raised intracranial pressure and thereby white matter injury, treatment of PHVD should be considered when ventricular dilatation is rapidly progressive. In this paragraph, we will demonstrate how ventricular measurements are performed and will refer to reference values. The most frequently used measurement of the lateral ventricles is the so-called ventricular index (VI), introduced by Levene in 1981. It is defined as the distance between the falx and the lateral wall of the anterior

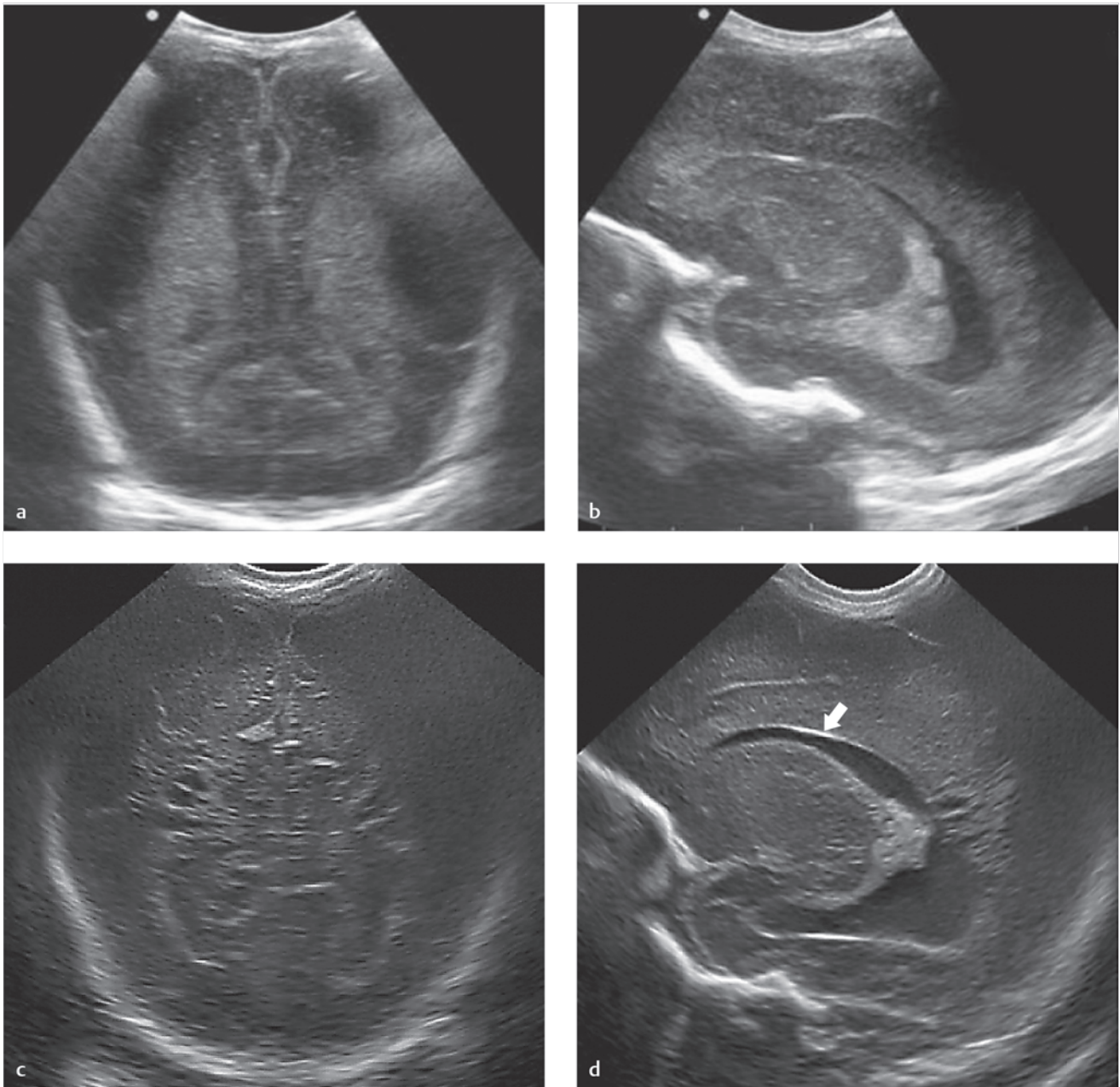


Fig. 3.24a–d Preterm neonate, GA 34 weeks. **a, b** Coronal, resp. parasagittal cUS images on the first day of life showing PVE in the frontal and parietal white matter, physiologic at this age. **c, d** Coronal, resp. parasagittal cUS images performed 1 month later, after the child had developed necrotizing enterocolitis. Now showing cystic lesions in the parietal white matter. In addition, there is mild dilatation of the lateral ventricle and echogenic ventricular lining (*arrow*), the first related to white matter loss, the latter to a small IVH.

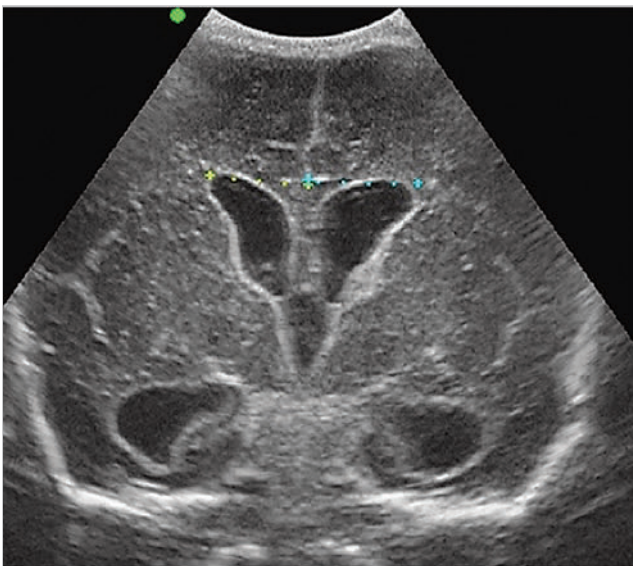


Fig. 3.25 Coronal cUS image at the level of the third ventricle in a preterm neonate with PHVD. The VI is measured on both sides.



Fig. 3.26 Coronal cUS image at the level of the third ventricle in the same preterm neonate with PHVD. The AHW is measured on both sides.

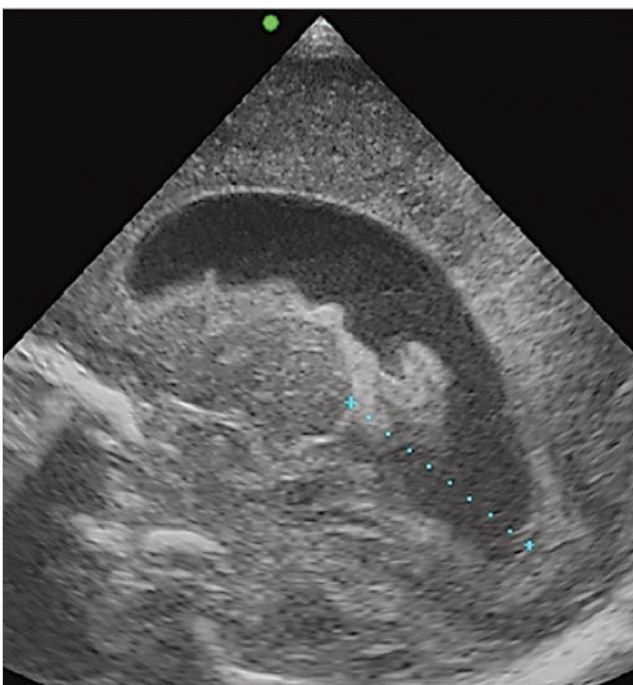


Fig. 3.27 Parasagittal cUS image through the left lateral ventricle in the same preterm neonate with PHVD. The TOD is measured. Note the blood clot continuous with the choroid plexus.

horns in the coronal plane. The VI is measured in the third coronal plane (at the level of the interventricular foramina of Monro) at the largest width of both lateral ventricles (► Fig. 3.25). The VI increases with age. Values above the 97th percentile indicate ventricular dilatation. The first sign of an increase in intracranial pressure is, however, not dilatation of

the lateral ventricles, but a change in ventricular shape with rounding of the frontal horns, so-called ballooning. This phenomenon results in an increase of the width of the anterior horns. The anterior horn width (AHW) is defined as the diagonal width of the anterior horn of the lateral ventricle, measured at its widest point in the coronal plane (► Fig. 3.26). The AHW remains constant with age. In the majority of neonates, the AHW is less than 3 mm. Values above 6 mm are associated with ballooning, and intervention should be considered. In extremely preterm infants, dilatation of the occipital horns often occurs before an increase in frontal horn size. The occipital horns are usually more dilated than the frontal horns and may even be the only site of ventricular dilatation. The thalamo-occipital distance (TOD) is defined as the distance between the outermost point of the thalamus at its junction with the choroid plexus and the outermost part of the occipital horn. It is measured in the parasagittal plane (► Fig. 3.27). The TOD remains rather constant with age.

The VI graph of Levene has an age range between 27 and 40 weeks. New reference values for the VI, AHW, and TOD were recently published by Brouwer et al, with an age range between 24 and 42 weeks. A summary is presented in ► Table 3.2.

3.4.2 Measurements of Cerebral Structures

Preterm infants have lower volumes of supratentorial white and gray matter on MRI performed at TEA compared with full-term infants. The corpus callosum (CC) is thinner and the cerebellar volume reduced.

The CC is the main white matter commissure connecting the cerebral hemispheres. It is essential for cognitive development and function. In a normal fetus, the CC grows rapidly, with an almost linear increase in length between 20 and 40 weeks of gestation, while the height remains rather constant during the

Table 3.2 Cross-sectional reference values (i.e., estimated means + 95% reference intervals, in millimeters) for the ventricular index (VI), anterior horn width (AHW), and thalamo-occipital distance (TOD) of 625 neonates from 24 to 42 weeks' gestational age (GA) (P, percentile; n = 625) (Brouwer et al, see reference)

GA (weeks)	VI (mm)			AHW (mm)			TOD (mm)		
	P 2.5	Estimated mean	P 97.5	P 2.5	Estimated mean	P 97.5	P 2.5	Estimated mean	P 97.5
24+0	6.8	8.0	9.4	1.1	1.5	2.8	11.2	14.5	18.7
25+0	7.0	8.3	9.7	1.1	1.5	2.8	11.4	14.7	19.0
26+0	7.2	8.5	10.1	1.1	1.5	2.8	11.6	15.0	19.3
27+0	7.4	8.8	10.3	1.1	1.5	2.8	11.8	15.2	19.6
28+0	7.6	9.0	10.6	1.1	1.5	2.8	11.9	15.4	19.8
29+0	7.8	9.3	10.9	1.1	1.5	2.8	12.0	15.5	20.0
30+0	8.0	9.5	11.2	1.1	1.5	2.8	12.1	15.6	20.2
31+0	8.2	9.7	11.5	1.1	1.5	2.8	12.2	15.8	20.3
32+0	8.4	10.0	11.8	1.1	1.5	2.8	12.3	15.9	20.5
33+0	8.6	10.2	12.0	1.1	1.5	2.8	12.3	15.9	20.5
34+0	8.8	10.4	12.3	1.1	1.5	2.8	12.4	16.0	20.6
35+0	9.0	10.6	12.5	1.1	1.5	2.8	12.4	16.0	20.6
36+0	9.2	10.8	12.8	1.1	1.5	2.8	12.4	16.0	20.6
37+0	9.4	11.1	13.1	1.1	1.5	2.8	12.4	16.0	20.6
38+0	9.5	11.3	13.3	1.1	1.5	2.8	12.3	15.9	20.6
39+0	9.7	11.5	13.5	1.1	1.5	2.8	12.3	15.9	20.5
40+0	9.9	11.7	13.8	1.1	1.5	2.8	12.2	15.8	20.4
41+0	10.0	11.9	14.0	1.1	1.5	2.8	12.1	15.7	20.2
42+0	10.2	12.0	14.2	1.1	1.5	2.8	12.0	15.5	20.0

same period. The cerebellum has important connections with supratentorial brain structures and the spinal cord. It plays an important role not only in motor control but also in language processing, auditory and visual memory, cognition, and social development and behavior. During the fetal period, growth and development of the cerebellum are rapid and critical.

In the human fetus, the CC and cerebellum are markers for brain development. This is related to the rapid growth of both structures and the fact that they are easily visualized by ultrasonography. There can be partial or complete agenesis of the CC. This may be an isolated finding but is also seen in association with other (more serious) central nervous system abnormalities and syndromes.

The cerebellar vermis is abnormal in the fetus with a Dandy-Walker malformation or variant and, again, in association with other central nervous system malformations and syndromes. The transverse cerebellar diameter (TCD) serves as a predictor of gestational age in the fetus. It is also used to assess cerebellar growth and to diagnose cerebellar hypoplasia when the gestational age is known.

In preterm infants, abnormal growth of the CC is associated with delayed cognitive and motor development. Injury to the cerebellum, a frequent complication in very preterm neonates, may severely disrupt its normal growth and development and is associated with abnormal motor and cognitive outcome and behavioral problems. Measurement of cerebral structures in the brain of the preterm neonate can be of clinical importance to diagnose and quantify brain abnormalities and altered development.

The length and height of the CC and the width (maximum anterior-posterior diameter) and height of the vermis are

measured in the midsagittal plane during scanning through the anterior fontanel (► Fig. 3.28). The TCD (widest diameter of the cerebellum) is measured in the coronal plane through the fourth ventricle, with the mastoid fontanel used as an acoustic window (► Fig. 3.29).

3.5 Preterm Infants: Pathology

3.5.1 Germinal Matrix–Intraventricular Hemorrhage

GMH-IVH remains a common neurologic complication of preterm birth, occurring in about 10 to 20% of preterm infants with a GA below 30 weeks. A large IVH and especially a hemorrhage with PVHI are often associated with an adverse neurologic outcome. The risk to develop PHVD increases when GMH-IVH is more severe. About 30 to 50% of infants with a large GMH-IVH will develop PHVD, and around 20 to 40% of infants with a severe GMH-IVH will consequently need a permanent ventriculo-peritoneal shunt. The presence of associated white matter injury due to a unilateral PVHI or the presence of more diffuse, bilateral white matter damage as well as the development of PHVD further increases the risk for an adverse neurodevelopmental outcome.

The classification system suggested by Volpe is suitable to describe early and late ultrasound appearances (► Table 3.3). It is better to avoid the use of grade 4 and instead provide a separate description of the size, site, and appearance of a parenchymal lesion. Making a distinction between a small hemorrhage



Fig. 3.28 Midsagittal cUS, preterm neonate, GA 32 weeks. The vermis height (D1) and width (D2) and callosal length (D3) are measured.

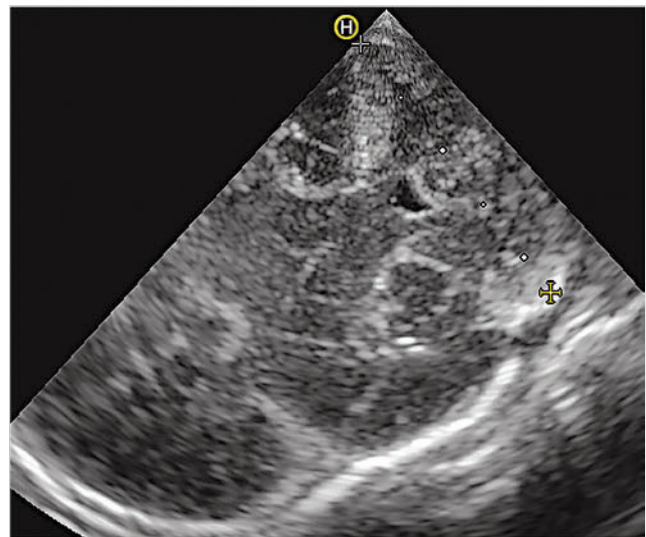


Fig. 3.29 Coronal cUS, with the mastoid fontanel used as an acoustic window. Preterm neonate, GA 27 weeks; postmenstrual age at scanning, 36 weeks. The TCD is measured.

Table 3.3 Grading of germinal matrix–intraventricular hemorrhage

Description	Generic term
Grade 1: GMH	GMH-IVH
Grade 2: GMH and small IVH without ventricular dilatation	GMH-IVH
Grade 3: GMH and large IVH with ventricular dilatation (clot fills > 50% of ventricle)	GMH-IVH and ventriculomegaly

restricted to the germinal matrix or a GMH with some blood ruptured through the ependyma into the ventricular lumen is not always possible. The use of the posterior fontanel as an alternative acoustic window has been advocated, showing improvement in the diagnosis of a small GMH-IVH (► Fig. 3.30). Using the posterior fontanel is also helpful for looking at the degree of dilatation/ballooning of the occipital horn in infants with PHVD (► Fig. 3.31). A GMH at a site other than the head of the caudate nucleus, like the roof of the temporal horn, often remains undiagnosed and will be diagnosed only when MR imaging is also performed.

A large GMH-IVH, grade 3, is diagnosed based on presence of a large clot in the ventricle, filling the ventricle more than 50%, as well as acute dilatation of the ventricle involved. A grade 3 IVH may lead to PHVD over a period of 1 to 3 weeks. The diagnosis of a grade 3 IVH cannot be made on a single examination performed during the second or third week, when ventricular dilatation is not acute but has occurred because of PHVD (► Fig. 3.32). The maximal extent of the hemorrhage may take a few days. Many centers therefore perform a first scan at the end of the first week. The evolution of a small GMH-IVH to a large hemorrhage would then be missed (► Fig. 3.33).

Blood can sometimes be seen in the cavum septum pellucidum. This is not an isolated finding but tends to occur in

combination with a GMH-IVH (► Fig. 3.34). Blood can also extend into the corpus callosum as a consequence of involvement of the septal vein (Dudink et al; ► Fig. 3.35).

A PVHI is usually unilateral, either globular in shape and communicating with the ventricle containing a moderate to large ipsilateral GMH-IVH, or triangular in shape, with the apex at the outer border of the lateral ventricle and not or partly communicating with the ipsilateral ventricle (► Fig. 3.36). In the past, PVHI was considered to be due to direct extension of the hemorrhage into the periventricular white matter, but this is no longer considered to be the most likely explanation for this type of parenchymal lesion. Most would now agree that this type of lesion is due to the presence of a GMH-IVH, which can lead to impaired venous drainage and subsequent venous infarction of the medullary veins of the white matter. This sequence of events can sometimes be followed with sequential ultrasound examinations, with change from a normal image to a stage of simple GMH-IVH and PVHI on the following day (► Fig. 3.37). Whereas the globular type of PVHI tends to evolve into a porencephalic cyst (► Fig. 3.38, ► Fig. 3.39, ► Fig. 3.40), the triangular type of lesion is more likely to evolve into multiple cysts, which are partly or even not at all communicating with the lateral ventricle and are therefore sometimes wrongly diagnosed as cystic PVL (► Fig. 3.41). This is especially likely to happen when sequential scans are not available and the initial GMH-IVH has been missed. A PVHI may also resolve with cystic evolution, with eventual ex vacuo dilatation on the affected side (► Fig. 3.42).

The PVHI is most often seen in the parietal lobe but can also develop in the frontal or temporal lobe, depending on the veins involved (see ► Fig. 3.42; ► Fig. 3.43). The site of the lesion in relation to the area of the trigone of the lateral ventricle is important for outcome prediction. If the lesion is anterior to the trigone (frontal or temporal lobe), the development of a

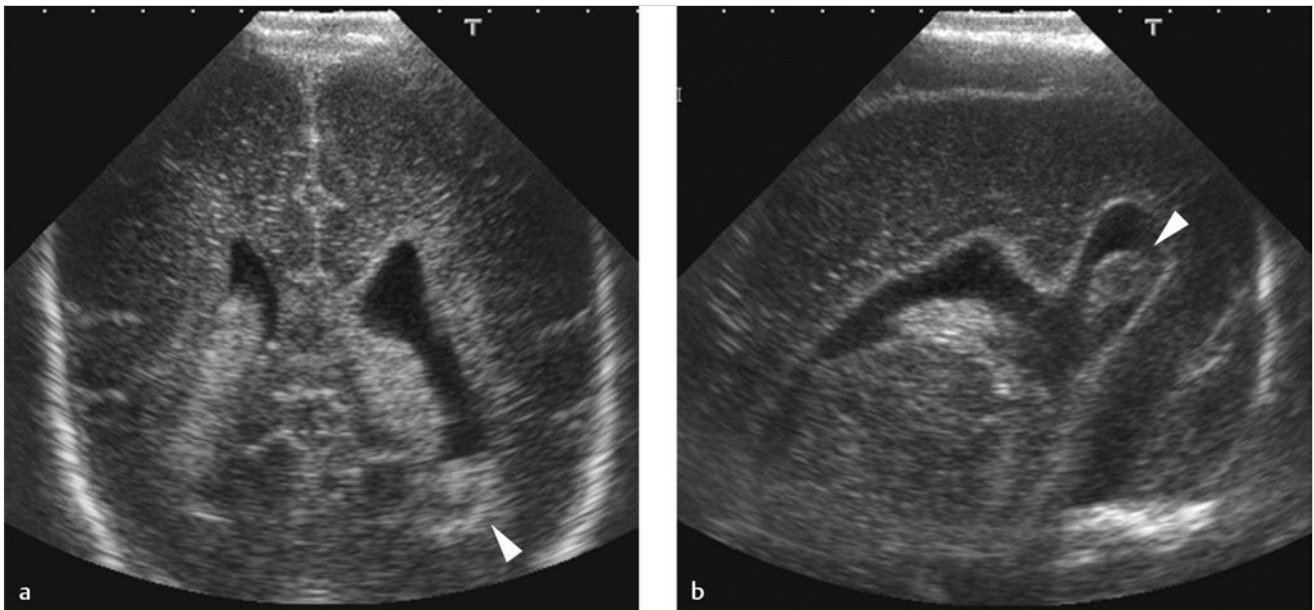


Fig. 3.30a,b a Preterm infant, GA 26 weeks. The coronal view, angling backwards, shows a small clot in the left ventricle (*arrowhead*). b The image taken through the posterior fontanel confirms the presence of an IVH (*arrowhead*).

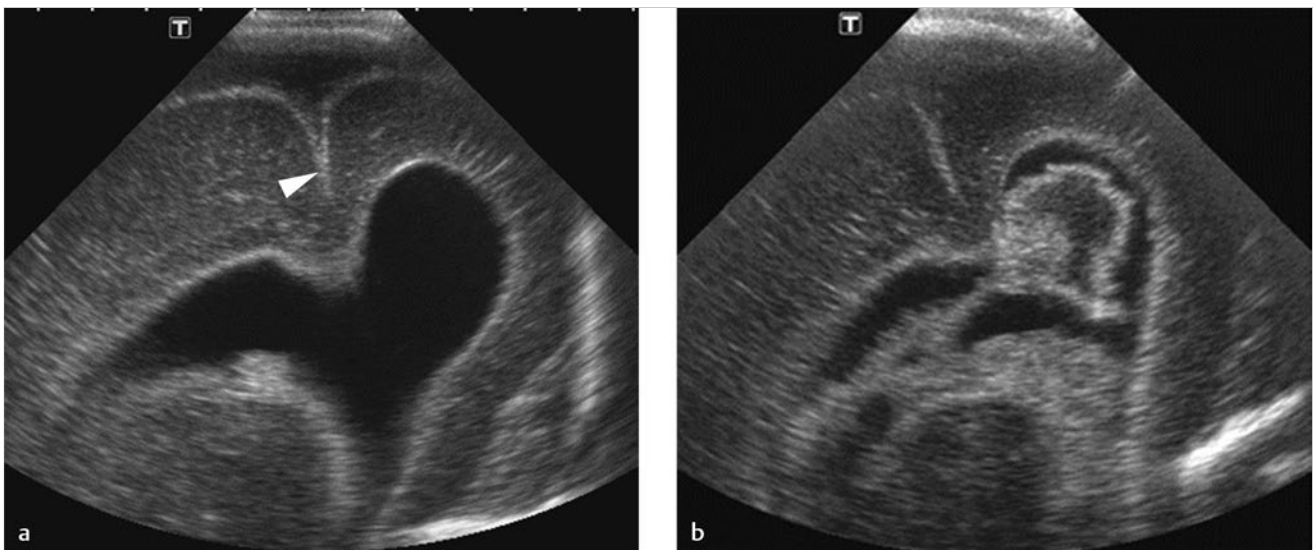


Fig. 3.31a,b Parasagittal views of another infant, taken through the posterior fontanel, showing dilatation of the right occipital horn, posterior to the calcarine fissure (*arrowhead*, a). A large clot is seen in the left occipital horn (b). Enlargement of the occipital horns is present bilaterally.

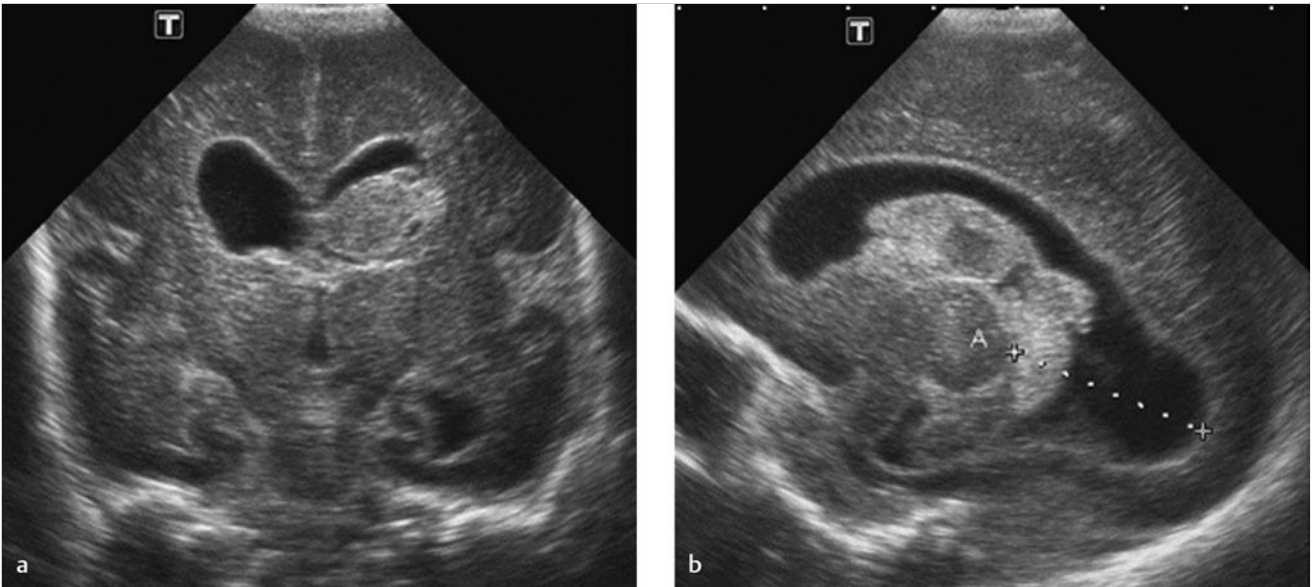


Fig. 3.32a,b Preterm infant, GA 26 weeks. A large GMH-IVH is present on the left. While there is a clot filling more than 50% of the ventricle, there is also PHVD. The TOD is measured in the parasagittal view. The white matter does not appear to be involved.

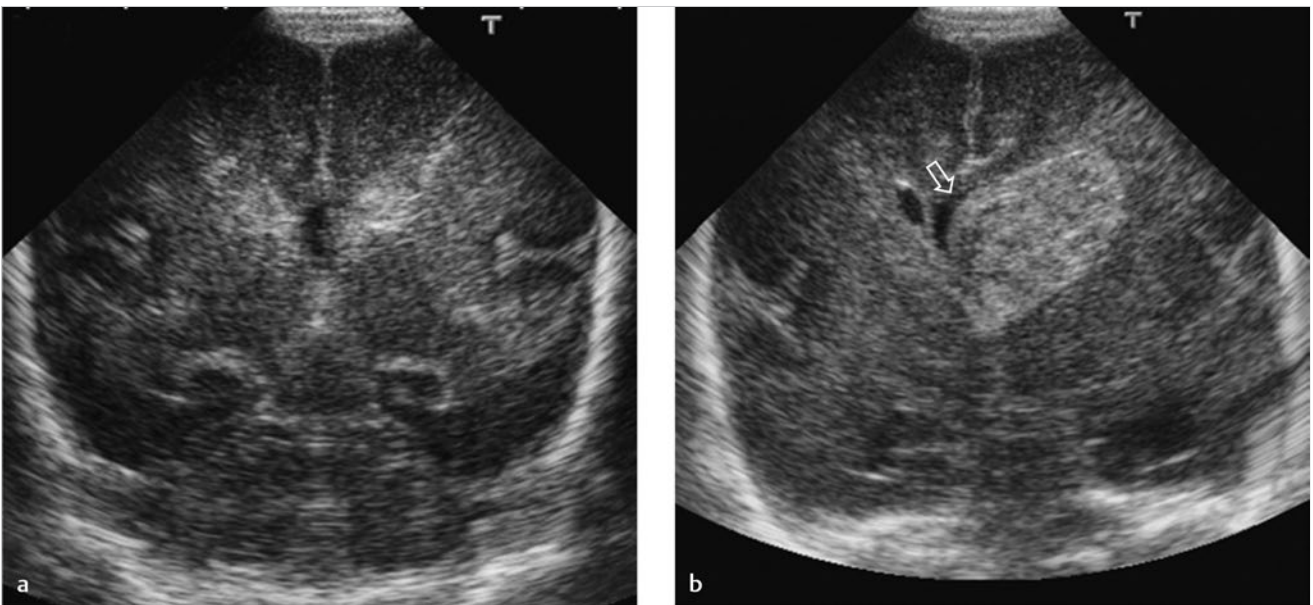


Fig. 3.33a,b Preterm infant, GA 26 weeks. A bilateral GMH-IVH is seen on the day of birth. On day 3, a large GMH-IVH is now present on the left, with acute dilatation of the left ventricle. Also note the pressure effect on the cavum septum pellucidum (arrow).